THE UNIVERSITY OF CHICAGO

BIOMECHANICS, EVOLUTION, AND MODULATION OF SUCTION FEEDING MECHANISMS IN FISHES

A DISSERTATION SUBMITTED TO

THE FACULTY OF THE DIVISION OF THE BIOLOGICAL SCIENCES

AND THE PRITZKER SCHOOL OF MEDICINE

IN CANDIDACY FOR THE DEGREE OF

DOCTOR OF PHILOSOPHY

GRADUATE PROGRAM IN INTEGRATIVE BIOLOGY

BY

KATRINA ROSE WHITLOW

CHICAGO, ILLINOIS

AUGUST 2022

For Mom and Dad

TABLE OF CONTENTS

LIST OF TABLES

LIST OF FIGURES

ACKNOWLEDGEMENTS

This dissertation was influenced and enabled by the support of many people and institutions. First and foremost, my co-advisors Mark Westneat and Callum Ross provided critical mentorship for my growth as a scientist and teacher. Through equipment failures, leaking tanks, surgical complications, COVID shutdowns, and more, I knew that I had their support and faith. My skills from resilience to writing and everything between have improved during my time at the University of Chicago, thanks to Callum and Mark. I am perhaps even more grateful for the experiences I had with Mark and Callum outside of the research lab. Mark facilitated two fantastic fieldwork experiences for me, which could not have been more different but were equally rewarding: tromping through swampy rivers in southern Illinois to collect bowfin and diving the beautiful reefs of Mo'orea to film and collect wrasse. Callum brought me into the Human Body course as a TA the last two years of my PhD, where I found a real passion not only for learning the details of human anatomy and physiology, but also for teaching and interacting with students. I am certain these experiences helped me secure my faculty position, not to mention that they were extremely fun!

My committee members Michael Coates and Melina Hale provided helpful guidance and feedback throughout my PhD. Melina welcomed me to her lab for my first rotation as a PhD student, where I learned several techniques and explored the new-to-me field of neurobiology. She has further served as a great role model and constructive committee member, despite my shift into biomechanics of feeding. Mike's been an incredible source of information on the anatomy and fossil record of the fishes I studied, always encouraging me to explore aspects of fish evolution relevant to my work, which would have been inaccessible without his guidance.

I am grateful to my previous research mentors, Chris Oufiero and Paul Brunkow, who both taught me so much and encouraged me to pursue a scientific career. Paul was the first professor to welcome me in his lab as a junior at Southern Illinois University Edwardsville, where he taught me about morphometrics, data collection, and how to approach scientific questions. His mentorship helped form the foundation for my scientific approach and career, and I strive to play a similar role in the lives of my future students. Chris took me on as a master's student at Towson University, where I found my love of working with fishes in the lab. Chris helped me learn everything from computational analysis in R to publishing research papers, and so much of how I approach my work still stems from the lessons he taught me.

A huge thanks to my colleagues and collaborators, in particular Nicholas Gidmark and Elska Kaczmarek for numerous insights and discussions about XROMM and more. I owe a special thanks to Sofia Garrick and Dakota Lane, who helped with the painstaking process of digitizing data for this thesis. Thank you both for being wonderful to work with.

Broader institutional support and funding were critical to this dissertation. To Audrey Aronowsky and other members of the OBA and Darwin Cluster administrative group, thank you. Thank you to Stephanie Palmer and Urs Schmitt-Ott for guiding me as a first and second year through my qualifying exams. Vicky Prince, thank you for the opportunity to serve as an instructor of record for the TA training course for the BSD – this opportunity was critical to my decision to pursue teaching further for my career. The University of Chicago Hind's Fund and Organismal Biology and Anatomy Internal Core Facilities Grant provided financial support for my research. The NSF provided funding for the University of Chicago XROMM Facility, which

was critical for this dissertation. The UC Animal Resources Center provided space, care, and CT scanner training and access. The UC PaleoCT lab provided access to microCT scanning. The Shubin lab provided staining chemicals and equipment. The Keck Facility and Brainerd Lab at Brown University provided resources for additional data collection.

I am thankful to my colleagues in the Westneat lab for so many things, including our shared love of fish. Andrew and Chloe first welcomed me into the lab, where we were later joined by Sam, Lily, and Linnea. To Andrew, I am grateful for your mentorship and listening ear. I really enjoyed our discussions of swimming mechanics and other fish room gossip. Chloe's friendship transformed my graduate school experience (and truly, my life) in the second half of our time together, and I am so glad that we started having our chats late in lab and over coffee with a side of sass. Mental health is something I often encouraged others to look after, but was never so good about myself, until Chloe encouraged me to change that. Lily was a great friend and mentor for the brief time we were able to be in lab together amidst the pandemic. Sam has been a wonderful collaborator on all things fish XROMM, and I am grateful for her friendship both in lab and underwater. Linnea, thank you for being a bright spot at the end of my dissertation and providing endless optimism.

I am grateful to the Ross lab for providing me a second home during my thesis work. The people in Ross lab brought a rich diversity of scientific thought (not to mention XROMM expertise) to my UC experience. Discussing biomechanics with folks who work on everything from opossum chewing to primate locomotion broadened my knowledge and was a true pleasure. Thank you all for welcoming a fishy friend into your group and for allowing an unfused dentary-articular combination to count in mandible meeting. Court and Kelsey, thank you for showing

me the ropes and always encouraging me. Kelsey helped make the Ross lab and the entire IB program a warm and supportive place to work, always making sure everyone had a place to be themselves. I am lucky to call them a friend. Michael and Myra, it was wonderful to start our times at UC together and thank you for showing me the joys of "gangstagrass". JD, your support in the lab was truly essential, and your friendship outside the lab was too. Kara, thank you for everything, I am so grateful for our coffee chats and time together in the anatomy lab. Hannah, Peishu, and Alec, you three have provided me with so much comedic relief these last few years and I look forward to seeing you all do great things.

My fellow IB students have provided endless support, encouragement, and opportunities for decompressing throughout my time at UChicago. Thank you to the class above me: Kelsey, Stephanie B, and Erick, for creating such a supportive environment in the program and welcoming me as a first year student. I owe a special thanks to the senior Hale Lab students who saw me through my first rotation project and served as my secondary SAC committee, Hilary, Brett, Adam, and Katie. Hilary also became my perpetual SICB buddy and helped me get back into SCUBA, and for that I am eternally grateful. Thank you TBell crew for all the spice and good times. To Sang, thank you for fueling my bagel addiction, listening to all my woes, and always giving me a reason to laugh. You're the real MVP!

I am incredibly grateful to many friends, and friends who might as well be family, for their support throughout my time at UChicago. My SCUBA crew has given me endless support and a wonderful way to get my mind off work. Your friendships have been essential for my success, and blowing bubbles with you is one of my favorite things. Katie and Sarah, I don't even know where to begin – thank you for everything. I'm not sure how I made it as far as I did

without you and while I will absolutely cheer you on, you're both never actually allowed to leave Chicago unless it's to come closer to South Bend. Thank you to Cabin Club for providing a way out of the city and (much needed) forced relaxation these past two years. To Kevin, Nikia, and John, thank you for all the time sitting in front of my computer yelling at video games together. One of the absolute highlights of the pandemic is that Wednesday nights are now a hangout time regardless of time zones. Jess, I am in shock that we've not managed to get more margaritas during these past 6 years, but I know there will be more soon and I can't wait. Thank you to all the friends who have laughed, cried, swam, eaten stupidly spicy wings, tacos, fondue (eaten anything, really), climbed, drank beer, dissected, gotten coffee, blown bubbles, traveled, crafted, taught, camped, hiked, played games, boated, fished, and so much more with me throughout my time at UChicago.

Finally, I owe the biggest thank you to my family. The Whitlows, Griffises, Meyers, Shadleys, Babiks, Londons, Hunleys, Fosters, Clarks, and Rideouts, I love you all. Especially to my parents and Seth - your constant love, support, and encouragement was essential. Seth, you are my rock, and Mom and Dad, you've always been my biggest cheerleaders. Thank you.

ABSTRACT

Numerous jawed vertebrate species use suction feeding to capture evasive prey by rapidly expanding the skull and pulling water into the mouth. Many biomechanical mechanisms specific to this behavior are unknown, and how this behavior has evolved through time is still under investigation. In this thesis I quantify cranial kinematics for two non-teleost actinopterygian taxa using X-Ray Reconstruction of Moving Morphology (XROMM), exploring how mobile skeletal elements may drive suction feeding success. Furthermore, I compare the contribution of each cranial bone to changes in oral cavity volume across four species spanning the gnathostome phylogeny. In chapter 1 I introduce the field of suction feeding biomechanics, providing morphological and phylogenetic context for the subsequent chapters, and set up specific questions that are addressed in this thesis. In chapter 2 I describe the cranial kinesis employed during suction feeding by *Polypterus bichir*, a member of the earliest branching actinopterygian clade. I quantify the precise 3D motions of the ceratohyal and find that these motions are strongly associated with prey motion and the peak rate of volume expansion during suction strikes. I describe and employ a new method of quantifying the relative contribution of individual bones to volume change (RCVC) during suction feeding strikes. I also explore the mechanics of jaw opening in *P. bichir*, including the role of the sternohyoideus muscle in depressing the hyoid during suction feeding. In chapter 3 I quantify the suction feeding kinematics of *Amia calva* feeding on both evasive and non-evasive prey, finding that strikes on evasive feeder fish are statistically distinct from those on worms. This chapter provides another dataset for understanding the variability and modulation of suction feeding strikes in fishes. I further explore the role of the sternohyoideus muscle in depressing the hyoid and generating

force for suction feeding in *A. calva*. In chapter 4 I measure the RCVC (relative contribution to volume change) during suction feeding across four species: *P. bichir, A. calva, Protopertus annectens,* and *Chitala blanci*. These species span the gnathostome phylogeny and have distinct morphologies. Our analysis reveals variation in which bones drive volume change during suction feeding. In chapter 5 I provide a summary of the findings and impacts of this dissertation and lay out several future directions for study to expand upon this work.

CHAPTER 1: INTRODUCTION

Successfully acquiring food is essential for an organism's survival and fitness, providing the energy required to grow, reproduce, navigate the environment, and escape predation; this ultimately impacts the evolution of both predators and prey, and the maintenance of species through time. Fishes, the most species-rich vertebrate group, must navigate the complex underwater environment while capturing their prey. The skulls of jawed fishes are highly kinetic and complex, enabling rapid expansion of the oral cavity to draw prey into the mouth via suction feeding. Suction is achieved through precise coordination of cranial skeletal elements, beginning with the oral jaws opening and ending with water passing posteriorly through the opercular opening (Tchernavin, 1948). This progressive "anterior to posterior wave" of volume increase creates a pressure gradient between the mouth and surrounding water, pulling a bolus of water, hopefully containing a prey item, into the oral cavity (Bishop et al., 2008; Jacobs and Holzman, 2018). The prey item is frequently then snagged on teeth or gill rakers to prevent escape, while the jaws begin to close and the operculum opens to allow some of the water to continue flowing out through the gills.

Suction feeding in fishes has been studied extensively and from various perspectives, including the fields of morphology, biomechanics, skeletal linkages, performance, dietary specialization, power, hydrodynamics, flow regimes, and evolution of fish skulls and feeding mechanisms (Bishop et al., 2008; Camp and Brainerd, 2014; Kane and Higham, 2014; Lauder, 1982; Provini et al., 2022; Wainwright and Bellwood, 2002; Wainwright et al., 2015; Westneat, 2004). However, due to the complex nature of fish skulls, the complex environment the animals eat in, and the immense diversity of species that may differ in any of these aspects, there are

many outstanding questions in the field of fish feeding biomechanics. In this chapter I will lay out a general background on suction feeding in fishes, exploring previously unknown variables and mechanics of the species examined for this thesis. I describe several remaining questions in the field, their relevance, and the specific questions answered in the subsequent chapters of this dissertation.

BASIC MECHANICS OF SUCTION FEEDING AND DIVERSITY IN FISH SKULLS

In its most simplified geometric form, a fish skull can be modeled as an oblong cone or series of ellipses that expands and contracts in a coordinated fashion to generate a pressure gradient between the oral cavity and the outside of the skull (Muller and Osse, 1984; Muller et al., 1982; Van Wassenbergh and Aerts, 2009). This basic pattern of anterior to posterior motion in fishes begins with a rapid increase in gape, driven by neurocranial elevation and jaw depression, potentially alongside maxillary and/or premaxillary protrusion (Lauder, 1982; Liem, 1980). Subsequently, the hyoid depresses and, in certain species, flares laterally, expanding the oral cavity ventrally and pulling the prey item further into the mouth. Finally, strikes conclude with opercular flaring, allowing a water bolus to exit the oral cavity posteriorly without dislodging the prey item or allowing it to escape back through the jaws (Bishop et al., 2008; Jacobs and Holzman, 2018; Van Wassenbergh and Aerts, 2009).

The timing of pectoral girdle retraction, where it occurs, does not fall strictly into this anterior to posterior pattern. The pectoral girdle is sometimes considered part of the head as it articulates with the cranium and forms the posterior boundary of the gill apparatus (Tchernavin, 1948). More often it is treated as a distinct unit and boundary between the body and head, as it is

connected to the body by hypaxial muscles and to the hyoid apparatus of the skull via the sternohyoideus muscle (Camp, 2019). The likely importance of this connection between axial and cranial components – namely, the ability of body muscle to alter pectoral girdle position, and therefore the position of the branchial apparatus and ventral hyoid arch - has long been noted (Tchernavin, 1948). Recent work has emphasized the importance and variability of this connection, demonstrating that axial muscles contribute substantially to suction generation across bony fishes (Camp and Brainerd, 2014; Li et al., 2022; Lomax et al., 2020; Van Wassenbergh et al., 2007; Whitlow et al., 2022)

There is wide variability among species in the relative mobility of each of cranial, hyoid, and pectoral girdle elements, and subsequently, we presume, in their importance for the suction feeding apparatus. Many species (like many teleosts and one holostean, *Amia calva*) use eight or more independently mobile elements (stiff components, like sets of bone and/or cartilage), expanding their skulls laterally, dorsoventrally, and anteriorly (Lauder, 1979). Other species may even protrude the entire oral jaws anteriorly (such as in the dramatic strike of the slingjaw wrasse *Epibulus insidiator*; Westneat and Wainwright, 1989), while others are more restricted in one or more of these axes of mobility. For instance, the actinopterygian *Polypterus* lacks the ability to swing their jaws forward but exhibits substantial dorsoventral and lateral mobility (Lauder, 1980; Whitlow et al., 2022). Furthermore, the relative size of bones, size and orientation of musculature, and linkages connecting these bones and muscles all vary through the evolutionary history of fishes (Ferry-Graham et al., 2001b; Westneat, 2004). For example, the teleost *Chitala blanci* has a dorsoventrally broad and laterally compressed skull (Li et al., 2022), while the skull

of *Atractosteus spatula* is laterally broad and dorsoventrally compressed (Lemberg et al., 2019). However, all these species successfully suction feed!

Importantly, none of the motions described above operates completely independently of the others. The elevation of the neurocranium, driven by contraction of the epaxial musculature, results in elevation of the suspensorium and therefore may contribute to gape expansion. Posterior and ventrally directed forces applied to the anterior and ventral aspect of the hyoid arch, whether powered by a contracting sternohyoideus, hypaxial muscles, or both, result not only in retraction and depression of the ceratohyal, but also result in movement of the suspensorium and lower jaw. In many species jaw depression is also driven in part by opercular rotations and translations and how exactly this mechanism works together with ceratohyal movement has yet to be elucidated. A central aim of this thesis is to explore these complex feeding kinematics in more detail using 3D imaging techniques applied to fish species in key phylogenetic positions in the tree of life.

PHYLOGENETIC CONTEXT

This thesis explores suction feeding in the early branching actinopterygian fishes *Polypterus* and *Amia*, and across the sarcopterygian-actinopterygian divide to compare lungfishes and teleost as well, so it is important to understand how these species are related and grouped. Fig. 1.1 shows the broad phylogenetic relationships relevant to this thesis, the gnathostomes or jawed vertebrates. The first split shown is between organisms with a non-ossified, cartilaginous skeleton, Chondrichthyes (sharks, skates, and rays) and Osteichthyes (bony fishes). Osteichthyes encompasses bony fishes, including tetrapods (land animals, ranging

from amphibians and reptiles to humans), which are grouped at the far right. Dipnoi and *Latimeria* (lungfishes and coelacanths) are the closest living relatives to tetrapods. Collectively these three groups (Tetrapoda, Dipnoi, *Latimeria*) comprise the clade Sarcopterygii, or lobe-finned fishes. The rest of the gnathostome tree constitutes the actinopterygians, or ray-finned fishes. This clade consists of teleosts, which include most common reef and game fish, as well as species such as gars, bowfin, paddlefish, sturgeon, reedfish, and bichirs. Reedfish and bichirs together comprise the Polypteriformes, the earliest-diverging clade of extant actinopterygians (Giles et al., 2017). While we now know that many features of *Polypterus* that appear primitive are actually reversals (Giles et al., 2017), we can gain insight about basal feeding mechanics that fossil species may have used via inferences from data collected in bichirs. The Neopterygii consists of three primary clades: Teleostei, Amiiformes (which consists of only one extant species), and Lepisosteiformes (which contains seven extant species in two genera). Amiiformes are often regarded as "living fossils" and have a rich fossil record which demonstrates many characteristics seen in the extant species *Amia calva* are synapomorphies of the group (Grande and Bemis, 1998). Combined with the recent re-evaluation of feeding kinematics in the lepisosteiform *Atractosteus spatula* (Lemberg et al., 2019) the data gathered in this thesis provide insight regarding strike mechanics in three key taxa across the gnathostome tree.

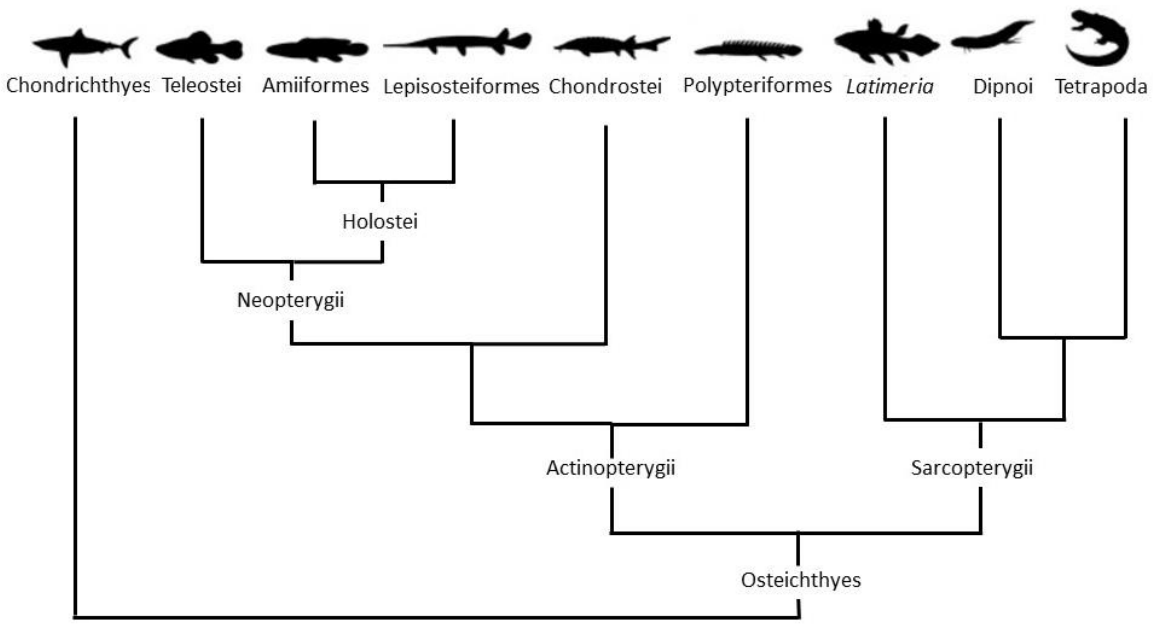

Fig. 1.1. Phylogeny of jawed vertebrates. Adapted from Giles et al., 2017; Wilhelm et al., 2015.

MORPHOLOGICAL OVERVIEW OF *AMIA* AND *POLYPTERUS*

Amia and *Polypterus* are biomechanically interesting as they have disparate pectoral girdle and cranial morphology and mobility, which may affect how motions of the pectoral girdle, hyoid, mandible, and cranium are coordinated and modulated to execute successful suction feeding strikes. For example, both species have gular plates, but *Amia* has a single midline plate and numerous branchiostegals posterior to this (Fig. 1.2A), while *Polypterus* has paired gular plates that touch at the midline when at rest (Fig. 1.2B) (Allis, 1897; Allis, 1922). The maxilla in *Amia* is capable of a large amount of anteroposterior swing, pivoting around a peg-like articulation with the neurocranium (Fig. 1.2E), while the maxilla in *Polypterus* is immobile relative to the cranium and suspensorium (Fig. 1.2F) (Allis, 1897; Allis, 1922; Lauder,

1980). The placement, orientation, and lateral mobility of articulations between the neurocranium and suspensorium also differ among these species. In *Polypterus* the hyomandibula has a very loose soft tissue connection with the rest of the suspensorium (Fig. 1.2H), explored in Chapter 2, while *Amia* has a more rigid suspensorium (Fig 1.2G). Finally, *Amia* has a second jaw opening mechanism, functionally similar to that of teleosts, and further possess a dual joint between the suspensorium and the lower jaw (Lauder, 1979; Lauder, 1980).

These species also have a number of similarities in cranial anatomy and mechanics. They share a ligamentous connection between the hyoid and mandible that enables lower jaw depression via hyoid movement (Lauder, 1980). Previous work demonstrated that *Polypterus* and *Amia* both generate substantial suction during feeding and have similar degrees of lateral mobility in the cranium (Lauder, 1980). Furthermore, these species are both elongated and have extensive body musculature, implying that they may generate similar degrees of power generated using the hypaxial and epaxial muscles during suction feeding.

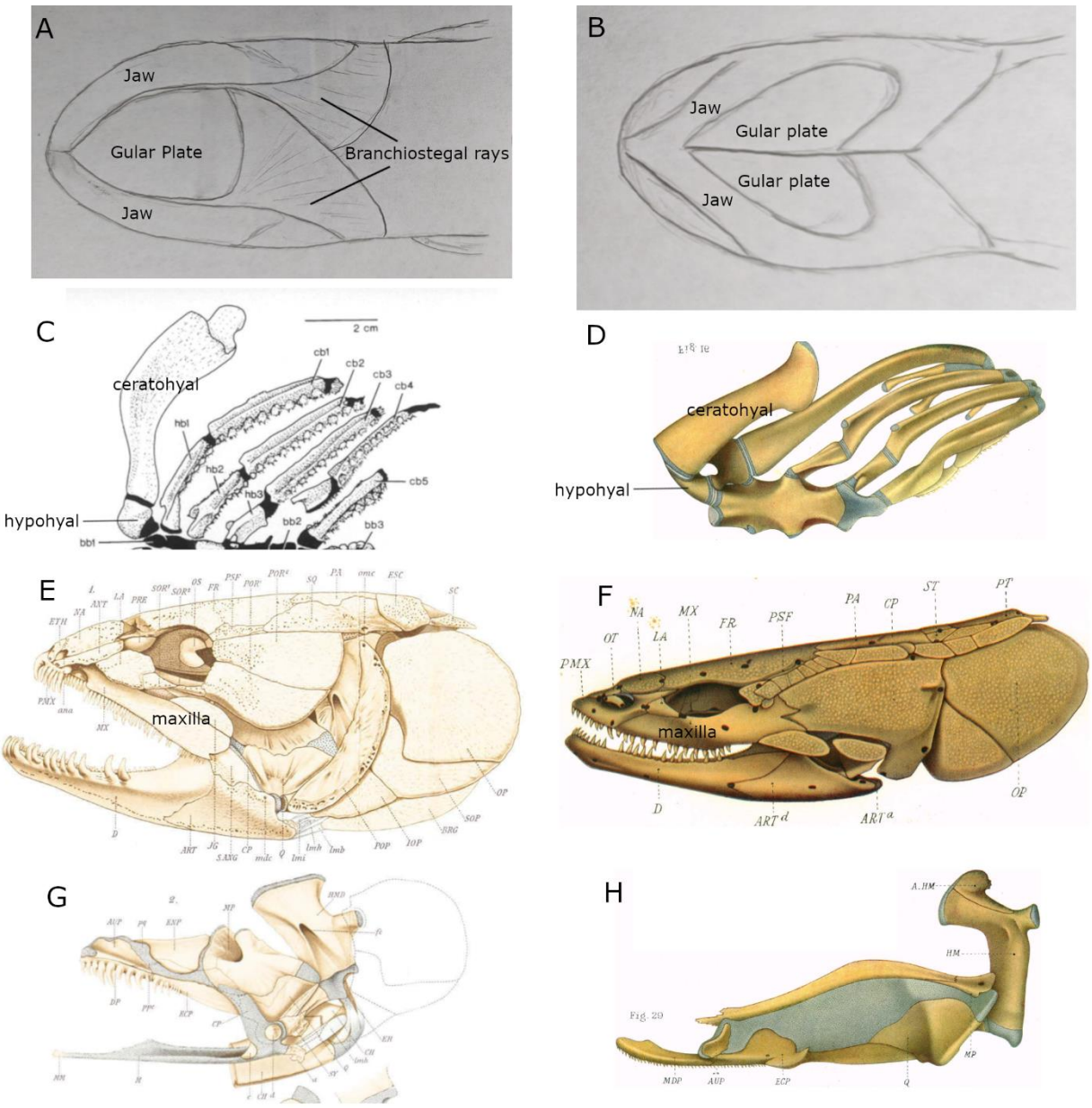

Fig. 1.2. Suspensorial and hyoid anatomy of *Amia calva* and *Polypterus bichir*. A, C, E, and G show *Amia calva* specimens, B, D, F, and H show *Polypterus bichir.* A and B show ventral views of intact specimens illustrating the anatomy and placement of the gular plate(s). C and D show the branchial basket bones only, from a ventral view. E and F show intact skeletonized skulls from a lateral view. G and H show the suspensory apparatus only, also from a lateral view. C is modified from Grande and Bemis, 1998. E and G are modified from Allis, 1897 and D, F, and H are modified from Allis, 1922.

JAW DEPRESSION MECHANISMS IN NON-TELEOST ACTINOPTERYGIAN FISHES

There are two principal mechanisms by which actinopterygians depress the jaw: using hyoid-driven and opercular driven linkages. The existence of each linkage has been clearly demonstrated, although which components actuate the motion and the best models to predict jaw depression are still being explored (Camp and Brainerd, 2015; Whitlow et al., 2022). Here I lay out the basics of each linkage, then explore remaining questions in the ventral system in greater detail. In the hyoid-driven system, the hyoid is retracted, putting the mandibulohyoid ligament into tension and depressing the lower jaw (Lauder, 1980). In the opercular linkage, relative motion of the suspensorium (and therefore, the quadratomandibular joint) and the operculum either moves the suspensorium forward (Camp and Brainerd, 2015) or puts the interoperculomandibular ligament into tension (Liem, 1970) and depresses the lower jaw. In most actinopterygians both mechanisms are important, however some of the taxa considered in this thesis lack the interoperculomandibular ligament, and therefore are thought not to utilize opercular rotations in enacting jaw depression.

In this thesis I focus primarily on the ventral mechanism, which involves the hyoid arch and mandibulohyoid ligament, as the specific drivers of this system appear to vary across taxa (Lomax et al., 2020). We know that the axial muscles are active, inserting on the pectoral girdle to either stabilize or retract it. Simultaneously, the sternohyoideus muscle (which originates on the cleithrum of the pectoral girdle and inserts on the hypohyal, or the anterior hyoid) is active, retracting the hyoid. However, the pectoral girdle may or may not be mobile (Lauder, 1980), so the sternohyoideus may shorten, lengthen, or stay the same length while activating. Under the first scenario, the pectoral girdle serves as a steady anchor point for the sternohyoideus to pull

against, so that contraction of the sternohyoideus retracts the hyoid by itself (Lauder, 1980). Under the second scenario, the pectoral girdle is mobile, being pulled posteriorly by the hypaxial muscles, and the sternohyoideus is active to maintain its length against axial muscle forces (either maintaining length or lengthening), transferring force from the motion of the pectoral girdle to retract the hyoid (Camp and Brainerd, 2014; Camp et al., 2015; Van Wassenbergh et al., 2005). Under the third scenario the pectoral girdle is mobile and the sternohyoideus shortens, both the axial and sternohyoideus muscles contribute work to jaw opening (Camp et al., 2018; Lomax et al., 2020; Van Wassenbergh et al., 2007). Detailed kinematic evidence thus far has supported only the latter two mechanisms and suggests that the relative size of the sternohyoideus and hypaxial muscles may mediate which of these scenarios occurs in each species (Lomax et al., 2020). However, previous analyses suggest that a mobile pectoral girdle during feeding is unique to teleosts (Lauder, 1980), implying that *Amia* and *Polypterus* may not have a mobile pectoral girdle at all (scenario 1).

Further motivation for evaluation of jaw opening mechanisms in non-teleost actinopterygian fishes stems from work on the alligator gar (*Atractosteus spatula*) Lemberg et al 2019. Alligator gar are holostean fishes that perform a lateral snap to bite their prey, but these fish are also capable of generating suction through a surprising degree of mobility in the cranium (Lemberg et al., 2019). Lemberg demonstrated that the pectoral girdle retracts during strikes by alligator gar (Lemberg et al., 2019), and therefore jaw depression is powered at least in part by axial muscles. Chapters 2 and 3 of this thesis extend the work of Camp, Lemberg, Lomax, and others to analyze the role of the sternohyoideus muscle and quantify the mobility of the pectoral girdle in *Polypterus* and *Amia.*

Amia calva and teleost fishes share an independently evolved but functionally similar additional jaw opening mechanism through the opercular apparatus. While the connections between mobile elements of this system have been known for over 50 years (Liem, 1970), specifics of their function have only recently been re-evaluated in the largemouth bass, *Micropterus salmoides* (Camp and Brainerd, 2015). These fish possess an interoperculomandibular ligament, behind the quadratomandibular joint, which transfers forces through the interopercle to the lower jaw. Many 2D analyses have estimated the outputs from this system using a four-bar linkage model (Muller, 1989; Westneat, 2004), which we now know overestimates jaw depression due to the non-planar nature of the opercular motion (Camp and Brainerd, 2015). There is also an important role for neurocranial and suspensorial elevation in moving the jaw joint to effect jaw opening (Camp and Brainerd, 2015), though the interoperculomandibular ligament is necessary for normal mouth opening (Liem, 1970). However, these mechanisms have yet to be explored outside of teleosts.

USING XROMM TO SEE INSIDE THE FISH SKULL

The XROMM (X-ray Reconstruction of Moving Morphology) workflow (Brainerd et al., 2010) enables new insights into the detailed mechanisms driving suction feeding in fishes. Where researchers previously relied on combinations of light camera video or particle image velocimetry for examining live feeding fish, sometimes combining these observations with manual manipulations of post-mortem specimens, XROMM allows us to "look inside" the skull of a fish during the feeding strike. By using biplanar videoradiography of live specimens implanted with radio-opaque markers performing a behavior and integrating the marker positions

with CT data of the bone and marker meshes, we can animate the bones and measure their motion. This method also enables measurement of the length changes of muscles as well as the volume of the oral cavity during a strike.

WHAT DRIVES SUCCESSFUL SUCTION FEEDING?

Fishes can successfully generate suction in a variety of ways. Each mobile element in a fish's skull may be moved to develop sub-ambient pressure in the oral cavity by increasing the total oral cavity volume. This pressure difference is what determines the magnitude of force applied to a prey item and is therefore central to the question of what drives suction feeding. However, the extent to which a given bone contributes to increasing the volume of the oral cavity has not yet been explored, though we have numerous ways of modeling the volume of the oral cavity (Bishop et al., 2008; Camp et al., 2015; Muller et al., 1982; Van Wassenbergh and Aerts, 2009).

Importantly, not all species that suction feed show the same degree of mobility in each skeletal element. For example, bowfin (*Amia calva*) expand their skulls relatively evenly in all directions: laterally, dorsoventrally, and anteriorly, while slingjaw wrasses emphasize anterior expansion by throwing the oral jaws forward. In perhaps the most mobility-limited suction feeders, lungfishes, the highly fused skulls do not appear to allow for lateral expansion, meaning that suction forces are driven by the jaws, hyoid, and pectoral girdle (Gartner et al., 2022). One can imagine that each of these degrees of freedom (mediolateral, anteroposterior, dorsoventral) is important to successful suction feeding for a given species, and in this thesis I seek to understand how (and how much) each mobile element in the skull contributes to the generation of suction.

I use two methods for this investigation. First, I employ a novel bone motion freezing method created during this dissertation (Whitlow et al., 2022). This method leverages previous methods used to model the volume of a fish's oral cavity using XROMM data (Camp et al., 2015), extending the initial framework to allow for manipulation of the animation. Specifically, we apply an iterative motion freezing approach to understand how the volume change over a given time interval shifts when a given bone is not allowed to move relative to the neurocranium. The sums of these impacts are used to calculate the relative contribution to volume change (RCVC) for each bone, one method of understanding the role of a given bone in changing the oral cavity volume and generating suction (explored in detail in chapters 2 and 4). Second, I relate the velocity of a given bone's motion to the resulting acceleration of the prey item in *Polypterus* feeding strikes, providing further support to the conclusions from RCVC in chapter 2.

NOTES ON MODULATION AND NEURAL CONTROL OF STRIKES

Coordination and modulation of feeding and locomotor systems is critical in fishes for successfully securing food. For example, suction feeding demands a burst of axial muscle contraction timed with skull expansion, parrotfishes use their pectoral fins as paddles and brakes during their cyclic biting of algae on coral, gars use body muscles to execute a quick sideways snap at their prey, and many fishes use their body's momentum to ram feed. Coordination can be defined as the integration of movement across multiple functional components of an organism to achieve a specific task or goal (Ram and Ross, 2019; Rice and Westneat, 2005). Modulation can be defined as: "the ability of an organism to consistently alter its behavior pattern in response to differing stimuli" (Matott et al., 2005). The extensive literature on skull mechanics during

feeding in fishes provides a strong framework for exploration of the modulation and coordination of this system from evolutionary, ecological, biomechanical, and neurobiological perspectives.

Actinopterygian fishes are an ideal system in which to address questions about modulation and coordination for several reasons. First, they have extensive diversity in cranial linkage structure and mobility, and we have background knowledge of how these linkages work (Lauder, 1980; Westneat, 2004). Second, there are a number of lineages with diverse trophic strategies whose feeding and locomotion have each been scrutinized from both biomechanical and ecological perspectives (Wainwright et al., 2004; Westneat, 1990; Westneat and Walker, 1997), providing a basis for hypothesis-driven research into coordination of these systems. Finally, behavioral or kinematic modulation in the feeding system has been demonstrated in sharks (Ferry-Graham, 1998; Gardiner et al., 2017; Matott et al., 2005), teleosts (Kane and Higham, 2015; Van Wassenbergh and De Rechter, 2011; Wainwright and Lauder, 1986), reptiles (Montuelle et al., 2009; Montuelle et al., 2012a), and mammals (Iriarte-Díaz et al., 2011; Ross et al., 2007a; Vinyard et al., 2008). However, the most recent evaluation of holosteans (*Amia calva* and *Lepisosteus occulatus*) and bichirs (*Polypterus senegalus*) found no modulatory ability in these species (Lauder, 1980).

This suggests three broad scenarios: 1) the ability to modulate feeding behavior has evolved several times, and sharks and teleosts evolved modulatory abilities separately from tetrapods, 2) the ability to modulate feeding behavior is basal to gnathostomes but the holostean and bichir lineages lost this ability, or 3) the ability to modulate feeding behavior is basal to gnathostomes and persists in holosteans and bichirs but researchers have not yet found the right suite of feeding conditions to elicit a modulated response. We note that there are many, more

minor, variations possible within these broad scenarios, as the degree of modulation possible or realized can vary within lineages and is a relative measurement. While scenario 1 is feasible, recent evidence shows that gars can modulate their hyoid motion (separating depression from retraction via coordination with the hyoid constrictor muscles) in order to delay suction (Lemberg et al., 2019), falsifying the hypothesis that no holosteans can modulate suction feeding kinematics. Furthermore, while prey treatments were varied in Lauder's study (1980), recordings appear to have been taken consistently from the top of the tank, meaning prey placement was stereotyped, thereby allowing limited opportunities to modulate outside of prey type driven factors.

Modulation and coordination patterns are likely to co-evolve with species ecology and may even change within a given individual or species depending upon a number of conditions. Recent work by Kane and Higham (2015) has begun tackling an interesting multidimensional framework in which coordination operates, where cranial morphology and kinematics, locomotor specialization, and trophic strategy all interact to produce an "integration space". One idea they propose is that specialists (which eat a narrow subset of the available food items and/or employ a restricted locomotor repertoire) are likely to have a well-defined and constrained coordination pattern, while generalists may be able to better modulate how they coordinate their fins, body, and cranium during a feeding event. Therefore, we examined the ability to modulate in the generalist *Amia calva* (Mcallister et al., 2019) as this species readily feeds on live feeder fish, worms, and even dead pieces of fish or freeze-dried krill in the laboratory.

There is also debate in the literature about the neural drivers and underlying mechanisms of modulatory abilities in fishes. Specifically, researchers have questioned whether fishes that

modulate strike kinematics across prey types are simply selecting from a repertoire of pre-programmed strike patterns, or whether aspects of the strike may be altered once the strike is initiated in a form of "feed-back" integration to further modulate the strike (Aerts, 1990; Gidmark et al., 2012; Liem, 1978; Nemeth, 1997a; Van Wassenbergh and De Rechter, 2011; Vinyard, 1982). Pre-strike sensory information is certainly utilized in determining how a predator approaches and captures prey, demonstrated clearly by removing visual or lateral line sensory inputs (Gardiner and Motta, 2012). However, it is possible that these inputs are not the *only* determinant of strike kinematics. This question must also be examined in strikes where sensory feedback is received or altered mid strike, such as when a live prey item attempts an escape response. In such work, evidence of modulatory ability in response to a prey escape has been found in some studies (Aerts, 1990; Van Wassenbergh and De Rechter, 2011).

THESIS CHAPTER OVERVIEW AND SPECIFIC AIMS

This dissertation tests hypotheses about pectoral girdle mobility, mechanisms and modulation of intracranial kinesis, and drivers of successful suction feeding in fishes using XROMM. Chapters 2 and 3 investigate the detailed kinematics and biomechanics of two basal actinopterygian lineages, *Polypterus* and *Amia*. From an evolutionary perspective, these species are important as they represent some of the earliest-branching living lineages of ray-finned fishes. From a biomechanical perspective, these taxa may serve as models for unique morphologies and linkage systems.

With Chapter 2, I address three main questions in *Polypterus bichir*. First, I investigate the kinematics and relative timing of neurocranial elevation, cleithral retraction, suspensorial and opercular flaring, and jaw and hyoid depression. This is the first time that suspensorial or

pectoral girdle motions have been described in any polypterid, and the first explicit quantification of kinematics in *P. bichir* specifically. Second, I quantified the relative contributions to oral cavity expansion of the bones that drive suction feeding in *P. bichir* using a novel metric, the relative contribution to volume change (RCVC). Finally, I elucidate the role of the sternohyoideus muscle in the linkage between the hypaxial muscles and lower jaw by measuring its length change during the strike.

In Chapter 3 I examine *Amia calva* feeding mechanics and modulation. First, I ask: what are the kinematics and relative timing of neurocranial elevation, cleithral retraction, suspensorial and opercular flaring, and jaw and hyoid depression in *Amia calva*? These kinematics expand upon previous descriptions and I further explore how they compare with *P. bichir* to understand key differences in the relative mobility of these non-teleost actinopterygian fish. Second, I explore how the timings, magnitudes, and velocities of these kinematics vary in strikes on evasive vs. non-evasive prey by comparing strikes on feeder fish and worms. This work demonstrates a prey type effect and confirms that non-teleost actinopterygians can modulate their strike mechanics. I explore the broader neuromechanical implications of these results. Third, I elucidate the role of the sternohyoideus muscle in the linkage between the hypaxial muscles and lower jaw, using methods from Chapter 2. Finally, I explore the roles of the two joints between the lower jaw and the suspensorium in *Amia calva*, attempting to identify the true axis of rotation between these bones by exploring how they translate relative to one another at the quadrate and symplectic.

In Chapter 4 I use the data on *Polypterus* and *Amia* presented in Chapters 2 and 3, along with comparisons from two other fishes, to explore the relative roles of each bone in generating

suction. The four species analyzed are morphologically and evolutionarily distinct and provide a basis for understanding how diverse fishes drive volumetric expansion of the oral cavity. With these datasets I first explore how we can describe and quantify the contributions that each mobile skeletal element makes to the volumetric expansion of the skull. The primary goal here was to understand how each skeletal element contributes to the generation of suction and prey capture. Next, I ask whether species with distinct morphologies display unique patterns of RCVC contributions during feeding strikes, and explore the roles of bone size, shape, and mobility in the pattern of volume change throughout a strike. I then explore whether the primary contributor to peak volume expansion rate varies across species. The time at peak volume expansion rate is when the highest suction forces are generated, so with this question I explored which bones are likely responsible for generating the greatest suction forces through volumetric expansion of the skull. Finally, I explore how inclusion or exclusion of the cleithrum as the full posterior boundary of the oral cavity changes these findings. There is some debate as to the best method of accounting for soft tissue around the cleithrum in these endocasts, and we do not yet know with confidence how the esophageal opening (and the posterior boundary of the oral cavity) moves with the cranium or pectoral girdle during strikes.

In sum, this thesis develops our understanding of specific feeding mechanics in two non-teleost actinopterygians and quantifies the drivers of volume expansion across four aquatic feeders. In chapters 2, 3, and 4 I lay out the motivations, methods, findings, and implications for the specific questions and aims of this dissertation. In chapter 5 I explore the evolutionary and biomechanical implications of these findings and outline promising avenues for future work.

CHAPTER 2: CERATOHYAL MOTION DRIVES MANDIBULAR DEPRESSION AND ORAL CAVITY VOLUME CHANGE IN *POLYPTERUS BICHIR* SUCTION FEEDING[1]

ABSTRACT

Many fishes use substantial cranial kinesis to rapidly increase buccal cavity volume, pulling prey into the mouth via suction feeding. Living polypterids are a key lineage for understanding the evolution and biomechanics of suction feeding due to their phylogenetic position and unique morphology. *Polypterus bichir* have fewer mobile cranial elements compared to teleosts (e.g., immobile [pre]maxillae) but successfully generate suction through dorsal, ventral, and lateral oral cavity expansion. However, the relative contributions of these motions to suction feeding success have not been quantified. Additionally, extensive body musculature and lack of opercular jaw opening linkages make *P. bichir* of interest for examining the role of cranial vs. axial muscles in driving mandibular depression. Here we analyze the kinematics of buccal expansion during suction feeding in *P. bichir* using X-Ray Reconstruction of Moving Morphology (XROMM) and quantify the contributions of skeletal elements to oral cavity volume expansion and prey capture. Mouth gape peaks early in the strike, followed by maximum cleithral and ceratohyal rotations, and finally by opercular and suspensorial abductions, maintaining the anterior-to-posterior movement of water. Using a new method of quantifying bones' relative contributions to volume change (RCVC) we demonstrate that ceratohyal kinematics are the most significant drivers of oral cavity volume change. All measured cranial

[1] This chapter was originally published as: Whitlow *et al.* 2022. Ceratohyal motion drives mandibular depression and oral cavity volume change in *Polypterus bichir* suction feeding. Journal of Experimental Biology (2022) 225, jeb243283.

bone motions, except abduction of the suspensorium, are correlated with prey motion. Lastly, cleithral retraction is largely concurrent with ceratohyal retraction and jaw depression while the sternohyoideus maintains constant length, suggesting a central role of the axial muscles, cleithrum, and ceratohyal in ventral expansion.

INTRODUCTION

Suction feeding - rapid oral cavity expansion that draws prey into the mouth - is considered to be the ancestral feeding mode for osteichthyan fishes (Jacobs and Holzman, 2018; Lauder, 1985). Most prior research on suction feeding mechanics has focused on derived teleosts with highly mobile skulls and numerous mechanisms for cranial expansion and successful suction feeding. For instance, teleosts share two mechanisms for jaw depression, one driven by pectoral girdle and hyoid mobility (a mechanism common to actinopterygian fishes) and one driven by opercular mobility (thought to exist only in teleosts and *Amia*) (Camp and Brainerd, 2015; Lauder, 1980). Furthermore, many studies highlight protrusible jaws, which bring the oral jaws closer to the prey, focus suction forces more directly at the prey, and increase the rate and magnitude of forces imparted to the water bolus by increasing volumetric expansion of the buccal cavity (Alexander, 1967; Kane and Higham, 2014; Lauder, 1982; Liem, 1980; Westneat and Wainwright, 1989). However, not all cranial skeletal elements show the same degree of mobility in all suction feeding species, and the relative importance of each bone's kinematics for generating suction forces is unknown. Here we examine suction feeding in polypterid fishes, the most rootward living actinopterygian fish, which are thought to have a relatively simplified feeding system with no (pre)maxillary protrusion and a single mechanism of jaw depression

(Lauder, 1980). Despite this reduced cranial mobility, *Polypterus bichir* are successful suction feeders, exhibiting the classic anterior-to-posterior wave of skull expansion. In *P. bichir,* lateral skull expansion and hyoid depression occur and are likely important for successful suction feeding (Lauder, 1980), but we do not fully understand their contributions to the volumetric expansion of the buccal cavity, their impact on prey motion, or their role in successful prey capture.

Suction feeding is powered in part or whole by the axial muscles, with variable contributions from smaller cranial muscles, which in some cases serve to redirect forces rather than generate power directly (Camp and Brainerd, 2014). This paper focuses on the ventral linkages and drivers of jaw opening in *P. bichir*, as mechanisms of cranial elevation—driven by epaxial muscles—have been elucidated previously (Lauder, 1980). In most bony fishes, as in polypterids, the hypaxial and sternohyoideus muscles are both active during suction feeding, driving ceratohyal motion and ultimately contributing to jaw depression (Tchernavin, 1948). Hypaxial muscles insert on the cleithra, while the sternohyoideus runs between the cleithra and the anterior ceratohyals. Both muscles are active at the start of a feeding strike in *Polypterus* (Lauder, 1980) and there are three major ways that these muscles may work in concert or opposition to drive ventral expansion. First, the hypaxials may isometrically or eccentrically stabilize the cleithrum, while the sternohyoideus pulls against this "anchor" to retract and depress the ceratohyal, as proposed for bichirs, bowfin, and gar (Lauder, 1980). Second, the hypaxials may retract the cleithrum, while the sternohyoideus is isometrically active or lengthening, its activity serving to transfer force generated by the hypaxials, as demonstrated in largemouth bass and several clariid catfishes (Camp and Brainerd, 2014; Camp et al., 2015; Van Wassenbergh et

al., 2005; Van Wassenbergh et al., 2007). Third, the two muscles may work in concert, both shortening to retract the cleithrum and the ceratohyal, as seen in one clariid catfish, bluegill sunfish, and striped surfperch (Camp et al., 2018; Lomax et al., 2020; Van Wassenbergh et al., 2007). The relative sizes of the sternohyoideus and hypaxial muscles are thought to determine which of these mechanisms is utilized for a given species (Lomax et al., 2020), suggesting that *P. bichir's* extensive hypaxial muscles may drive hyoid motion indirectly through a ligament-like function of the sternohyoideus.

A deeper understanding of the mechanics of jaw opening, oral cavity volume change, and suction feeding forces in *P. bichir* and other actinopterygians requires the ability to precisely quantify motions of internal skull structures such as the hyoid arch and its connections to the cleithrum and mandible. Here, we use the X-ray Reconstruction of Moving Morphology (XROMM) workflow (Brainerd et al., 2010) and dynamic endocast modeling (Camp et al., 2015) to quantify cranial kinesis and measure volumetric expansion of the oral cavity in *P. bichir* during feeding. We test the relationships between these motions and suction feeding forces and explore the role of the sternohyoideus and ventral hyoid arch in jaw opening in this species with three sets of analyses.

We first quantify the kinematics and relative timing of neurocranial elevation, cleithral retraction, suspensorial and opercular flaring, and jaw and hyoid depression in *P. bichir*. We hypothesized that jaw depression and neurocranial elevation precede ceratohyal depression, followed by abduction of the suspensorium and operculum, as this would maintain the anterior to posterior wave of cranial expansion thought to be common to all aquatic suction feeders.

Second, we investigated the kinematic drivers of successful suction feeding in *P. bichir* using two metrics: first by measuring motion (acceleration) of marked prey items throughout the strike and cross-correlating this motion with bone velocity; and second by employing a novel bone freezing method to measure the instantaneous contribution of each bone's motion to buccal cavity volume change. Importantly, the neurocranium was used as a frame of reference to make these measurements and therefore contributions of the neurocranium to suction generation were not measured in this study. We hypothesized that ceratohyal and jaw depression are the most important factors in successful suction generation due to their substantial and rapid motion, while lateral flaring of suspensorium and operculum influence suction generation to lesser degrees.

Finally, we evaluate the role of the sternohyoideus muscle in the linkage between the hypaxial muscles and lower jaw by measuring sternohyoideus length and translations at key points in this linkage. We hypothesized that, as in bass, the cleithrum moves posteriorly during the strike in *P. bichir*, and the sternohyoideus functions isometrically to transmit that force into displacement of the ceratohyal, which in turn transmits force to the mandible through the mandibulohyoid ligament (MHL).

METHODS

Animals and care: Three live specimens (standard lengths 23.5, 23.0, and 25.0cm) of the Nile Bichir (*Polypterus bichir lapradei* Lacepède 1803) were obtained from the aquarium industry and housed singly at the University of Chicago. Fish were fed worms or live feeder fish three times weekly. Individual fish responded best to different custom tank designs, so certain individuals were transferred to an 11.4 cm wide tank on the day of or the night before data

collection but were otherwise housed in 20+ gallon aquariums. Other individuals were housed for the duration of their data collection in a "tunnel tank", which consisted of a 24 cm by 33 cm rectangular area with a tunnel extension of 47 cm by 3.75 cm. All husbandry and experimental protocols were approved by the University of Chicago IACUC (protocol #72365).

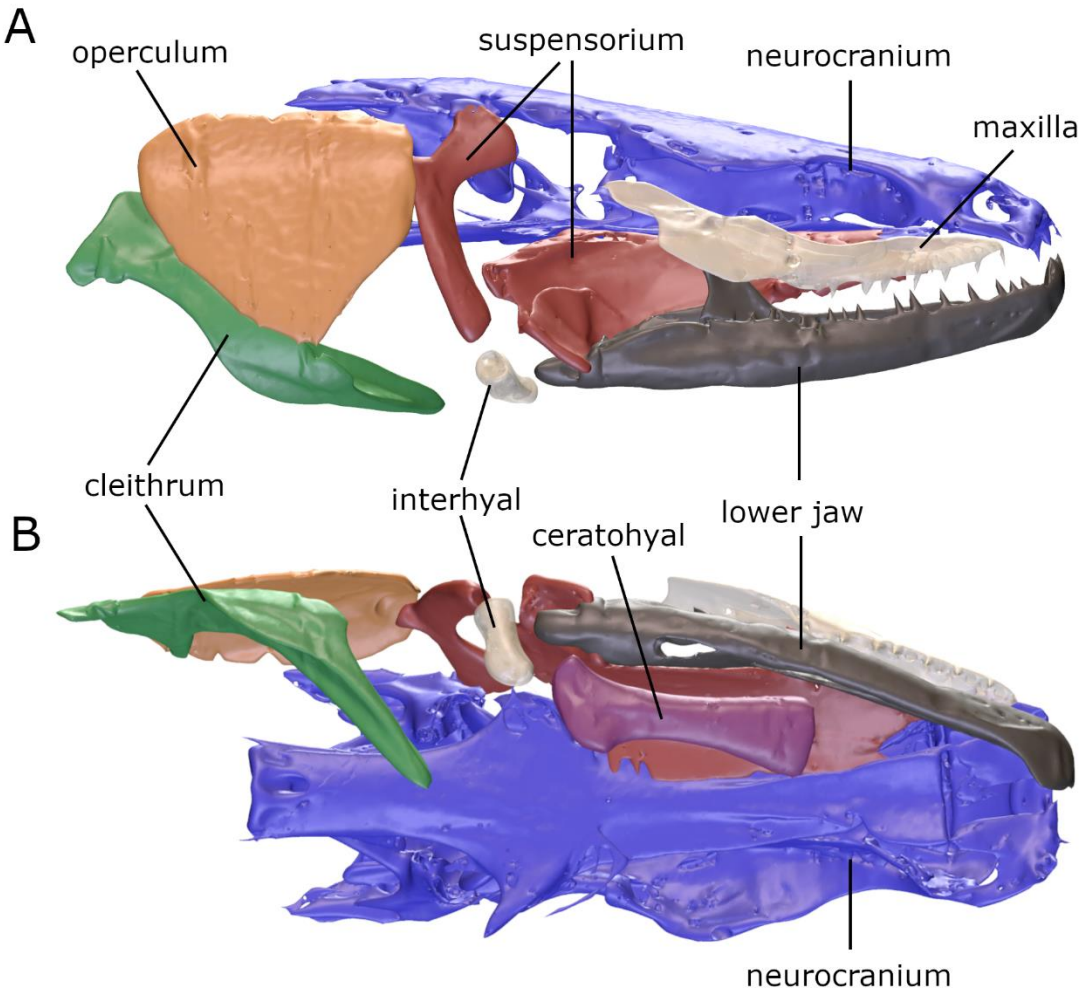

Fig. 2.1. Cranial skeletal anatomy of *P. bichir*. Rigid bodies measured and linkage-central bones in the skull and cleithrum from two views: (A) lateral and (B) ventral. Colored bones are rigid bodies animated in this study, while pale bones (interhyal and maxilla) are shown for context but were not animated.

Surgical marker implantation: Fish were anesthetized with 0.07- 0.3 g L^{-1} MS-222 (added progressively, buffered 2x by weight with sodium bicarbonate) and implanted with 3-6 radio-opaque tantalum beads (1 mm or 0.8 mm) in each bone or structure of interest: neurocranium, mandible, ceratohyal, suspensorium, operculum, cleithrum, and body (Fig. 2.1; Fig. 2.S1). The suspensorium (palatoquadrate + hyomandibula) was treated as a single rigid body due to firm connections between the bones (Allis, 1922) and we confirmed a lack of flexion between the two bones using pairwise inter-marker distance comparisons from 10 animated trials (within palatoquadrate = 0.1 ± 0.007 mm, within hyomandibula = 0.074 ± 0.005 mm, between bones = 0.11 ± 0.003 mm). Body markers were implanted bilaterally approximately 6-10 cm behind the cleithrum along the most lateral points of the fish's body, with two markers just dorsal to a frontal plane through the vertebral centra and one just ventral on each side. Body plane markers were used to animate a reference plane from which to measure neurocranial elevation and cleithral retraction (*sensu* Camp and Brainerd, 2014). Bone markers were implanted unilaterally (right side) by hand drilling and press-fitting markers into a hole of the same diameter as the marker. Soft tissue markers were injected using a hypodermic needle of a diameter slightly larger than the marker (16 gauge), and body plane markers were placed by separating two rows of scales and puncturing the skin between them using a #11-blade scalpel.

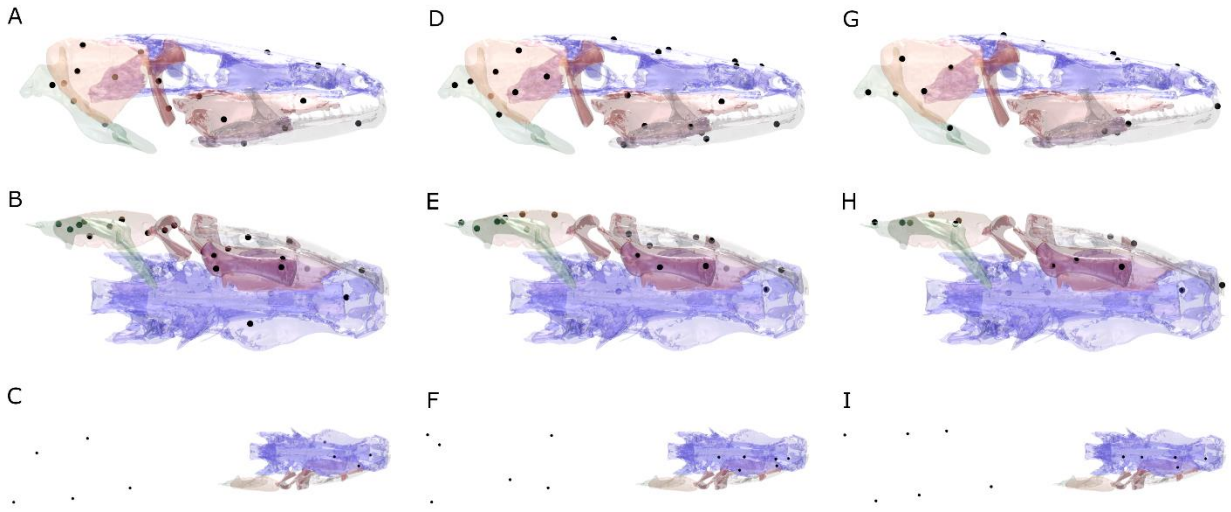

Fig. 2.S1. Marker implant sites for all individuals, superimposed on P3 CT scan. A-C) P1 A) Lateral B) Ventral and C) Dorsal view. D-F) P2 D) Lateral E) Ventral and F) Dorsal view. G-I) P1 G) Lateral H) Ventral and I) Dorsal view. In C, F, I) all markers except Neurocranial and Body Plane are hidden for clarity.

CT scanning: A microCT (taken post-mortem; GE Phoenix v|tome|x 240 kV/180 kV scanner, University of Chicago Paleo-CT facility) or CT scan (taken under MS-222 sedation; Vimago L Base version, EpicaScanner) of each animal was used to create 3D polygonal meshes of each bone in Amira 5.5.0 (FEI Company, Hillsboro OR), allowing precise measurement of bead placements within the bones.

XROMM data collection and animation: P. bichir were filmed feeding in custom-built tanks (described under "animal care", designed to minimize the attenuation of x-rays through large quantities of water in the capture volume) using two pairs of roughly orthogonal X-ray sources and image intensifiers. 16 of 18 strikes used in this study were collected at the University of Chicago XROMM facility, using high-speed video cameras (Xcitex XC-2M) controlled by ProCapture motion capture software. Two additional strikes by one individual from this study

were recorded at the Keck XROMM Facility at Brown University using Phantom v.10 high-speed cameras (Vision Research, Wayne, NJ, USA). All data were collected at 500 Hz using a shutter speed of 1/1000 s; the two strikes recorded at Brown did not show any kinematic differences from the 16 strikes obtained at University of Chicago.

To ensure that the feeding event occurred within the XROMM capture volume, fish were trained to strike at a minnow (*Pimephales promelas*, ~3 – 4 cm) when it was released from behind a trapdoor. Eighteen usable trials were obtained (7, 7, and 4 from each fish), two of which were failed strikes (the feeder fish was not captured). Failed strikes did not differ kinematically from successful ones, so the 18 trials were pooled together for kinematic descriptions and volumetric simulations. The two failed strikes were removed from analyses that involved prey acceleration as those prey accelerations could have been induced by the predator, by an escape response, or some other hydrodynamic effect that we could not account for. A subset of trials with a slightly higher degree of noise in rigid body transformations was removed from the volumetric analysis due to a disproportionate effect of noise on the relative contribution calculations (see "Volumetric analysis" section). This resulted in a reduced sample size of 13 strikes (7 and 6 from two fish) for the volumetric analysis.

XMALab (version 1.5.5; Knorlein et al., 2016) was used to remove image distortion, compute 3D camera positions, and track tantalum markers in each sequence. The XYZ coordinates of each marker were triangulated and used to calculate the rigid body transformation of each bone, which were exported from XMALab unfiltered. Data with obvious high-frequency noise (from the operculum and suspensorium) were later filtered using a low-pass Butterworth

filter at a cutoff frequency of 50 Hz in R (version 3.5.3). Mean precision for co-osseous inter-marker distances from *in vivo* data was 0.109 mm (Table 2.S1) (Brainerd et al., 2010).

Table 2.S1. Precision information from *in vivo* co-osseous pairs of intermarker distances.

P1 Collected at UC	Standard deviations of pairwise intermarker distances within each rigid body			
	Min	Max	Mean	SEM
Body Plane	0.16	2.734	0.76	0.086
Ceratohyal	0.075	0.236	0.13	0.008
Cleithrum	0.071	0.115	0.088	0.003
Lower Jaw	0.086	0.125	0.099	0.003
Neurocranium	0.078	0.119	0.094	0.002
Operculum	0.069	0.123	0.096	0.002
Suspensorium	0.07	0.149	0.112	0.003

P1 Collected at Brown	Standard deviations of pairwise intermarker distances within each rigid body			
	Min	Max	Mean	SEM
Body Plane	0.07	0.848	0.251	0.046
Ceratohyal	0.04	0.104	0.062	0.006
Cleithrum	0.04	0.049	0.044	0.002
Lower Jaw	0.051	0.068	0.058	0.003
Neurocranium	0.042	0.131	0.069	0.006
Operculum	0.038	0.041	0.039	0.002
Suspensorium	0.04	0.106	0.068	0.007

P2	Standard deviations of pairwise intermarker distances within each rigid body			
	Min	Max	Mean	SEM
Body Plane	0.145	2.184	0.604	0.063
Ceratohyal	0.090	0.174	0.125	0.007
Cleithrum	0.086	0.188	0.121	0.005
Lower Jaw	0.107	0.209	0.155	0.010
Neurocranium	0.092	0.194	0.123	0.003
Operculum	0.086	0.131	0.112	0.003
Suspensorium	0.093	0.171	0.122	0.013

Table 2.S1. Continued

P3	Standard deviations of pairwise intermarker distances within each rigid body			
	Min	Max	Mean	SEM
Body Plane	0.118	2.061	0.5	0.036
Ceratohyal	0.086	0.125	0.102	0.002
Cleithrum	0.08	0.114	0.094	0.002
Lower Jaw	0.086	0.134	0.107	0.003
Neurocranium	0.079	0.271	0.144	0.007
Operculum	0.074	0.123	0.095	0.003

Animations of these bone meshes were generated and motion was quantified using Maya 2018 (Autodesk, Inc., San Rafael, California) and the XROMM Maya Tools shelf version 2.2.3 (https://bitbucket.org/xromm/xromm_mayatools/src/master/). Bone mesh animations were checked against MayaCams to verify proper alignment and calibration (see Fig. 2.2). We used a combination of anatomical coordinate systems (ACSs) and joint coordinate systems (JCSs) to describe various components of motion in the *P. bichir* skull during feeding strikes. An ACS refers to a 3-axis coordinate system digitally fixed to a bone, which is used to measure the translation of any object relative to that bone (Brainerd et al., 2010). Relative motion (both translation and rotation) between two bones is described using a JCS (Grood and Suntay, 1983), which in Maya consists of two ACSs – one parented to each bone of interest (Brainerd et al., 2010; Gidmark et al., 2015). Importantly, JCS rotational axes do not stay orthogonal: the Z axis is fixed to the proximal bone and the X axis is fixed to the distal bone, while the Y axis is calculated as close as possible to the normal of the other two axes (Brainerd et al., 2010). We used a global ACS to measure the motion of the prey item through world-space and calculate the Euclidean distance of prey motion. We took the first and second derivatives of this Euclidean distance to calculate the velocity and acceleration of the prey item, respectively. All values

reported are peak magnitudes and timings averaged by trial (± standard error), while figures show values averaged by time (trials aligned to 0 ms at peak gape prior to averaging).

Kinematic analyses: In order to quantify the overall kinematic pattern of *P. bichir* strikes, we used JCSs oriented along anatomical directions (AP = anteroposterior, DV = dorsoventral, ML = mediolateral), thereby describing the rotations of bones in a manner comparable to that used to report data collected from lateral light camera video recordings (i.e., Grubich, 2001; Lauder, 1980; Lemberg et al., 2019; Markey et al., 2006; Sanford, 2001; Westneat and Wainwright, 1989). Each JCS was oriented such that the highest degree of motion is captured by the Z-axis to minimize non-linear distortions introduced by measuring with Tate-Bryan angles in Euler space (Manafzadeh and Gatesy, 2020). Specifically, the Z-axes for neurocranial elevation, lower jaw depression, cleithral retraction, and ceratohyal depression were all oriented mediolaterally, in order to capture rotations in sagittal planes, while the Z-axes for suspensorial and opercular abduction were oriented anteroposteriorly, in order to capture rotations in transverse planes. Fig. 2.3 shows the placement of each JCS when the fish is in resting pose (solid colored bones). The neurocranium and cleithrum were measured relative to a body plane averaged across five or more body markers (after Camp and Brainerd, 2014), and the cleithrum, operculum, suspensorium, lower jaw, and ceratohyal were measured relative to the neurocranium (note that cleithral rotations were quantified in two coordinate systems to detangle the impact of neurocranial rotation and vertebral column bending from this measurement). Z-axis rotations for this overall kinematic description dataset were standardized to a starting point of 0° by subtracting the mean of the first 25 frames recorded before the strike, during a period with relatively little intracranial movement.

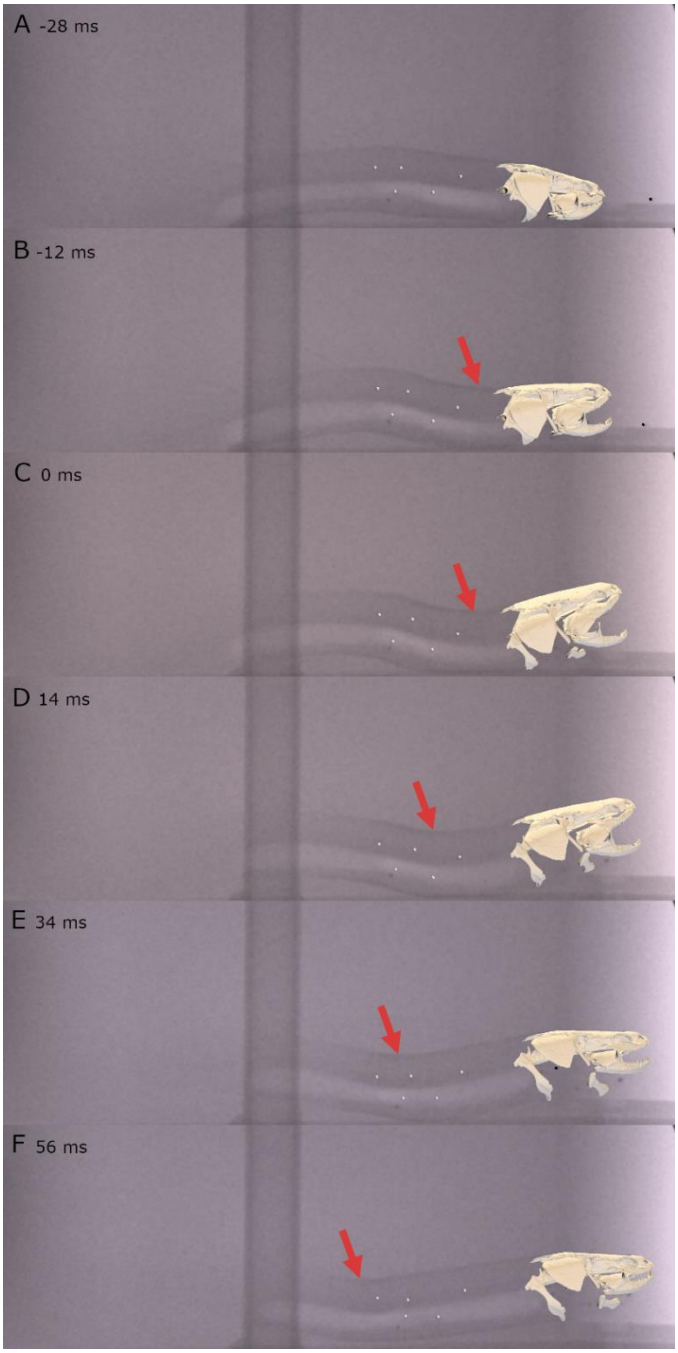

Fig. 2.2. Still frame sequence of X-Ray video and corresponding XROMM animation. Skull and body postures in 6 frames: (A) just prior to motion onset (-28 ms), (B) halfway between motion onset and maximum gape (-12 ms), (C) maximum gape (0 ms), (D) early in compressive phase (14 ms), (E) midway through compressive phase (34 ms), (F) mouth closed (56 ms). The black sphere visible in (A) (B) and (E) overlays a 1 mm marker implanted in the feeder fish. White spheres overlay markers used to animate body plane. Red arrows highlight a posteriorly traveling wave of vertebral bending.

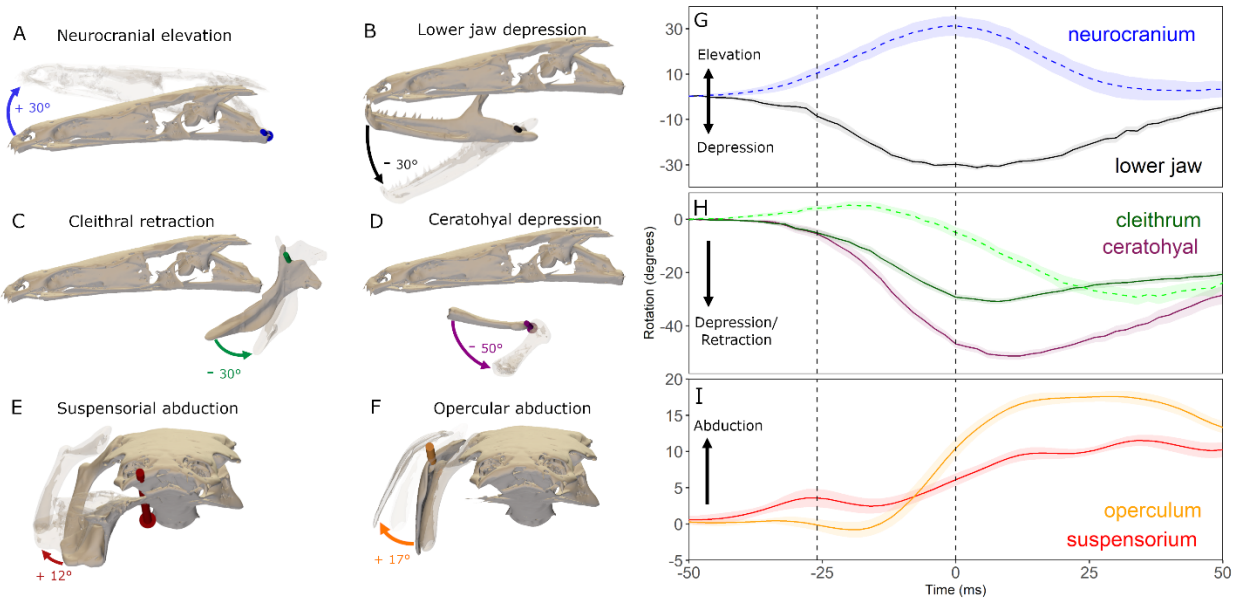

Fig. 2.3. Mean rotations of largest magnitude axes for anatomically-oriented JCSs. (A-F) Z-axes for each anatomically-oriented JCS used to measure the primary motion captured for each bone in lateral single-camera studies. Colors correspond to kinematic traces shown in G-I, and the value listed is the highest mean rotation. (A) Neurocranial elevation, medial view. (B) Lower jaw depression, medial. (C) Cleithral retraction (rotation about a mediolateral axis), medial. (D) Ceratohyal depression, medial. (E) Suspensorial abduction (rotation about an anteroposterior axis), anterior. (F) Opercular abduction (rotation about an anteroposterior axis), anterior. (G-I) Shows mean ± SEM of z-axis rotations (largest axis of expected rotation) of bones from all tracked strikes across three individuals (11 trials for suspensorium, 16 trials for operculum, 18 for all other variables). All rotations were zeroed to average resting position by subtracting average motion during the first 25 frames recorded. Rotations for G and H are unfiltered, rotations in panel I (suspensorial and opercular motion) were smoothed using a 50 Hz low-pass Butterworth filter. Vertical lines denote onset of prey motion (-26 ms) and peak gape (0 ms). Dashed lines (neurocranium and cleithrum) were measured relative to a body plane and solid lines were measured relative to the neurocranium.

Initial observations and associations with volume and suction (described below) revealed substantial rotations of the ceratohyal around all three axes, so ceratohyal kinematics were further analyzed using a JCS placed in a "joint-oriented" position: with the X-axis aligned with the long axis of the bone, allowing direct measurement of ceratohyal long-axis rotation. This JCS is shown in Fig. 2.4A-B and was used to quantify the rotations and translations about each axis

of the ceratohyal relative to the neurocranium. For this dataset, we show the untransformed (i.e., not "zeroed") axes of rotation and translation, as these axes represent a full six degrees-of-freedom joint pose as rotations from an arbitrary resting position. Additionally, we visualized these motions using an instantaneous helical axis (Berme et al., 1990; Iriarte-Diaz et al., 2017), which completely describes bone motion as rotation about and translation along a single axis, using published MATLAB code (available at https://github.com/jdlaurence/XROMM_HelicalAxis). We selected the time point of peak ceratohyal velocity, or the time point at which the ceratohyal is rotating most rapidly (-14 ms before peak gape, Table 2.1), as a representative point for visualizing this axis of rotation during ceratohyal depression.

Table 2.1. Mean peak magnitude and time to peak for bone locator velocity and maximum cross-correlation and lag times between each bone velocity and prey acceleration (trace data shown in Fig. 2.6).

Bone Locator	Number of trials	Peak velocity (mm s^{-1})	Time to peak velocity (ms)	Max. cross-correlation (R)	Lag at max cross-corr (ms)
Ceratohyal anterior	(n=16)	1560 ± 80.8	-14.3 ± 1.24	0.302	6
Ceratohyal posterior	(n = 16)	709 ± 42.7	-14.8 ± 1.80	0.26	8
Lower Jaw	(n = 16)	1918 ± 92.1	-16.9 ± 1.44	0.303	2
Operculum	(n = 14)	568 ± 40.1	-1.3 ± 3.83	0.219	20
Suspensorium	(n = 9)	414 ± 45.0	0.4 ± 6.14	0.101	34

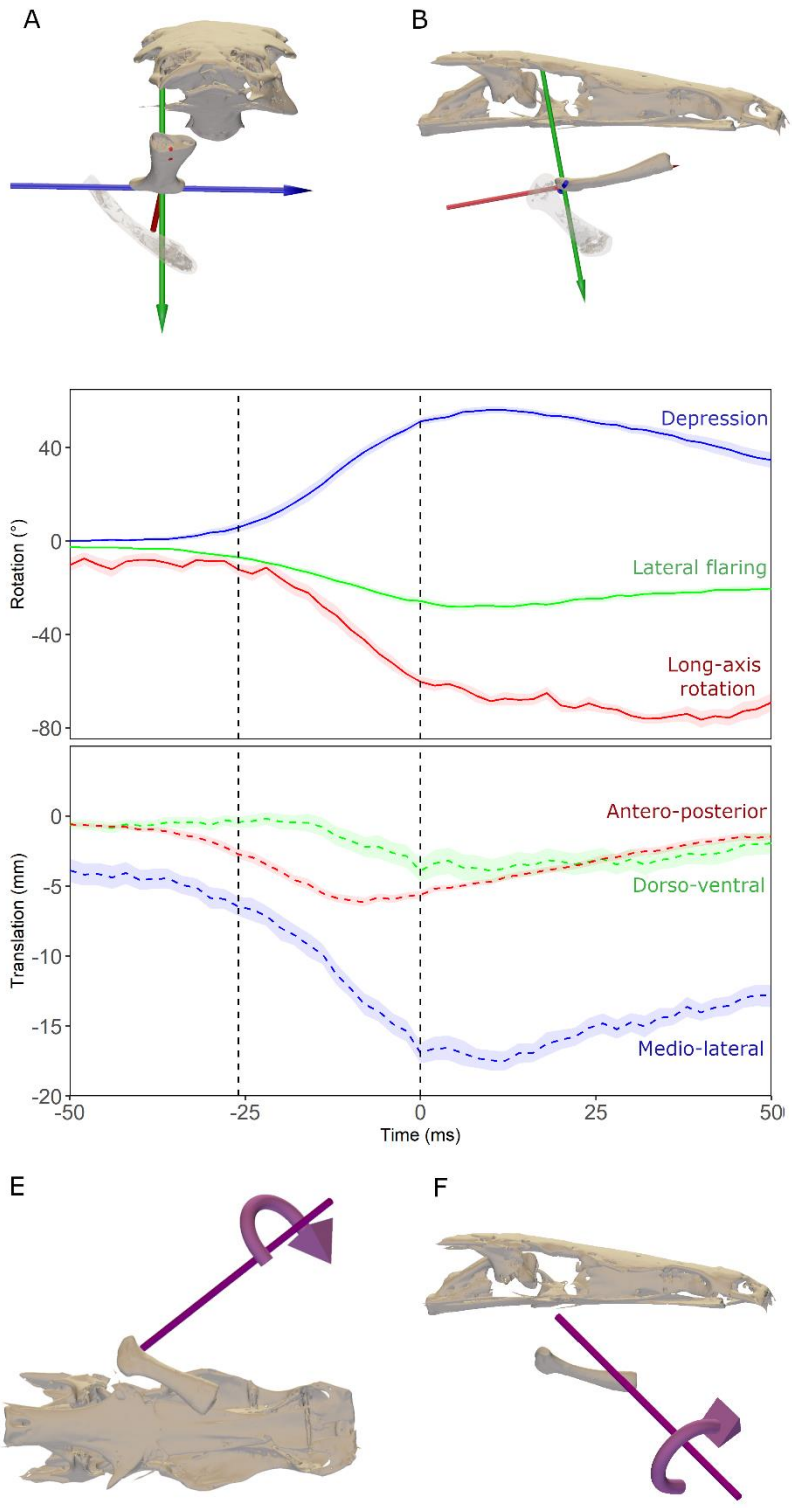

Fig. 2.4. Mean 3D kinematics of the ceratohyal relative to the neurocranium measured using a joint-oriented JCS. Panels (A) anterior and (B) lateral view show the position of the neurocranium, hyomandibula, and distal JCS at mouth closed or resting position (solid bones) and at maximum gape (transparent bones). This JCS was positioned to enable measurement of long-axis rotation of the ceratohyal. Note that the interhyal (between hyomandibula and ceratohyal, Fig. 2.1) is not shown here as it was not animated in this study. (C) and (D) show means ± SEM of 18 trials across three individuals, with rotations about each axis in panel (C) (solid lines) and translations along each axis in panel (D) (dashed lines). Vertical lines denote the onset of prey motion (-26 ms) and peak gape (0 ms). (E) and (F) show the instantaneous helical axis of the ceratohyal from a representative trial at -14 ms before peak gape, or peak ceratohyal velocity (as calculated in Fig. 2.6) in (E) ventral and (F) lateral view. The helical axis follows a right-hand rule designation, indicating that the ceratohyal is being depressed at this time, with the direction of rotation about the cylindrical axis shown (also see Video 2.2).

Testing correlates of prey acceleration: To estimate the contributions of each axis of cranial kinesis to prey motion, we used an ACS system paired to the neurocranium to quantify relative motions of the points on the lower jaw, ceratohyal, operculum, and suspensorium that experienced the greatest displacements. In addition, for the ceratohyal, we selected both anterior and posterior points, as this bone undergoes substantially different motions at each end. We calculated the velocity (derivative of the Euclidean distance traveled) for each of these points relative to the neurocranium. We then used cross-correlation analyses to determine the temporal relationships between velocity of motion at each key point and prey acceleration, a proxy for suction force. We compare the velocity of bones and acceleration of prey because the acceleration of water around a prey item is thought to determine the force applied to that prey, and is driven by the rate of cranial expansion (Holzman et al., 2008; Wainwright and Day, 2007). Analyses of bone velocity to prey velocity provided similar results and are therefore not included in the present study. Cross-correlations calculate the linear correlation between two time series across a set of lags, where, for each lag, one signal is shifted in time relative to the other. We calculated maximum (positive) cross-correlations from 50 ms before and after peak gape (100 ms total) using a modified version of the R function ccfDis (matools package, https://aaronolsen.github.io/software/matools.html), which adds "NA" buffers corresponding to the lag time between each concatenated time series to prevent overlap of signals from different trials when time series are shifted. We tested significance for each motion pair after Olsen et al. (2019), where we randomly inverted one signal for each trial generating a null distribution of 999 unique iterations for all bones except the suspensorium (this bone was properly animated in a lower number of trials and thus could only have 256 unique randomized iterations). Due to the

concatenation of time series from all trials required for this statistical test, we do not present ± standard error of R values for this cross-correlation dataset.

Volumetric analysis: We expanded our testing of the contributions of the operculum, suspensorium, ceratohyal, and jaw to suction generation using volumetric analysis and virtual iterative bone freezing experiments. The instantaneous volume of the oral cavity was measured by creating a dynamic digital endocast of the right side of the head, and reported volume measurements are doubled to reflect total mouth volume (*sensu* Camp et al., 2015). In Maya, locators were attached to the oral surfaces of the animated cranial bones, and their locations over time were calculated. The locator positions were then imported into MATLAB (R2020a), where, for every frame, an alpha shape was calculated from the constellation of locators, and its volume was computed using code adapted from (Camp et al., 2015) (Fig. 2.S2A-B). Adapted code may be accessed at: https://github.com/jdlaurence/dynamicEndocastByBone.

In order to measure the instantaneous contributions of the lower jaw, ceratohyal, suspensorium, and operculum to the overall change in oral cavity volume, we developed a new method of digitally freezing bones to the neurocranium. We chose not to measure the RCVC of the cleithrum, as there is not clear evidence that cleithral retraction will directly change the shape of the posterior oral cavity. Traditionally, freezing a degree of freedom in a biomechanical system to assess its impact on a motion involves holding that degree of freedom frozen for the duration of the motion (Bernstein, 1967; Olsen, 2019a; Vereijken et al., 1992). However, given the extreme range of motion in bones like the ceratohyal and lower jaw and potential for inter-bone interaction effects at different points in a strike, we progressively froze the given bone relative to the neurocranium for short time increments (5 frames, 10 ms), on a rolling basis over

the duration of a trial. This allows an instantaneous quantification of the effect of a given bone's motion on volume change throughout the strike, rather than averaged across total strike duration. We selected five frames as our preferred freezing interval as this was a short enough period to avoid creating any joint poses that could not easily be achieved by cadaveric manipulations or observed during *in vivo* data collection, which we confirmed by importing alpha hulls back into Maya for visualization (see Fig. 2.S2B-J). Additionally, we examined the Delta Volume Full traces (difference of total endocast volume between consecutive increments) with different increment values and noted that the peak at maximum expansion rate began to widen at increments above 10-15 ms, suggesting over-smoothing.

The individual skeletal element freezing was performed by the MATLAB function 'dynamicEndocastByBone', which calculates the transformation matrix describing the motion of the reference bone (neurocranium) from one time step, *t,* to the next, *t+1* (where *1* is one increment of five frames), and then applying that transformation matrix to the bone to be frozen. So, at every *t+1* frame, five alpha shapes were calculated: the alpha shape from baseline animation with all bones moving and four alpha shapes with a single bone (lower jaw, ceratohyal, suspensorium, or operculum) 'frozen' in its position relative to the neurocranium at frame *t.* Consequently, the difference in any frame *t+1* between the frozen volume and the baseline volume represents the impact of that frozen bone on the overall volume change at that time.

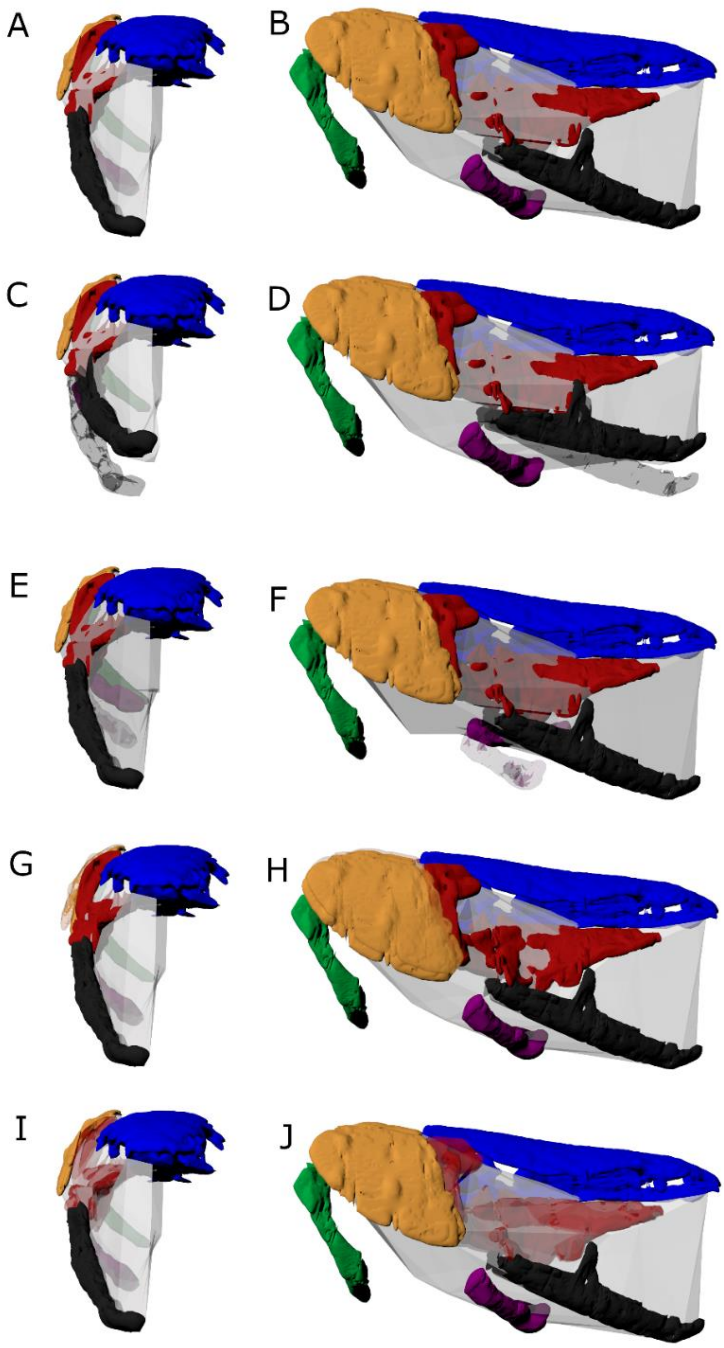

Fig. 2.S2. Oral cavity volume endocast alpha hulls at maximum gape, anterior and lateral views. A & B) Reference volume, all bones unfrozen. C-J) "Frozen" volumes, with solid bone at frozen position (held to neurocranium from 5 frames prior) and transparent bone at reference position for: jaw (C & D) ceratohyal (E & F) operculum (G & H), and suspensorium (I & J).

To quantify the relative contributions of each bone and normalize this to the change in volume at a given time point, we took the difference between the overall volume change and the frozen volume change for each bone and divided it by the sum of absolute volume changes for all frozen bones. Thus, the instantaneous relative contribution to volume change (RCVC) of the *i*th bone ($RCVC_{Bone_i}$) is represented by the following equation:

$$RCVC_{Bone_i} = \frac{\Delta V_{Full} - \Delta V_{FrozenBone_i}}{\sum_{j=1}^{n} \left| \Delta V_{Full} - \Delta V_{FrozenBone_j} \right|}$$

Where for a given time increment: ΔV_{Full} is the change in endocast volume without any bones frozen, $\Delta V_{FrozenBone_{i/j}}$ is the change in endocast volume with the *i*th or *j*th bone frozen, and n is the number of bones frozen (i.e., does not include the neurocranium). A bone's RCVC is a unitless ratio of its impact on endocast volume change to the sum of all bones' impacts on volume change at a given time point. We use the sum of impacts of all frozen bones in the denominator rather than the total volume change to avoid singularities and magnified noise effects associated with the small denominators that occur when the net volume change approached zero but individual bones were still moving. Thus, RCVC constitutes a stable measure of the impact of a given bone's motion on the volume change of the buccal cavity relative to the cumulative impact (in absolute terms) of all bones. Importantly, the absolute value signs in the denominator of the equation remove the directionality of volume change; only when all bones are contributing to expansion (RCVC is positive for all bones) or all are contributing to compression (RCVC is negative for all bones), can RCVC be interpreted as the relative contribution to overall oral volume expansion or contraction, respectively. For example, if a

bone's RCVC is positive, then that bone is contributing to oral cavity volume expansion, but the oral cavity could be experiencing either net expansion or contraction at that time.

All volumetric data were smoothed using a three-frame moving average filter. Trials in this analysis were cut off at -35 to 50 ms before extracting bone contribution peak magnitudes and times because high amounts of noise prior to the onset of bone motion led to false peaks in some values. We tested for significant differences between bone's RCVCs at several time points among all (n = 13) *P. bichir* strikes pooled using a one-way ANOVA and post-hoc Tukey HSD tests. For this analysis, we selected the time at each bone's peak RCVC, time at peak total volume, and time at peak rate of volume change as our time points of interest.

Examining evidence for a cleithrum-hyoid-jaw linkage: To evaluate the role of pectoral girdle displacement and sternohyoideus function on ceratohyal and lower jaw kinematics, translation of the cleithrum and ceratohyal were measured relative to the neurocranium using ACSs. Specifically, we quantified the displacement magnitudes of the most ventrolateral aspect of the cleithrum (lateral sternohyoideus origin), the most anterior aspect of ceratohyal (sternohyoideus insertion), most posterior aspect of ceratohyal (mandibulohyoid ligament origin), ventral lower jaw just anterior to the palatoquadrate joint (mandibulohyoid ligament insertion), and most anterior aspect of the lower jaw (to measure jaw depression). We quantified these motions in all three anatomical planes, measuring protraction-retraction (anteroposterior translation), elevation-depression (dorsoventral translation), and adduction-abduction (mediolateral translation). The relationship between retraction of the cleithrum, depression and retraction of the ceratohyal, and depression and retraction of the lower jaw were analyzed pairwise across bones using cross-correlations. Cross-correlation provides a measure of association between two time series

variables across a series of lags (see above), so we use them here to investigate potential cause-effect relationships among kinematics of different overall excursion magnitude. We report the highest (absolute value) cross-correlations from 50 ms before and after peak gape (100 ms total) across trials and the lag time at which the maximal cross-correlation occurred. Variables with consistent (low deviation) lag times and high R values are identified as motions likely to be causally linked (e.g., driven by the same musculature or motion of one bone actuating motion of another in a linkage). A distance tool was used to measure the length of the sternohyoideus muscle, approximated with locators at the insertion and origin sites of the muscle (both lateral and medial origins).

RESULTS

Suction feeding in *Polypterus bichir* involves a highly kinetic skull, with elevation of the neurocranium and depression of the lower jaw initiating a rapid increase in gape to begin the strike, followed by cleithral retraction and ceratohyal depression, and finally by lateral abduction of the operculum and suspensorium. *P. bichir* employ forward-directed ram feeding in addition to suction, and a wave of dorsoventral bending travels posteriorly down the body (Fig. 2.2). Prey acceleration peaks rapidly and the prey maintains relatively constant velocity through the expansive phase of the strike, slowing once it reaches the back of the pharynx. Prey acceleration was most strongly cross-correlated with lower jaw and anterior ceratohyal velocity. The ceratohyal undergoes complex 3D motions, depressing, retracting, flaring laterally and rotating about its long axis. Changes in oral cavity volume were driven initially by the lower jaw, then the ceratohyal, and finally by the operculum. The sternohyoideus muscle does not shorten during

strikes and this study supports force transmission between the ceratohyal and lower jaw through the MHL.

Kinematic pattern of Polypterus bichir *feeding strikes*

P. bichir feeding strikes start with a rapid gape increase, driven by neurocranial elevation (maximum 33.6 ± 4.67° SEM relative to the body plane) and lower jaw depression (maximum -34 ± 0.79° relative to the neurocranium) (Fig. 2.2, Fig. 2.3, Table 2.S2). Shortly after the onset of cranial elevation and jaw depression, the ceratohyal begins depressing (maximum -55.3 ± 1.55°), reaching its peak 14 ± 3.01 ms after maximum gape. Posterior rotation of the cleithrum relative to the neurocranium (maximum -32.4 ± 0.97°) follows a pattern similar to the ceratohyal, peaking slightly earlier at 10.7 ± 3.0 ms after peak gape. Posterior rotation of the cleithrum relative to the body plane reached a minimum of 7.6 ± 1.21° at -24.5 ± 2.24 ms and a maximum of -31.5 ± 3.11° at 37.6 ± 3.77 ms. Finally, the operculum and suspensorium abduct, reaching their peaks of 19.1 ± 1.0° and 12.8 ± 1.1° at 24.6 ± 2.17 ms and 30.9 ± 6.6 ms after peak gape, respectively (Fig. 2.3, Table 2.S2). Opercular adduction (average peak of -3.7 ± 0.61° across trials) also occurs at the onset of the strike, at -15.9 ± 6.48 ms before peak gape (Fig. 2.3).

The ceratohyal of *P. bichir* exhibited substantial rotation about each axis, in addition to the anatomically-oriented z-axis (depression) described above. Noting substantial long-axis rotation of the ceratohyal in our animations, we quantified the motion of this bone using an additional set of JCSs, oriented such that the x-axis directly measured long-axis rotation of the bone (Fig. 2.4). Translation and rotation data in this "joint-oriented" JCS measured relative to the neurocranium (Fig. 2.4) demonstrate that the ceratohyal rotates -80.0 ± 2.89° about its long axis, 60.1 ± 1.5° about a mediolaterally oriented z-axis, and -28.1 ± 1.98° around a primarily

dorsoventral axis. Additionally, the ceratohyal translates in all 3 of these directions, with particularly high lateral (-14.5 ± 0.71 mm) and posterior (-6.03 ± 0.32 mm) translations. We also visualized ceratohyal movement using an instantaneous helical axis, which describes rigid motion as a rotation and a translation along a single axis, shown in Fig. 2.4E-F. At peak ceratohyal velocity, the axis of rotation of the ceratohyal is at approximately 45° to both the mid-sagittal and frontal planes. This axis is dorsal and anterior to the joint of the ceratohyal with the interhyal when measured relative to the neurocranium (Fig. 2.4E-F).

Table 2.S2. Mean peak magnitude and time to peak for z-axis rotation values.

Bone	**Number of Trials**	**Maximum Z axis rotation (°)**			**Time to peak Z rotation (ms)**		
Ceratohyal	(n = 18)	-55.3	±	1.55	14.1	±	3.01
Lower Jaw	(n = 18)	-34.0	±	0.79	3.7	±	1.98
Cleithrum	(n = 18)	-32.4	±	0.97	10.7	±	3.00
Neurocranium	(n = 18)	33.6	±	4.67	5.0	±	5.24
Operculum	(n = 16)	19.1	±	1.00	24.6	±	2.17
Suspensorium	(n = 11)	12.8	±	1.10	30.9	±	6.60

Drivers of oral cavity volume change

Volumetric analysis shows that oral cavity volume began increasing at -28.8 ± 1.61 ms across all measured trials, peaking to 13.5 ± 0.9 cm^3 at 11.5 ± 1.88 ms. The absolute rate of volume change peaked at -10.9 ± 1.00 ms (Table 2.2, Fig. 2.5). Across trials, the relative contribution to volume change (RCVC) of the lower jaw reached the highest peak of 0.77 ± 0.03 first in the strike at -26.3 ± 1.34 ms and was significantly different from all other bones at this time ($p < 0.0001$). The ceratohyal RCVC peaked later in the strike and contributed slightly less to instantaneous volume change, reaching a peak of 0.61 ± 0.04 at -4.6 ± 3.17 ms, also significantly higher than all other bones at this time ($p < 0.0001$). The suspensorium reached the

lowest peak RCVC of 0.48 ± 0.09 shortly after peak gape at 5.4 ± 1.84 ms (Table 2.2) and was statistically different from the ceratohyal and lower jaw ($p < 0.01$), but not the operculum ($p = 0.561$) at this time. Finally, the operculum RCVC reached the latest peak of 0.63 ± 0.06 at 10.0 ± 3.50 ms and was significantly different from all other bone's RCVC at this time ($p < 0.01$). When considering each bone's peak RCVC regardless of time point, significant differences were found only between the lower jaw and the suspensorium ($p < 0.01$).

At the point of maximum rate of volume change, the ceratohyal's RCVC was significantly higher than all other bones ($p < 0.0001$), followed by the lower jaw and operculum (which were not statistically different, $p = 0.91$), and finally the suspensorium (Table 2.2). At maximum total volume, the operculum's RCVC was highest and significantly different from the lower jaw and ceratohyal ($p < 0.01$), but not from the suspensorium ($p = 0.23$). Analysis of the RCVC of each bone averaged by time point shows that the lower jaw contributes most strongly to volume changes from the onset of the strike until 14 ms before peak gape (Fig. 2.5). Between -14 ms and peak gape, the contributions of the ceratohyal rapidly overtake those of the lower jaw (Fig. 2.5). Just prior to peak gape (-4 ms) the operculum RCVC overtakes the ceratohyal contributions, and the operculum contributes most substantially to volume change at the end of the strike. Suspensorial RCVC also peaks later in the strike, overtaking ceratohyal contributions at 2 ms, but never reaches a higher RCVC than the operculum (Fig. 2.5).

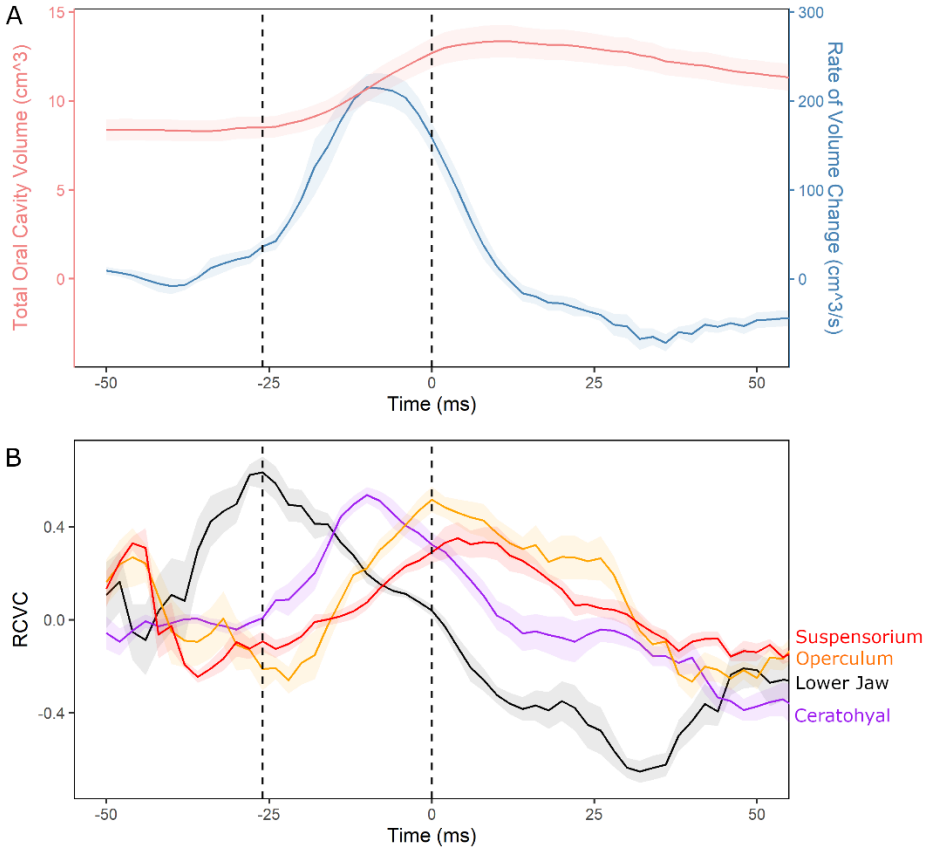

Fig. 2.5. Change in oral cavity volume and relative contribution of each rigid body. (A) Change in oral cavity volume during feeding strikes. Total volume (salmon-colored line) was calculated directly from the endocast, while rate of volume change (blue line) was calculated as the derivative of total volume, or the volume change from one frame to the next. (B) Relative contribution to volume change (RCVC) of each rigid body or skeletal element to summed delta volume. Each line is a ratio of that bone's contribution to the summed or absolute delta volume (see Methods for details). Lines show mean ± SEM of strikes across two individuals (7 trials for suspensorium, 11 trials for operculum, 13 for all other variables). Vertical lines denote onset of prey motion (-26 ms) and peak gape (0 ms).

Table 2.2. Absolute delta volume and bone RCVC magnitudes at overall peaks, time of maximum total volume, and time at maximum delta volume (trace data shown in Fig. 2.5).

	Absolute Delta Volume (cm^3 freeze $interval^{-1}$)	Lower Jaw RCVC	Ceratohyal RCVC	Operculum RCVC	Suspensorium RCVC
Peak magnitude	2.3 ± 0.167	0.77 ± 0.033	0.61 ± 0.035	0.63 ± 0.063	0.48 ± 0.093
Time at peak	-10.9 ± 1.00	-26.3 ± 1.34	-4.6 ± 3.17	10.0 ± 3.50	5.4 ± 1.84
Magnitude at peak total volume	0.45 ± 0.067	0.25 ± 0.026	0.51 ± 0.030	0.22 ± 0.027	0.07 ± 0.030
Magnitude at peak delta volume	-	-0.36 ± 0.049	0.05 ± 0.061	0.40 ± 0.076	0.20 ± 0.035

Correlates of prey acceleration

Cross-correlation analyses demonstrated that displacement velocities for all bones except the suspensorium were significantly associated with prey acceleration ($p < 0.05$, determined by null distributions with > 999 unique combinations for all bones except suspensorium). Statistical power for the suspensorium was lower than for other bones due to a reduced total number of successful trials in which this rigid body was effectively reconstructed (9 trials, null distribution included 256 unique combinations). Displacement velocity of the anterior lower jaw correlated most strongly with prey acceleration ($R = 0.302$) and had the lowest lag time at 1 ms (Fig. 2.6, Table 2.1). Anterior ceratohyal velocity followed shortly behind in both lag (3 ms) and maximum correlation ($R = 0.296$) (2.6, Table 2.1). We did not test the relationship between cleithral velocity and prey acceleration, as cleithral motion should indirectly contribute to suction generation through linkages with cranial elements measured in this study. The operculum had a relatively lower correlation with prey acceleration ($R = 0.219$) and a higher lag time at 10 ms (Fig. 2.6, Table 2.1). Finally, the suspensorium had the lowest cross-correlation ($R = 0.1$) and the highest lag time (17 ms).

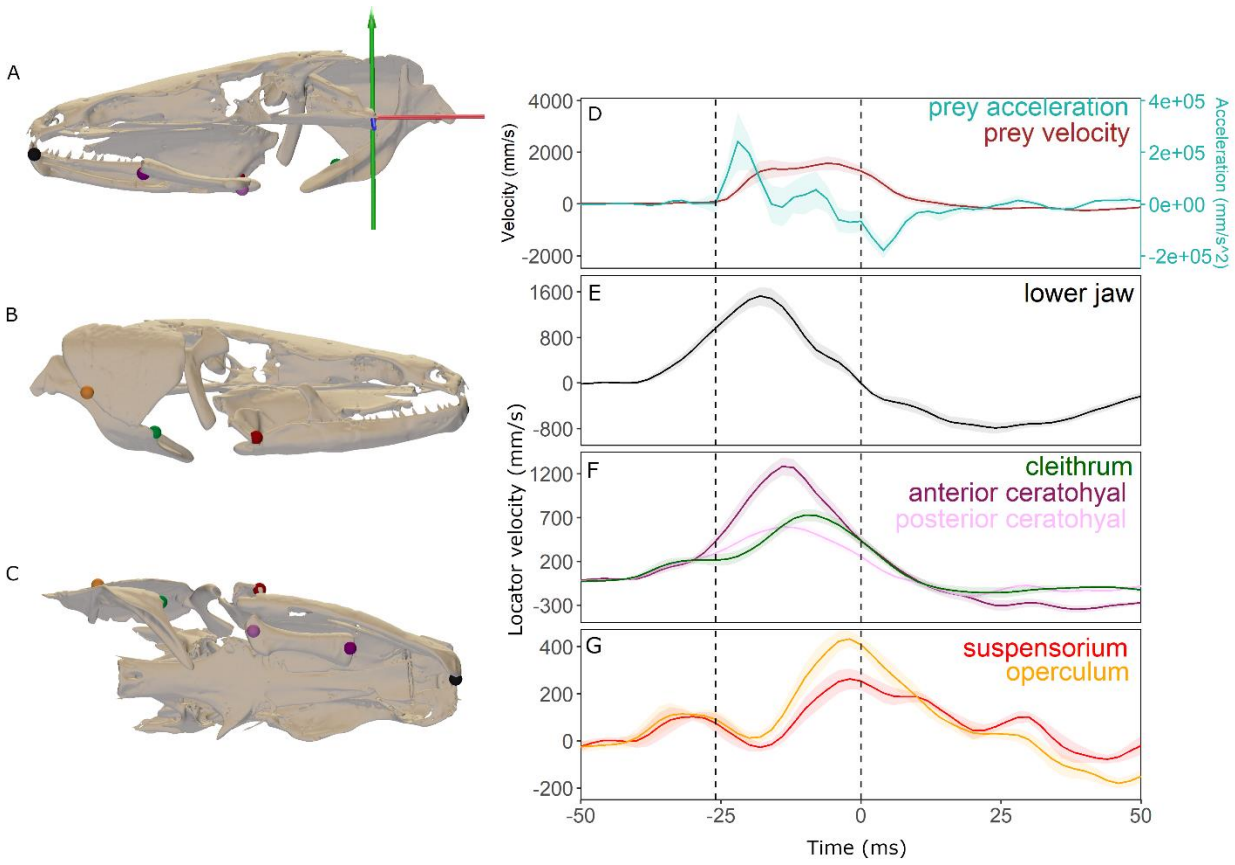

Fig. 2.6. Mean displacement velocity of bone points of interest. (A-C) Locators for each bone used to measure the point undergoing the highest degree of motion during a strike. Colors correspond to kinematic traces shown in E-G. (A) Medial view with ACS coordinate system paired to the neurocranium (from which each locator's displacement velocity was calculated). (B) Lateral view. (C) Ventral view. (D-G) Mean ± SEM of all successful strikes across three individuals (9 trials for suspensorium, 14 trials for operculum, 16 for all other variables). Prey data and rotations are unfiltered, except for suspensorial and opercular motion, which were smoothed using a 50 Hz low-pass Butterworth filter. Vertical lines denote onset of prey motion (-26 ms) and peak gape (0 ms). (D) Prey velocity and acceleration in world space. Panels (E-G) show locator displacements for each bone of interest, all measured relative to the neurocranium.

Cleithrum and jaw opening linkage mechanics

The insertion of the lateral sternohyoideus on the ventrolateral aspect of the cleithrum (Fig. 2.6) retracts to a maximum of -18.4 ± 1.18 mm relative to the neurocranium at 14.7 ± 3.70

ms (averaged across trials) (Table 2.S3). At the onset of cleithral motion, this point elevates slightly (2.1 ± 0.39 mm at -31.8 ± 2.14 ms), then depresses over an extended period, to a negative peak of -8.5 ± 0.43 mm at 36.7± 2.43 ms (Table 2.S3). The anterior ceratohyal, which is connected directly to the measured cleithral point by the sternohyoideus, retracts to a maximum of -20.5 ± 1.02 mm at 11.7 ± 1.91 ms and depresses to a negative peak of -20.7 ± 0.57 mm at 15.7 ± 3.03 ms (Table 2.S3). The posterior ceratohyal retracts much less (a peak of -5.5 ± 0.39 mm at -11.3 ± 1.42 ms) and elevates to a maximum of 3.9 ± 0.34 mm at 20.0 ± 3.28 ms. The largest translation of the posterior ceratohyal is lateral, to a peak of 16.3 ± 0.7 mm at 9.2 ± 1.73 ms (Table 2.S3). Distance measurements between the lateral-most and medial-most origins to a single insertion point of the sternohyoideus demonstrate that this muscle is not shortening during strikes; in fact, the muscle lengthens during the compressive phase (Fig. 2.7C).

The mandibulohyoid ligament (MHL) attachment on the lower jaw translates anteroposteriorly and dorsoventrally in phase with the posterior ceratohyal, reaching a posterior maximum of -3.5 ± 0.23 mm at -9 ± 1.48 ms, and ranging from a dorsal maximum of 3.2 ± 0.27 mm to ventral maximum of -2 ± 0.27 mm (Table 2.S3). The MHL attachment point on the lower jaw translates laterally to a peak of 7.3 ± 0.43 mm (Table 2.S3). Fig. 2.7 shows these motions averaged by time point across trials.

Cross-correlations demonstrate a strong relationship and minimal lag (1 ± 0.04 ms and 0.22 ± 0.22 ms, respectively) between the posterior translation of the lateral aspect of the cleithrum and the posterior and ventral translations of the anterior ceratohyal (R = 0.953 ± 0.011 and 0.944 ± 0.008, respectively). There is also a strong correlation between ceratohyal motion and lower jaw depression, with ventral translation of the anterior lower jaw (jaw depression)

strongly correlated with both posterior motion across the ceratohyal (R = 0.863 ± 0.015 and 0.867 ± 0.015, 5.1 ± 0.69 and -2.67 ± 0.4 ms lag) (anterior and posterior ceratohyal, respectively) and dorsoventral translation of the anterior ceratohyal (R = 0.773 ± 0.019, 5.78 ± 0.62 ms lag) (Fig. 2.7, Table 2.3). The lower jaw at the MHL attachment site shows relatively little motion (Fig. 2.7) and largely lower cross-correlations or more variable lag times with motion at the posterior ceratohyal. The clearest relationships are between posterior ceratohyal retraction and retraction of the lower jaw at the MHL (R = 0.91 ± 0.014 at 0 ms lag across all trials) and elevation of the posterior ceratohyal and elevation of the lower jaw at the MHL (R = 0.774 ± 0.033 at -7.11 ± 2.11 ms). (Table 2.3). Posterior translation of the cleithrum and ventral translation of the anterior lower jaw (R = 0.801 ± 0.024 with a 7.67 ± 1.26 ms lag) are also highly correlated.

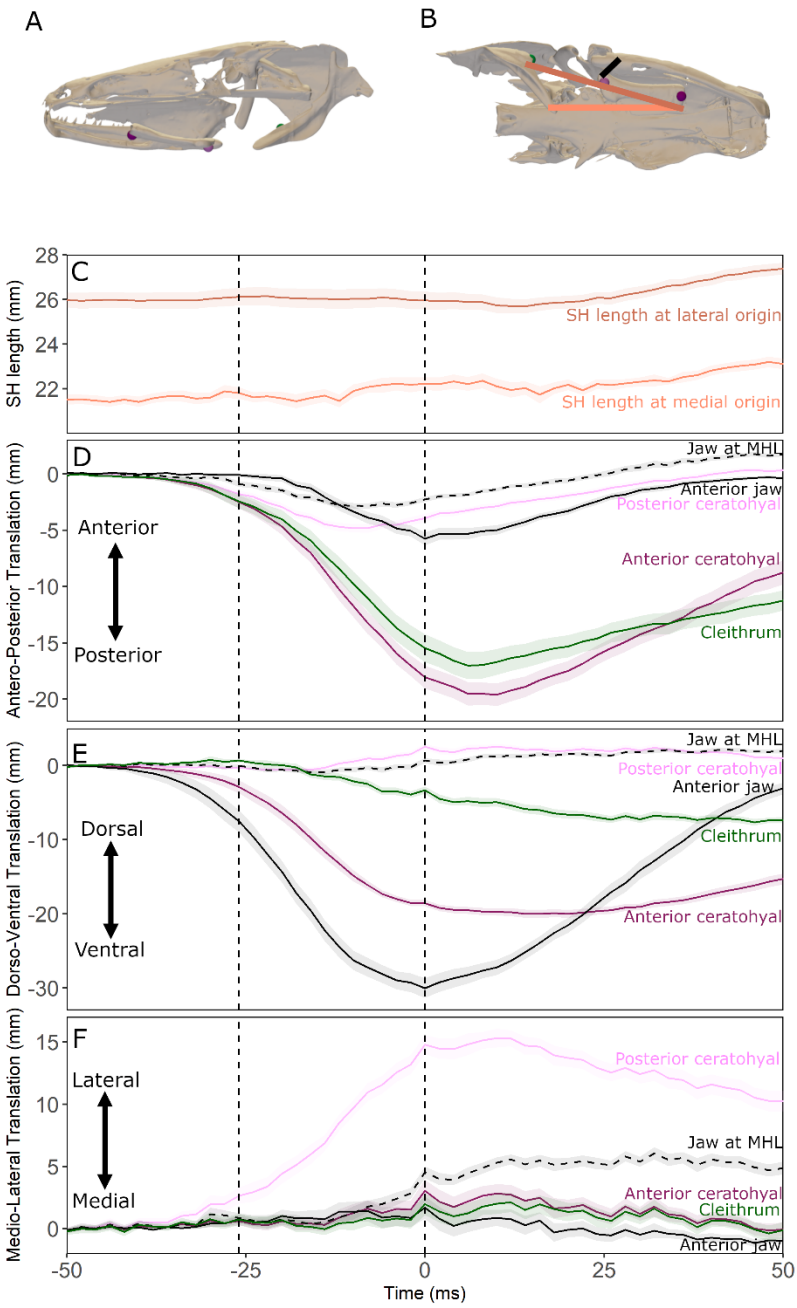

Fig. 2.7. Sternohyoideus length and translations of key points on cleithrum, ceratohyal, and lower jaw. (A) Medial view of the skull showing locators measured for anterior ceratohyal (dark purple), posterior ceratohyal (light purple), and ventrolateral cleithrum (green). (B) Ventral view of the skull showing locators measured and orientation of the lateral-most sternohyoideus (SH) origin (dark orange bar), medial-most SH origin (light orange bar), and mandibulohyoid ligament (black bar). (C) Length of sternohyoideus muscle from each origination point (to a single insertion point) across strikes, measured as the distance between origin and insertion points on the cleithrum and ceratohyal. (D-F) Translations of the lower jaw attachment of the MHL, anterior and posterior ceratohyal, and ventrolateral cleithrum in an anteroposterior (D), dorsoventral (E), and mediolateral (F) axis, all measured relative to the neurocranium using the same ACS as shown in Fig. 2.6. All lines in C-F show mean ± SEM of all tracked strikes across three individuals (18 trials). Vertical lines denote onset of prey motion (-26 ms) and peak gape (0 ms).

Table 2.S3. Mean magnitudes and timing of peak x, y, and z translations of anterior and posterior ceratohyal, lateral cleithrum, and jaw at mandibulohyoid ligament across trials, with translations calculated as in Fig. 7 but averaged the peak from each trial rather than by time point.

Bone	Translation Max/Min	Magnitude (mm)			Timing (ms)		
Anterior Ceratohyal	Peak Anterior	0.2	±	0.06	-44.3	±	1.36
	Peak Posterior	-20.5	±	1.02	11.7	±	1.91
	Peak Dorsal	0.2	±	0.05	-39.2	±	1.66
	Peak Ventral	-20.7	±	0.57	15.7	±	3.03
	Peak Lateral	4.9	±	0.67	1.6	±	4.27
	Peak Medial	-2.3	±	0.44	-5.4	±	7.54
Posterior Ceratohyal	Peak Anterior	0.9	±	0.15	18.9	±	9.79
	Peak Posterior	-5.5	±	0.39	-11.3	±	1.42
	Peak Dorsal	3.9	±	0.34	20.0	±	3.28
	Peak Ventral	-1.5	±	0.26	-16.8	±	5.37
	Peak Lateral	16.3	±	0.70	9.2	±	1.73
	Peak Medial	-1.0	±	0.17	-41.3	±	1.84
Cleithrum	Peak Anterior	0.4	±	0.14	-42.0	±	1.53
	Peak Posterior	-18.4	±	1.18	14.7	±	3.70
	Peak Dorsal	2.1	±	0.39	-31.8	±	2.14
	Peak Ventral	-8.5	±	0.43	36.7	±	2.43
	Peak Lateral	4.6	±	0.58	3.8	±	5.93
	Peak Medial	-3.1	±	0.47	2.9	±	8.00
Jaw at MHL	Peak Anterior	2.1	±	0.20	41.8	±	4.31
	Peak Posterior	-3.5	±	0.23	-9.0	±	1.48
	Peak Dorsal	3.2	±	0.27	32.2	±	5.06
	Peak Ventral	-2.0	±	0.27	-14.6	±	3.39
	Peak Lateral	7.3	±	0.43	24.7	±	3.74
	Peak Medial	-1.8	±	0.29	-27.9	±	3.70

Table 2.3. Peak cross-correlations and lag times between elements involved in lower jaw opening linkage, abbreviations are as follows: AP = anteroposterior, DV = dorsoventral, ML = mediolateral, with locators the same as shown in Fig. 2.6.

Link Responsible	Lead Variable	Lag Variable	Max Cross-Correlation	Lag time (ms)
Sternohyoideus directly	Cleithrum AP	Anterior Ceratohyal AP	0.95 ± 0.01	1.00 ± 0.40
		Anterior Ceratohyal DV	0.94 ± 0.01	0.22 ± 0.22
Sternohyoideus indirectly	Cleithrum AP	Posterior Ceratohyal AP	0.63 ± 0.03	9.00 ± 5.54
		Posterior Ceratohyal DV	0.45 ± 0.02	-38.33 ± 9.24
MHL directly	MHL Jaw AP	Posterior Ceratohyal AP	0.91 ± 0.01	0.00 ± 0.00
		Posterior Ceratohyal DV	0.69 ± 0.03	-10.89 ± 6.60
	MHL Jaw DV	Posterior Ceratohyal AP	0.60 ± 0.03	6.11 ± 4.66
		Posterior Ceratohyal DV	0.77 ± 0.03	-7.11 ± 2.11
	MHL Jaw ML	Posterior Ceratohyal AP	0.55 ± 0.03	-17.89 ± 6.15
		Posterior Ceratohyal DV	0.43 ± 0.02	25.33 ± 10.77
MHL indirectly	Anterior Jaw DV	Anterior Ceratohyal AP	0.86 ± 0.01	5.11 ± 0.69
		Anterior Ceratohyal DV	0.77 ± 0.02	5.78 ± 0.62
		Posterior Ceratohyal AP	0.87 ± 0.01	-2.67 ± 0.40
		Posterior Ceratohyal DV	0.55 ± 0.03	-9.56 ± 9.58
Both	Cleithrum AP	Anterior Jaw DV	0.80 ± 0.02	7.67 ± 1.27

DISCUSSION

The kinematics of the cranial bones of *P. bichir* during feeding strikes enable us to test hypotheses about the mechanisms driving the suction which underlies successful prey capture. In *P. bichir*, jaw opening initiates suction generation via rapid volumetric expansion of the oral cavity, while ceratohyal depression enhances and maintains suction and oral cavity expansion. Opercular abduction also contributes substantially to volume increase in the oral cavity, but its timing later in the strike serves not to generate suction directly but to maintain successful prey capture by allowing water to exit through the gills, maintaining the momentum of the water bolus throughout the strike. We also present new evidence for a previously proposed biomechanical linkage between the cleithrum, ceratohyal, and lower jaw. This linkage utilizes cleithral retraction to transfer power generated by the hypaxial muscles through an isometrical sternohyoideus muscle to the anteroventral hyoid arch, driving not only ceratohyal depression but also retraction and long-axis rotation, ultimately enabling jaw opening.

Kinematic patterns of Polypterus bichir *feeding strikes*

Suction feeding in *P. bichir* involves an anterior to posterior wave of motion in the body, cranium, lower jaw, and hyoid apparatus (Figs. 2 & 3), the same sequence utilized by teleosts and other aquatic suction feeders (Bishop et al., 2008; Jacobs and Holzman, 2018). This confirms previous work (Lauder, 1980) while expanding our knowledge of motion in bones such as the ceratohyal, cleithrum, and suspensorium, which are partially or wholly obscured and therefore unmeasurable by light camera video (Figs. 3 & 4). We additionally note substantial, previously undescribed, dorsoventral flexion in the vertebral column during *P. bichir* strikes, and posit that

these fish appear to utilize numerous intervertebral joints to accommodate a large degree of neurocranial elevation as recently described in both trout and frogfish (Camp, 2021).

Contrary to a previous hypothesis that the pectoral girdle of *Polypterus* serves as a stable anchor point for sternohyoideus muscle activity (Lauder, 1980), this study demonstrates that the cleithrum in *P. bichir* is highly mobile, undergoing substantial retraction during suction feeding strikes (Fig. 2.3). Interestingly, cleithral retraction relative to the neurocranium breaks the "anterior to posterior" pattern, as it peaks well before suspensorial or opercular abduction, although this pattern of mobility still holds within the skull. We demonstrate that cleithral mobility contributes to hyoid and lower jaw motion, though the power generated by the muscles that move it (hypaxial and sternohyoideus muscles) *a la* Camp and Brainerd (2014) remains to be quantified in this species.

Historically, hyoid bar motion in fishes was measurable only when the anteroventral hyoid apparatus depressed below the level of the jaws: XROMM enables measurement of the hyoid arch throughout a strike, allowing us to quantify the rotations and translations of the ceratohyal in all three anatomical axes (Fig. 2.4). We found not only the substantial depression and retraction of the ceratohyal previously described in fishes (Lemberg et al., 2019; Olsen et al., 2019), but also long-axis rotation, a previously unreported motion, which may be common across actinopterygians.

Drivers of suction in Polypterus bichir *feeding strikes*

Jaw opening, ceratohyal depression and retraction, and lateral abduction of the operculum relative to the neurocranium are all substantial contributors to suction generation in *P. bichir*,

with oral cavity volume change being primarily driven by these three bones in sequence (Fig. 2.5). Each of these bone velocities was significantly cross-correlated with prey acceleration, our proxy for suction. Neurocranial elevation also contributes to volume change and prey motion, but its contributions could not be directly measured in this portion of the study because the cranium served as a reference point. While prey acceleration alone underestimates the forces acting on the water (Holzman et al., 2008), motion of the prey item into the mouth to achieve prey capture is the ultimate goal of a suction feeding event and is therefore a useful measure of suction performance. The strongest correlations and shortest lag times were between prey acceleration and jaw velocity, followed closely by ceratohyal velocity (Fig. 2.6, Table 2.1). Furthermore, the highest overall RCVCs were produced by the lower jaw at the beginning of the strike, and the ceratohyal contributed the highest RCVC at the time of highest volume change (Fig 5., Table 2.2). This implies that, of the kinematics measured here, an increase in gape of the oral jaws anteriorly and depression of the ceratohyal posteriorly are the two primary sources of oral cavity volume expansion during suction feeding in *P. bichir*. Additionally, increases in prey acceleration and velocity begin during a period of the strike when only the neurocranium and lower jaw have moved substantially, suggesting that *P. bichir* strikes are initiated via flat-plate suction associated with jaw opening, and subsequent ceratohyal motion serves to maintain the velocity of the prey item. While this idea has been explored in previous work (Bishop et al., 2008; Jacobs and Holzman, 2018; Lemberg et al., 2019) the ability to quantify the association between 3D motion of individual skeletal elements and a prey item tracked throughout a feeding event allows a direct test of this hypothesis.

Lateral flaring of the suspensorium and operculum are also important to successful suction feeding in *P. bichir*, but not because it initiates negative pressure in the buccal cavity. Instead, lateral flaring continues the anterior to posterior wave of oral cavity expansion, maintaining the momentum of water through the mouth by allowing it to exit through the opercular opening. This is suggested in our study by the significant cross-correlation between opercular velocity and prey acceleration (at 16 ms) (Table 2.1) and by the high RCVC of opercular motion, which was significantly different from all other bones at its peak (Fig. 2.5, Table 2.2) of 10 ms, following prey ingestion into the oral cavity (coincident with a decrease in prey velocity, Fig. 2.6). Consideration of opercular kinematics (Fig. 2.3) and RCVC (Fig. 2.5) demonstrate that the operculum is contributing to an increase in volume at this time, as it is still abducting away from the neurocranium. Interestingly, the operculum may also play a role at the start of the strike by adducting slightly (Fig. 2.3), similar to the volume decrease seen in the "preparatory phase" before cranial expansion, noted in some teleosts (Lauder, 1980). The function of this opercular adduction is probably to ensure that suction generated by oral cavity expansion is directed forwards, not through the gill slits. Our interpretation of the role of the suspensorium is complicated by our inability to test statistical significance at the same level of confidence as other bones, but results from cross-correlation with prey acceleration and volumetric analyses support the notion that abduction of the suspensorium is a relatively minor contributor to suction generation. However, movement of the palate relative to the neurocranium and the relative mobility of the interhyal between suspensorium and ceratohyal provides an additional degree of freedom to ceratohyal motion, perhaps enabling the complex 3D motion in the ceratohyal discussed above (Fig. 2.4). As proposed previously (Lauder, 1980), the flexibility

afforded by the interhyal joint likely allows for an increased moment arm of the mandibulohyoid ligament relative to the lower jaw by enhancing the degree of posterior translation possible in the ceratohyal (Figs. 2.4 & 2.7).

Many previous studies have modeled hydrodynamics of fish suction feeding using geometric shapes like cones, with varying success and assumptions required (Bishop et al., 2008; Michel et al., 2015; Muller and Osse, 1984; Muller et al., 1982; Van Wassenbergh and Aerts, 2009). The use of 3D data collection and visualization techniques, such as CT scanning and the XROMM workflow, can be paired with hydrodynamic models to elucidate the role of each functional component of the fish skull during suction feeding. While such a combined model is outside the scope of the current study, the volume-based approach and prey acceleration measurements presented here lay the foundation for future modeling work in *P. bichir*, a species with important implications for our understanding of the evolution of suction feeding mechanics across fishes.

Cleithrum, hyoid, and jaw opening linkage mechanics

Our ability to measure ceratohyal kinematics in 3D allowed not only quantification of its contribution to oral cavity volume change but also its role in transmitting forces from the cleithrum to the lower jaw to drive jaw depression. Our data show that the cleithrum is retracted and rotated posteriorly during suction strikes (Fig. 2.3, Fig. 2.7), motion that must be generated by hypaxial muscle contraction (Allis, 1922). This posterior cleithral motion is then translated into ceratohyal retraction and depression, which in turn causes mandibular depression by applying a posteriorly and dorsally directed force to the posterior mandible, behind the axis of rotation (Fig. 2.7, Lauder, 1980). Retraction of the cleithrum begins while the posterior

ceratohyal moves posteriorly and the anterior ceratohyal moves ventrally and posteriorly. The posterior ceratohyal stops moving posteriorly about 11 ms prior to peak gape (Fig. 2.7D), followed by a slight dorsal translation and an increase in its rate of lateral translation (Fig. 2.7E-F). We propose that this "hard stop" on ceratohyal retraction occurs when the articulation of the ceratohyal with the interhyal and suspensorium has reached its limit; continued transmission of force to the cleithrum results in anterior depression and posterior "lateral flaring" of the ceratohyal. Lateral flaring of the ceratohyal may be the primary driver of abduction in the suspensorium, which begins to increase at this time (Fig. 2.3) (Video 2.1).

We conclude that the sternohyoideus muscle is contributing little, if any, power to drive hyoid motion, despite being active during strikes (Lauder, 1980). The sternohyoideus remains the same length during the expansive phase of feeding strikes in *P. bichir* (Fig. 2.7) so is incapable of contributing work to ceratohyal movements. This means that, as in bass, the axial muscles are the primary driver of ceratohyal motion in the expansive phase of the suction strike in *P. bichir* (Camp and Brainerd, 2014).

Data presented here support the theory that retraction of the ceratohyal drives jaw opening in *P. bichir*. Lauder (1980) hypothesized that jaw opening torques act on the jaw through the MHL, the connection of the lower jaw to the posterior ceratohyal. This ligament inserts on the ventral surface of the jaw and is positioned behind its axis of rotation (Fig. 2.7B), meaning that posterior and dorsal forces applied through the MHL will result in jaw depression (Lauder, 1980). Our data demonstrate that this MHL insertion point undergoes a measurable but small degree of motion during feeding (Fig. 2.7). The motion at this MHL insertion point which has the clearest implications for jaw opening, retraction, peaks at -9 ms, before maximal jaw

depression (Fig. 2.7, Table 2.S3) and is strongly cross-correlated with retraction of the ceratohyal (Table 2.3). Furthermore, although the jaw has not reached peak depression when the MHL insertion stops moving posteriorly (-9 ms), the jaw's peak velocity occurs before this point in the strike (-16 ms, Fig. 2.6), indicating that forces applied to the jaw at the MHL due to ceratohyal motions may be solely responsible for imparting the forces required for jaw opening.

There are two additional mechanisms that may contribute to jaw opening but were not directly measured in this study. First, while *P. bichir* lacks the levator operculi muscle thought to drive jaw depression via opercular rotation in *Amia* and teleosts (Allis, 1922; Camp and Brainerd, 2015; Lauder, 1980), we cannot rule out contributions from other muscles such as the adductor operculi or adductor hyomandibulae. It is plausible that the early opercular and suspensorial motions seen between -30 and -20ms (Fig. 2.3) are contributing to jaw depression early in the strike. Second, it is possible that once the jaw is opened far enough, the continued ventral movement of the anterior ceratohyal could affect additional jaw opening by applying force to the anterior lower jaw via some combination of the branchiomandibularis, interhyoideus (geniohyoideus superior in Allis, 1922), or intermandibularis posterior (geniohyoideus inferior in Allis, 1922) muscles. Regardless of the precise mechanism and origins of force transferred between the ceratohyal and the lower jaw, this study showed a clear relationship between ceratohyal motion and lower jaw depression (Table 2.3, Fig. 2.7), and further analysis is needed to understand the degree to which other mechanisms may mediate jaw opening.

Cleithral retraction also had a strong relationship with jaw opening, though with a lower R-value and more variable lags than seen for the cleithrum-ceratohyal or ceratohyal-jaw relationship (Fig. 2.7, Table 2.3). These slightly lower correlations and varied lag times are likely

due to the more complex nature of this linkage, with the cleithral motion input (via sternohyoideus muscle) driving complex three-dimensional ceratohyal motions (Figs. 4 and 7) in addition to the retraction likely causing jaw depression. Additionally, hyoid constrictor muscles may play a role in modulating the degree to which the ceratohyal depresses in response to a posteroventral force applied to its anterior aspect through the sternohyoideus, as seen in alligator gar (Lemberg et al., 2019). Future work modeling the expected linkage relationships compared to observed motions in this dataset will be of value for understanding the degree to which various muscular inputs are driving skeletal motions throughout the strike.

Implications for actinopterygian feeding evolution

Polypterids are commonly used as an analog for tetrapodomorph fishes (Lemberg et al., 2021; Markey, 2006; Markey and Marshall, 2007), as these fish are considered to be the extant sister taxa to all other living actinopterygians (Coates, 2017; Giles et al., 2017). While polypterid fishes have undergone a substantial independent evolutionary history and some notable reversals (Giles et al., 2017), the presence of broader functional characteristics, including linkages in the feeding apparatus, in both *P. bichir* and extant teleosts or other actinopterygian fish leaves the most parsimonious explanation that these characters are retained throughout the early actinopterygian lineage. For example, this study confirms that *P. bichir* has a highly mobile ceratohyal and cleithrum, both of which are also present in gars and derived teleosts (Camp and Brainerd, 2014; Camp et al., 2020; Lemberg et al., 2019).

A mobile cleithrum enables contracting hypaxial muscles and an active sternohyoideus to work in concert, directly driving complex ceratohyal motions which enable jaw opening and successful feeding via suction. Similar mechanisms recently described in largemouth bass (Camp

and Brainerd, 2014), bluegill (Camp et al., 2018), catfish (Camp et al., 2020), and now *P. bichir* emphasize that the importance of hypaxial muscle contraction for feeding is likely ubiquitous in suction feeding fishes (Tchernavin, 1948), though additional power contributions from the sternohyoideus are more variable (Lomax et al., 2020; Van Wassenbergh et al., 2007). Indeed, we know that this linkage is maintained even in highly derived teleosts, all of which share a second jaw opening mechanism wherein the operculum contributes to jaw opening (Camp and Brainerd, 2015; Olsen et al., 2017). Future work modeling the ability of each of these jaw opening linkages to cause mandibular depression in species that utilize both mechanisms could be useful in understanding the evolutionary maintenance of the pectoral girdle-hyoid-jaw linkage.

A deeper understanding of *P. bichir* suction feeding also helps us to examine the basic morphological and biomechanical building blocks of successful suction feeding in fishes and even aquatic-feeding vertebrates more broadly. *P. bichir* skulls are more mobile than those of lungfish or amphibians due to the capacity for lateral expansion of the suspensorium, but they lack the mobile maxilla or premaxilla common to teleosts and *Amia.* Here we demonstrate that *P. bichir* are effective suction feeders without a high degree of maxillary mobility, utilizing volumetric expansion generated primarily by oral jaw and ceratohyal motion (relative to the neurocranium) to pull prey items into their mouth (Figs. 2.5 & 2.6). We show that the impact of a mobile suspensorium on volumetric change in the oral cavity is relatively small. It is possible that this mobility is just as important for allowing the full range of motion seen in the ceratohyal (i.e., Fig. 2.4 & 2.7) as it is for its direct role in contributing to suction generation or oral cavity volume change. The role of a mobile suspensorium could be more rigorously tested by

examining other species with an immobile suspensorium using modeling and volume experiments similar to those presented here.

Conclusion

We demonstrate that jaw opening generates the suction forces that initiate prey motion during *P. bichir* feeding strikes. Complex ceratohyal motion enhances and maintains volumetric expansion to drive successful suction feeding in this species. Continued application of the volume modeling techniques developed in this study to other taxa will help elucidate the basic building blocks of suction feeding across actinopterygians. Kinematic evidence presented here supports a central role of the ceratohyal in mediating the biomechanical linkage between the cleithrum and lower jaw and suggests that motion in this linkage is powered by the axial muscles. Future modeling using these data could inform precisely how force is transmitted from the ceratohyal to produce jaw depression in actinopterygian fishes both without and in concert with an opercular jaw opening linkage.

ACKNOWLEDGEMENTS

We thank Samantha Gartner, Kelsey Stilson, Elska Kaczmarek, and Michael Coates for surgical assistance, technical help, and thoughtful discussions. Three constructive reviews greatly improved the manuscript. We thank Sofia Garrick for assistance with data processing and Dave Baier for Maya Tools. Thanks to the University of Chicago XROMM Facility, Brown University Keck Lab, University of Chicago Paleo-CT, University of Chicago Veterinary CT, University of Chicago Animal Resources Center, and University of Chicago Research Computing Center for facilities use and resources. This is University of Chicago XROMM Facility Publication #10.

COMPETING INTERESTS

The authors declare no competing or financial interests.

FUNDING

This work was funded in part by the University of Chicago Henry Hind's Fund and University of Chicago Integrative Biology Core Facilities Fund. Funding for the UChicago XROMM Facility was provided by National Science Foundation Major Research Instrumentation Grants MRI 1338036 and 1626552.

DATA AVAILABILITY

Raw videos, tracked trials, and bone meshes used in this manuscript are accessible on the XMA portal under identifier portal_base5 and can be accessed here: https://xromm.rcc.uchicago.edu/larequest.php?request=explorePublicMetadataStudy&StudyID=5&instit=portal_base.

CHAPTER 3: CRANIAL KINEMATICS AND MODULATION OF FEEDING STRIKES DUE TO PREY-TYPE EFFECTS IN *AMIA CALVA*

ABSTRACT

Variability in the biomechanics and kinematics of prey capture in vertebrates has been studied extensively, with evidence of multiple strategies for successful feeding in many groups. Early research into suction feeding strikes in fishes hypothesized that fish utilize a set of pre-programmed strike kinematics that cannot be altered once initiated. However, more recent evidence has demonstrated that teleosts not only deploy unique strike kinematics for different prey types, but that they also alter their kinematics in response to a prey item attempting to escape. It has not yet been explicitly investigated whether non-teleost actinopterygians can also modulate the strike in response to different prey types. Here we[2] examined the kinematics of suction strikes in the bowfin, *Amia calva,* a holostean fish most closely related to gars. We recorded *Amia* feeding on both feeder fish and worms, two types of live prey differing in evasiveness, using X-Ray Reconstruction of Moving Morphology (XROMM). We found significant prey type effects on the magnitude of pectoral girdle motions; timing of onset of jaw opening, ceratohyal depression, and neurocranial elevation; and peak velocities of all bone rotations except neurocranial elevation. These prey type effects demonstrate that the ability to

[2] This manuscript draft has the following coauthors: Katrina Whitlow, Callum Ross, Mark Westneat

modulate feeding strikes is primitive at least for actinopterygian fishes, and possibly for jawed vertebrates.

INTRODUCTION

Vertebrates consume a wide diversity of food types and sizes using variable strategies for prey acquisition and processing. For species that specialize on a single food source, having consistent and predictable feeding kinematics may allow for greater efficiency, but many animals consume a more generalist diet where a stereotyped set of feeding behaviors may not be sufficient. The ability to modulate feeding behavior in response to variables like prey type, environmental condition, and proprioceptive feedback impacts feeding performance in a wide range of vertebrates. We refer to consistent intra-individual variation in behavior in response to differing stimuli as modulation, following precedent in the aquatic feeding literature (Liem, 1978; Matott et al., 2005). Feeding behaviors and kinematics may vary at both the inter- and intra-individual levels. For example, lizards alter their jaw-neck-forelimb coordination patterns depending on prey size and speed (Montuelle et al., 2009; Montuelle et al., 2012a); primate chewing kinematics, muscle activity and bone strain vary across food types, individuals, and behaviors (Iriarte-Díaz et al., 2011; Reed and Ross, 2010; Ross et al., 2016; Vinyard et al., 2008); sharks change their feeding kinematics depending on the size and type of prey items (Ferry-Graham, 1998; Matott et al., 2005); and teleosts can alter their musculoskeletal kinematics in response to prey type, position, and evasiveness (see Kane and Higham, 2015; Van Wassenbergh and De Rechter, 2011; Wainwright and Lauder, 1986 for some examples).

Despite the widespread capacity for modulating feeding kinematics across vertebrates, the extent to which non-teleost fishes can modulate feeding kinematics, and the neural mechanisms sub-serving such modulation, remain unknown and understudied. Early research suggested that hydrodynamics necessitate a generalized kinematic pattern across all suction feeding fishes—an antero-posterior wave of cranial kinematics—and that this results in feeding strikes that are stereotyped within individuals and species (Liem, 1970; Nyberg, 1971). The idea that strikes are stereotyped has been disproven, although the extent to which individuals or species modulate their strike kinematics is not yet documented. For example, trophic generalists exhibit a repertoire of feeding patterns that may be employed for different prey types (Nemeth, 1997b; Rice et al., 2008; Van Wassenbergh et al., 2006). Other studies have shown that fish may actively regulate their strike in response to an escape attempt by a prey item (Van Wassenbergh and De Rechter, 2011). Furthermore, fishes may vary their strike kinematics and suction force due to internal motivation or other factors that cannot be controlled by an experimenter. For example, bluegill have been shown to vary their peak force exerted under experimental conditions despite consistent type, size, orientation and position of prey (Holzman et al., 2007).

A seminal study of *Amia calva* strike kinematics reported that they do not modulate their feeding kinematics between evasive (live goldfish) and non-evasive prey (pieces of smelt), suggesting that strike modulation capability might be limited to teleosts (Lauder, 1980). However, more recent evidence in the non-teleost alligator gar (*Atractosteus spatula*) suggests that this distant sister clade to *Amia* can modulate hyoid depression substantially across strikes (Lemberg et al., 2019). If gar can modulate their feeding behavior, it seems reasonable to hypothesize that *A. calva*, which are generalist predators, eating fishes, crustaceans, and even

insects (Mcallister et al., 2019), might be able to modulate strike kinematics in response to variation in prey type.

Amia feeding is also of interest from morphological, biomechanical, and evolutionary perspectives, as the species has a unique cranial morphology for which kinematics have not been fully characterized and shares several functionally similar traits with teleosts. Perhaps the most obvious is the forward swing of the maxilla during strikes, which has been modeled previously (Lauder, 1979) and constricts the anterior aperture through which suction forces are directed. *A. calva* possess two mechanisms for jaw opening; first, the primitive mechanism by which retraction of the ventral hyoid arch (ceratohyal and urohyal, illustrated in Fig. 1.2) exerts a posterodorsal force on the jaw behind and below its axis of rotation through the mandibulohyoid ligament, and a second mechanism (independently derived in teleosts and *Amia*) through which rotations of the opercular series exert force on the lower jaw through the interoperculomandibular ligament (Camp and Brainerd, 2015; Lauder, 1980; Olsen et al., 2017). While both of these mechanisms are likely to work in concert, whether the role of the sternohyoideus is to transmit force, generate force, or both—a question that has been explored in several teleosts (Camp and Brainerd, 2014; Camp et al., 2015; Camp et al., 2018; Camp et al., 2020; Lomax et al., 2020; Van Wassenbergh et al., 2005; Van Wassenbergh et al., 2007) and the non-teleost actinopterygian *Polypterus bichir* (Whitlow et al., 2022)—is currently unclear. Despite sharing several functional feeding characters with teleosts, *A. calva* are most closely related to the family Lepisosteidae (gars), but have been evolving independently for over 250 million years and are divergent in their skull morphologies and feeding mechanics (Grande and

Bemis, 1998; Hughes et al., 2018; Lauder, 1980; Lemberg et al., 2019; Near et al., 2012; Thompson et al., 2021).

In this study, we used the XROMM (X-Ray Reconstruction of Moving Morphology) workflow to reconstruct the motion of five cranial, one hyoid, and two pectoral girdle bones in *Amia calva* feeding on live minnows and worms. We quantify feeding kinematics in this species, expanding on, and adding precision, to data on cranial, ceratohyal, and pectoral girdle motions. We investigate the role of the sternohyoideus muscle and pectoral girdle in driving jaw opening in this species. We evaluated whether *A. calva* modulate their strikes across prey types by documenting prey kinematics during strikes on evasive vs. non-evasive prey. Specifically, we compared the strike kinematic patterns, rigid body excursion magnitudes, onsets of bone motion, velocities of bone motion, sternohyoideus muscle shortening, oral cavity volume and expansion rate, and induced prey motion in strikes on feeder fish (evasive) and worms (non-evasive) prey.

METHODS

Specimen acquisition, care, and surgical procedures

All husbandry and experimental protocols were approved by the University of Chicago IACUC (protocol #72365). Three live specimens (410 mm, 460 mm, 510 mm total length) of bowfin (*Amia calva;* Linnaeus, 1766) were obtained from the Big Muddy River in Jackson County, IL using a seine net and transported to the University of Chicago. Some molecular (Bermingham and Avise, 1986) and morphological evidence (Sinopoli, 2019) supports splitting *Amia calva* into several previously lumped synonyms, and our specimens were likely the

nominal subspecies of *A. reticulata* or *A. piquotii*. Fish were housed singly leading up to experiments and were fed worms or live feeder fish three times weekly. For ease of training and data collection, fish were temporarily housed in custom-built "tunnel tanks" (a 25 cm tall tank with a large "home" rectangle of 43 cm by 38 cm and a tunnel extension of 39 cm long by 10 cm wide) prior to and during data collection.

Fish were anesthetized with 0.06-0.15 g L^{-1} buffered MS-222 (added progressively) and surgically implanted with bone and soft tissue markers following previously reported methods (Whitlow et al., 2022). Briefly, 3-6 radio-opaque tantalum markers (1mm or 0.8mm) were implanted in each structure of interest: neurocranium, mandible, maxilla, ceratohyal, suspensorium, operculum, cleithrum, supracleithrum, and body (Fig. 3.1).

Data collection and animation

Animals were filmed feeding in the University of Chicago XROMM facility using high-speed video cameras (Xcitex XC-2M) at 500 fps and 1/1000 s shutter speed. X-Rays were generated (90-105 kV and 12.5-63 mA) and captured using two pairs of roughly orthogonal X-ray sources and image intensifiers. The elongated tunnel of the custom-built tanks (described above) was placed in the x-ray capture volume and food items were presented at the end of the tunnel. Individuals were fed live earthworms (*Lumbricus*, 7-11 cm long) and feeder fish (comet goldfish (*Carassius*) and minnows (*Pimephales*); 4-8 cm long) to test for kinematic and biomechanical differences when feeding upon evasive vs. sessile prey. Prey items were marked with 1-2 tantalum markers (1 for feeder fish, implanted just above the anal fin, 2 for worms, implanted approximately 1/4 and 3/4 down the length of the worm) to track the motion of the prey item during ingestion.

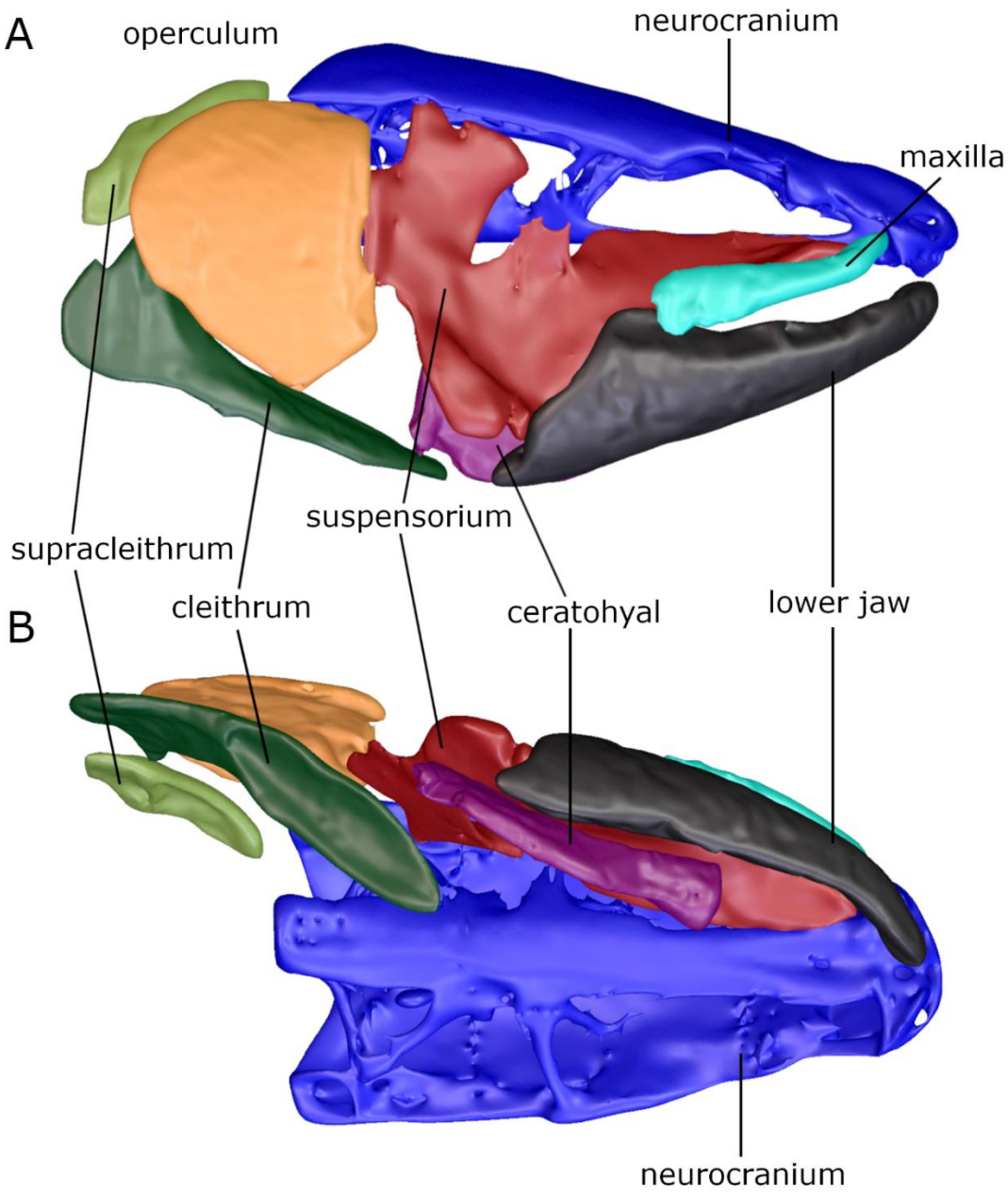

Fig. 3.1. Cranial and pectoral girdle skeletal anatomy of *Amia calva.* Anatomical diagram of the rigid body skeletal structures measured in this study, excluding body plane markers, from two views: (A) lateral and (B) ventral. Images are from live CT scans rendered in Maya.

A total of 21 feeding strikes across 3 individuals were analyzed for this study (12 on feeder fish, 9 on worms). Four of the strikes on feeder fish were unsuccessful, meaning the prey item was not captured, but these strikes displayed overall similar kinematics and are therefore included in all kinematic analyses except that of prey motion. Images were undistorted, camera positions were computed, and the XYZ positions of each tantalum marker were tracked in each feeding sequence using XMALab (version 1.5.5, Knorlein et al., 2016). Rigid body motions were calculated and filtered using a 50 Hz low-pass Butterworth filter.

Each fish was CT scanned (under MS-222 sedation; Vimago L Base version, EpicaScanner) in the University of Chicago Animal Resources Center. 3D slicer (https://www.slicer.org/; Fedorov et al., 2012) was used to segment scans and create 3D polygonal meshes of each bone for each individual, allowing precise measurement of bead placements within the bones. Maya 2018 (Autodesk, Inc., San Rafael, California) was used to place anatomical coordinate systems (ACSs) and 3D point locators on each set of meshes. To improve speed and replicability of data generation and export, the xromm-tools package (https://github.com/jdlaurence/xromm-tools) for R was used to apply rigid body transformations to each ACS and 3D point described below. To ensure data quality and accuracy, a subset of trials was animated in Maya using the XROMM Maya Tools shelf (version 2.2.3, https://bitbucket.org/xromm/xromm_mayatools/src/master/) following previously described methods (Brainerd et al., 2010; Whitlow et al., 2022).

Kinematic Analyses

Following methods described in Whitlow et al. (2022), joint coordinate systems (JCSs) were oriented along anatomical planes such that the highest degree of motion was captured by

the Z-axis (see Fig. 3.2). The Z-axes for neurocranial elevation, jaw depression, maxillary protrusion, ceratohyal depression, and cleithral and supracleithral retraction were oriented mediolaterally in order to capture rotations in the sagittal plane. Z-axes for suspensorial and opercular abduction were oriented anteroposteriorly, in order to capture rotations in a transverse plane. Neurocranial elevation was measured relative to a "body plane" formed by 5 or more markers in the body of the fish. All other bone kinematics were measured relative to the neurocranium.

We tracked the prey marker (closest to the mouth/first to cross into the oral cavity for prey with multiple markers) and calculated prey velocity and acceleration as the first and second derivatives of the Euclidean distance traveled relative to the prey's starting position (using XMALab 3D points only). Prey motions were only calculated and considered for successful strikes (8 on feeder fish, 8 on worms).

We used virtual locators placed on the tip of the ceratohyal and two locations on the cleithrum (medial and lateral edges of the ventral aspect of the bone) to approximate the length of the sternohyoideus muscle at its medial and lateral insertions, respectively. Similarly, the distance between virtual locators on the tips of the jaw and neurocranium was used to measure gape distance. All trials were standardized with time zero at the time of peak gape. Z-axis rotations and distances (gape, sternohyoid length) were standardized to a resting position of 0 (° or mm) by subtracting the mean of the first 25 frames recorded before a strike, a period with relatively little intracranial movement.

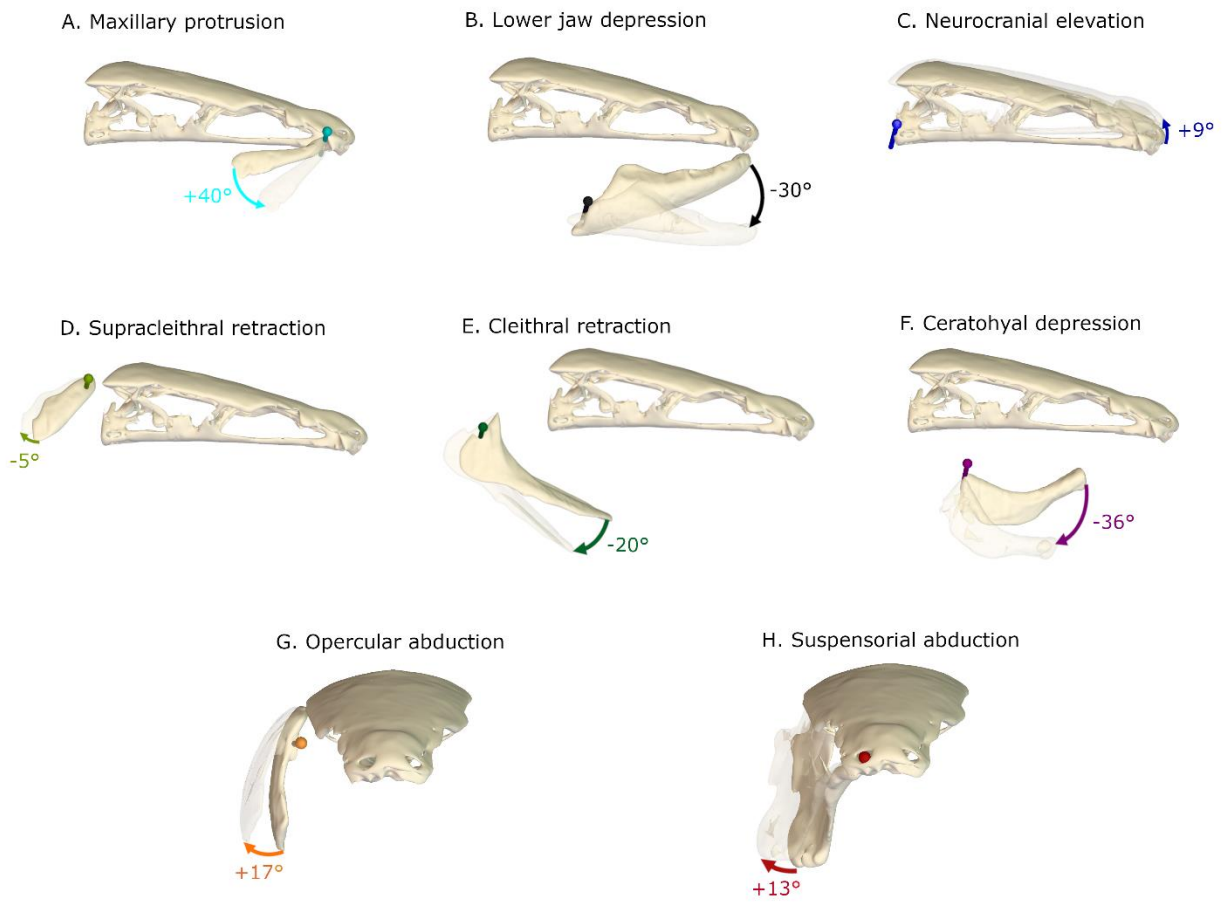

Fig. 3.2. Z-axes for each JCS used to measure primary motion captured for each bone. Colors correspond to kinematic traces shown in (Fig. 3.7 and 3.8). A-F show neurocranium and one other bone in lateral view. G and H show neurocranium and one other bone in rostral view.

Volumetric Analyses

Dynamic digital endocasts were generated using locators in one half of the oral cavity following previously established methods to measure the instantaneous volume of the oral cavity during each strike (Camp et al., 2015). In brief, the positions of these locators were exported from Maya and animated in Matlab using the xromm-tools workflow, described above. Following recently described methods (Whitlow et al., 2022), we used the

dynamicEndocastByBone package (https://github.com/jdlaurence/dynamicEndocastByBone) to calculate an alpha shape for each frame using this constellation of markers with an alpha of 2. Endocast volumes were imported back to Maya for visual confirmation of fit (see Fig. 3.3). From these endocasts we measured both the total volume achieved during a strike and the rate of volume change across each interval.

Statistical analyses

Collecting feeding strike data for two prey types allowed us to examine whether there was variation in the overall kinematic pattern; oral cavity volume expansion variables; or magnitudes, velocities, or timing of bone motions when *A. calva* were preying upon feeder fish (an evasive prey item) and worms (a sessile, and minimally evasive prey). Specifically, we calculated the following variables: peak rotation magnitude, time of peak magnitude, peak rotation velocity, onset of motion, and time of peak velocity of all z-axis rotations (jaw, maxilla, neurocranium, ceratohyal, cleithrum, supracleithrum, suspensorium, and operculum). For the jaw and ceratohyal, we also extracted the minimum velocity and time of minimum velocity, since these two bones are important drivers of the compressive phase of the strike to ensure the prey item does not escape the oral cavity. In order to reliably and reproducibly estimate onset of motion across bones with a wide range of overall rotation magnitudes, we utilized a custom R script that, for each trial, took onset as the first time point of at least 20 consecutive ms where the increase between consecutive rows was greater than 0.5% of the maximum magnitude reached for that bone in that trial.

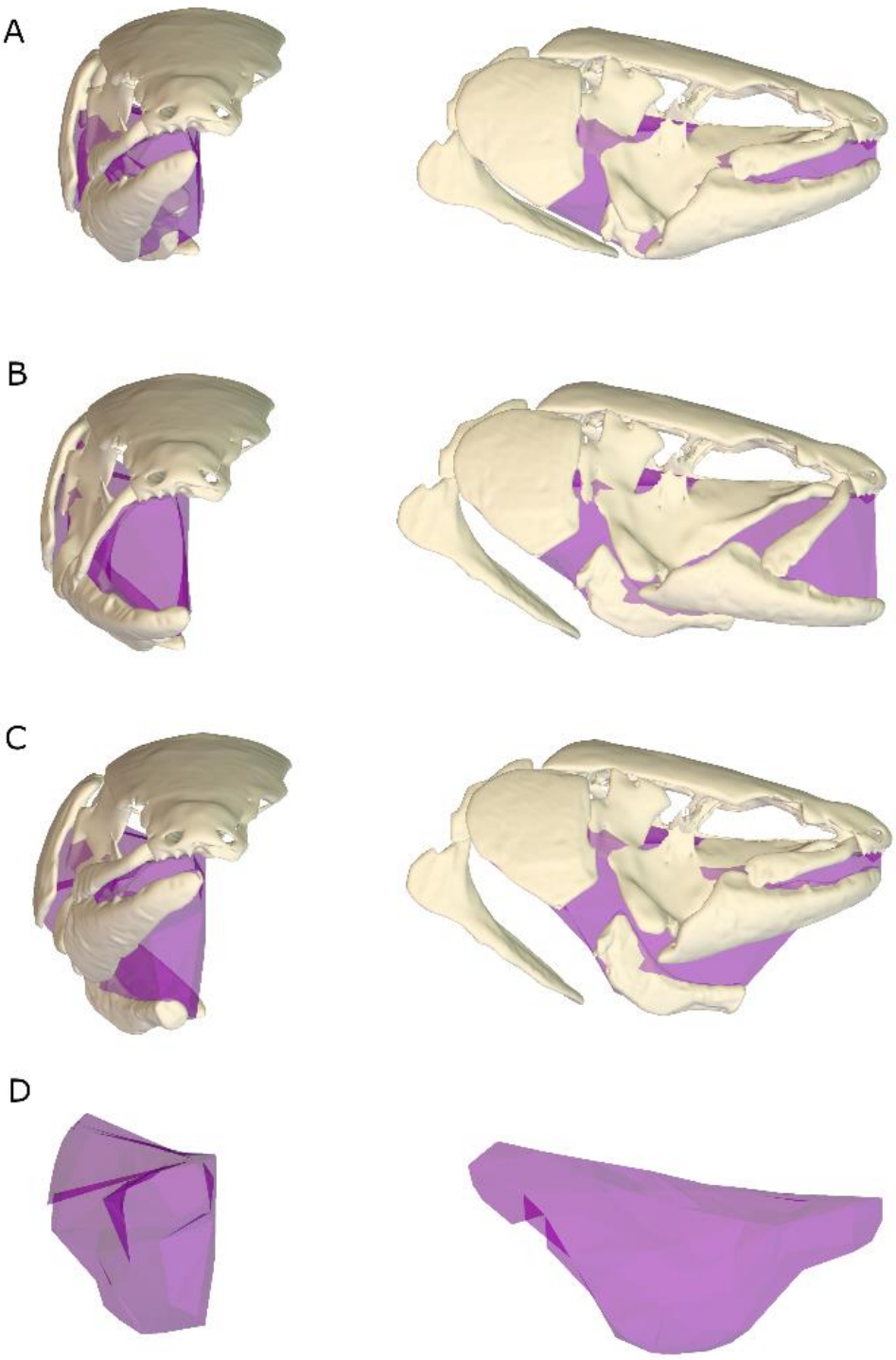

Fig. 3.3 Endocast modeling of oral cavity volume. Rostral (left) and lateral (right) views of stills from an XROMM animation with the dynamic digital endocast in purple. A) mouth closed, before strike; B) maximum gape; C) maximum oral cavity volume; and D) the endocast alone at maximum oral cavity volume.

After calculating each kinematic or timing variable (Table 1), we examined box and whisker plots for each variable by food type to gauge the amount of variability and overlap between interquartile ranges in our dependent variables. Since we measured numerous independent variables, many of which not only covary but may also be causally related, we selected a small subset of these variables that are likely to be associated with suction power or strike effort and which are not likely to be directly causally linked for further statistical analysis. Specifically, we separated velocity variables from magnitude and onset variables in our models, examining the peak rotation speed of the cleithrum, ceratohyal, and jaw separately from the onset of motion and peak magnitude of these same bones. This approach enabled us to examine the relative importance of timing and magnitude vs rate of rotations in the modulatory ability of *A. calva.* Using the R package jmv, we first tested these variables using MANCOVAs, with individual and prey type as factors and vertical position of the prey item relative to the head at the start of the strike as a covariate. Both models demonstrated no effect of the covariate prey position ($p = 0.379$ for onset + magnitude and $p = 0.764$ for velocity), so we dropped the prey position covariate from subsequent prey type analyses. Due to the potential for variability by individual we retained this in subsequent models. We separately ran two-factor ANOVAs on prey motion and oral cavity volume expansion rate to examine whether these variables were associated with prey type or individual.

Lastly, we noted substantial variation in neurocranial elevation that we hypothesized may have been due to the position of the prey item in the water column, rather than the prey type. We tested the role of prey starting position on neurocranial elevation relative to the body plane (in addition to examining prey position as a covariate for prey type variables). We used a multiple

regression model to test if the height of the prey item in the water column at the start of the strike (vertical position relative to the body plane at the time of jaw depression onset for each strike) was associated with neurocranial elevation or depression.

RESULTS

The overall kinematic pattern of *Amia calva* strikes is the classic anterior to posterior wave of motion, where jaw depression peaks first, followed by maxillary protrusion, ceratohyal depression, opercular abduction, and finally suspensorial abduction (Video 3.1). Cleithral retraction peaks shortly after the ceratohyal, while peak neurocranial elevation and supracleithral retraction were variable across strikes (Fig. 3.4). The sternohyoideus muscle shortens during cranial expansion and lengthens during cranial compression (Fig. 3.5). We found evidence of prey type effects on the onset, magnitude, and velocity of cranial motions, as well as the rate of oral cavity volume expansion, discussed below.

Kinematic pattern across Amia calva *feeding strikes*

A. calva feeding strikes start with rapid gape increase, driven by jaw depression (maximum -29.9 ± 1.81° SEM across all strikes; Table 3.1) and variable neurocranial elevation relative to the body plane. Almost immediately after peak gape, maxillary protrusion (forward swing of the distal end of the maxilla relative to the neurocranium) reaches its peak magnitude of 39.6 ± 3.51° at 2.0 ± 1.81 ms. Ceratohyal depression peaks shortly after gape, reaching a magnitude of -35.9 ± 1.89° at 21.8 ± 3.12 ms. Cleithral retraction follows ceratohyal depression, peaking to -19.6 ± 1.39° at 27.5 ± 2.91 ms. The supracleithrum was variable in peak timing, with

a small average retraction of -5.3 ± 0.61° at -12.7 ± 23.83 ms. The strike ends with lateral abduction of the operculum (peak 17.4 ± 0.91°) at 39.4 ± 4.39 ms and suspensorium (peak 12.6 ± 0.74°) at 54.1 ± 7.39 ms (Table 3.1). The prey item traveled an average total distance of 60.4 ± 5.12 mm, reaching a peak velocity of 2,871 ± 338 mm s^{-1}. The oral cavity volume reached a maximum of 87.04 cm^3 and a peak expansion rate of 610 $cm^3 ms^{-1}$.

Elevation of the neurocranium was substantial in some strikes (up to a single-strike maximum of 23.4°), but highly variable, sometimes not clearly elevating at all or even depressing (down to a single-strike maximum of -12.2°; Fig. 3.4, Fig. 3.6). The average neurocranial elevation across trials was 9.3 ± 1.44°, with the peak occurring at 22.2 ± 11.36 ms. Strikes with little to no elevation or even depression of the neurocranium were seen across prey types and in strikes from 2/3 fishes (Fig. 3.4, Fig. 3.6). A multiple regression of neurocranial elevation and depression demonstrated that maximal elevation was not associated with starting prey position ($p = 0.925$, $R^2 = -0.07$), but maximal depression was ($p = 0.03$, $R^2 = 0.245$). Examination of neurocranial elevation traces shows that the only strikes that include substantial neurocranial depression were on prey items low in the tank relative to the body plane of the fish at strike onset (Fig. 3.6). However, strikes on low prey items sometimes also resulted in high cranial elevation, and strikes on mid-column prey often did not result in clear elevation or depression (Fig. 3.6). Prey position was not statistically different across prey types ($p = 0.081$).

Table 3.1. Mean peak magnitude (°), time at peak magnitude (ms), time at motion onset (ms), of all z-axis bone rotations; length of sternohyoideus muscle (mm); prey motion (distance = mm), and maximum oral cavity volume (total = cm^3, rate of change = $cm^3\ s^{-1}$) across trials and separated by prey type.

		All trials			Feeder fish			Worm		
Lower Jaw	Peak magnitude	-29.9	±	1.80	-32.8	±	2.53	-25.6	±	1.59
	Time at peak	-0.2	±	0.35	-0.2	±	0.39	-0.2	±	0.70
	Onset	-66.2	±	6.03	-55.8	±	6.75	-81.7	±	9.04
Maxilla	Peak magnitude	39.6	±	3.51	45.5	±	3.93	32.3	±	5.57
	Time at peak	2.0	±	1.81	1.6	±	2.83	2.5	±	2.13
	Onset	-60.9	±	5.44	-51.0	±	4.80	-73.2	±	9.80
Neurocranium	Peak magnitude	9.3	±	1.44	10.1	±	1.86	7.5	±	2.40
	Time at peak	22.2	±	11.36	39.8	±	12.51	-20.0	±	15.83
	Onset	-52.7	±	9.98	-34.8	±	6.63	-95.6	±	20.21
Ceratohyal	Peak magnitude	-35.9	±	1.89	-38.7	±	2.56	-31.8	±	2.18
	Time at peak	21.8	±	3.12	25.7	±	4.89	16.0	±	1.36
	Onset	-57.4	±	5.42	-46.0	±	5.12	-74.5	±	8.25
Cleithrum	Peak magnitude	-19.6	±	1.39	-22.0	±	1.66	-16.0	±	1.86
	Time at peak	27.5	±	2.91	30.2	±	4.61	23.5	±	1.92
	Onset	-59.9	±	6.12	-49.5	±	6.17	-75.5	±	10.31
Supracleithrum	Peak magnitude	-5.3	±	0.61	-6.5	±	0.66	-3.2	±	0.75
	Time at peak	-12.7	±	23.83	20.7	±	23.64	-62.7	±	44.05
	Onset	-70.8	±	19.99	-56.9	±	16.80	-96.3	±	46.90
Operculum	Peak magnitude	17.4	±	0.91	18.3	±	1.27	16.1	±	1.22
	Time at peak	39.4	±	4.39	35.0	±	4.10	46.0	±	8.99
	Onset	-33.4	±	4.44	-26.5	±	4.89	-43.7	±	7.20
Suspensorium	Peak magnitude	12.6	±	0.74	12.8	±	1.11	12.5	±	0.92
	Time at peak	54.1	±	7.39	56.8	±	9.98	50.0	±	11.47
	Onset	-57.6	±	14.94	-33.8	±	7.63	-93.2	±	32.77
Medial Sternohyoideus	Peak stretch	3.1	±	0.24	3.3	±	0.32	2.7	±	0.37
	Peak shorten	-1.1	±	0.17	-0.9	±	0.15	-1.6	±	0.31
Lateral Sternohyoideus	Peak stretch	1.7	±	0.27	2.1	±	0.36	1.1	±	0.31
	Peak shorten	-2.2	±	0.37	-2.0	±	0.44	-2.6	±	0.66
Prey Item	Peak distance	60.41	±	5.231	55.52	±	5.391	65.31	±	9.02
	Time peak dist.	127.13	±	23.768	142.50	±	38.981	111.75	±	28.878
Maximum Volume	Total Volume	87.0	±	2.16	88.1	±	3.27	85.7	±	2.81
	Rate of Volume Change	610	±	38.5	678	±	56.4	526	±	33.8

Table 3.2 Peak velocity (mm s^{-1}) of all z-axis bone rotations and prey across trials and separated by prey type.

		All trials			Feeder fish			Worm		
Lower Jaw	Peak dep. vel.	1767	±	196	2220	±	247	1088	±	78
	Peak elev. vel.	-1899	±	178	-2053	±	241	-1668	±	256
Maxilla	Peak velocity	2546	±	391	3150	±	573	1640	±	259
Neurocranium	Peak velocity	581	±	76	681	±	103	341	±	29
Ceratohyal	Peak dep. vel.	1675	±	146	1965	±	200	1241	±	75
	Peak elev. vel.	-1143	±	129	-1240	±	191	-997	±	146
Cleithrum	Peak velocity	858	±	71	1005	±	87	638	±	67
Supracleithrum	Peak velocity	658	±	77	805	±	88	439	±	102
Operculum	Peak velocity	1172	±	104	1425	±	117	794	±	81
Suspensorium	Peak velocity	995	±	91	1141	±	127	774	±	82
Prey Item	Peak velocity	2871	±	338	3165	±	401	2577	±	562

Both the medial and lateral portions of the sternohyoideus muscle (SH) shorten and lengthen at different times during the strike (Fig. 3.5), though the magnitude and timing vary substantially across trials (but not with prey type). The medial SH shortens to -1.2 ± 0.17 mm before peak gape, at -35.4 ± 26.21 ms and lengthens to 3.1 ± 0.27 mm at 108.2 ± 20.34 ms. The lateral SH shortens to -2.2 ± 0.37 mm before peak gape, at -4.6 ± 14.8 ms and lengthens to 1.7 ± 0.27 mm at 58.8 ± 35.8 ms.

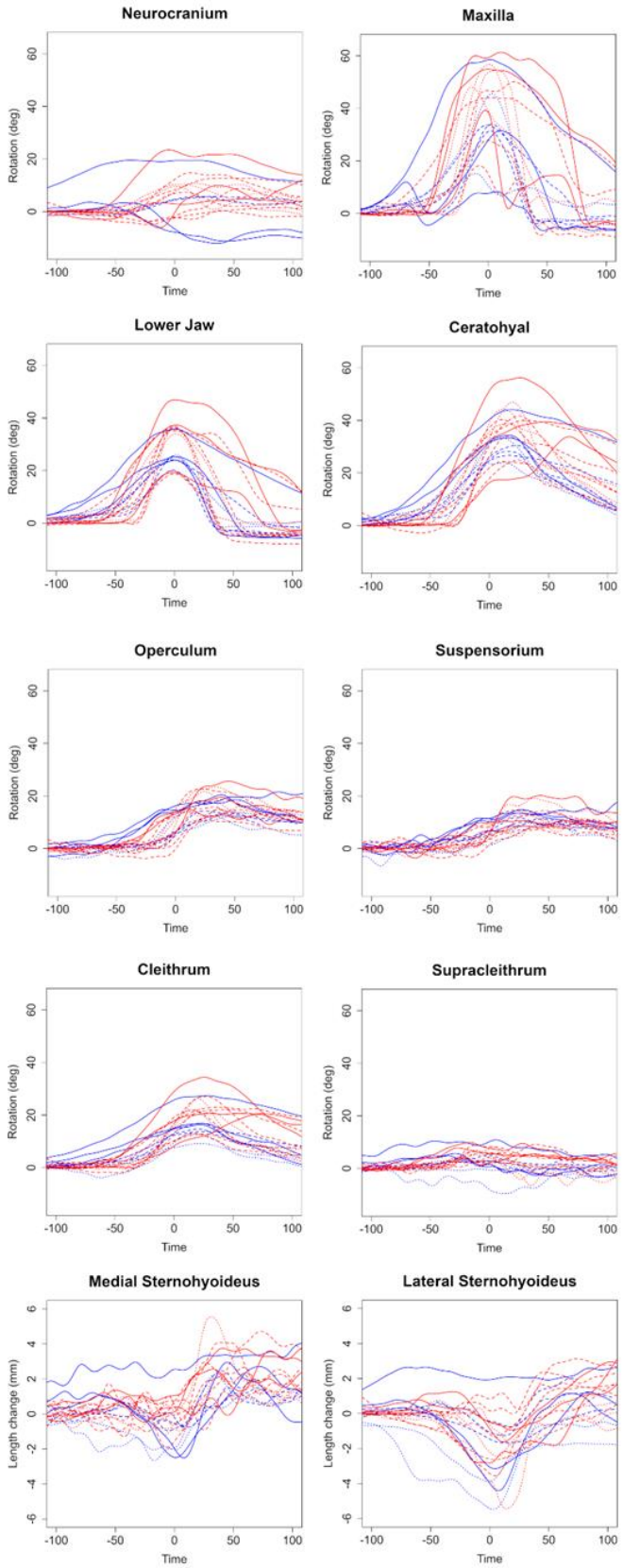

Fig. 3.4 Variability in kinematics across strikes. Individual trial kinematic traces for neurocranial elevation, maxillary protrusion, jaw depression, ceratohyal depression, opercular abduction, suspensorial abduction, cleithral retraction, supracleithral rotation, medial sternohyoideus length change, and lateral sternohyoideus length change. All rotations were zeroed to average resting position by subtracting average motion during the first 25 frames recorded.

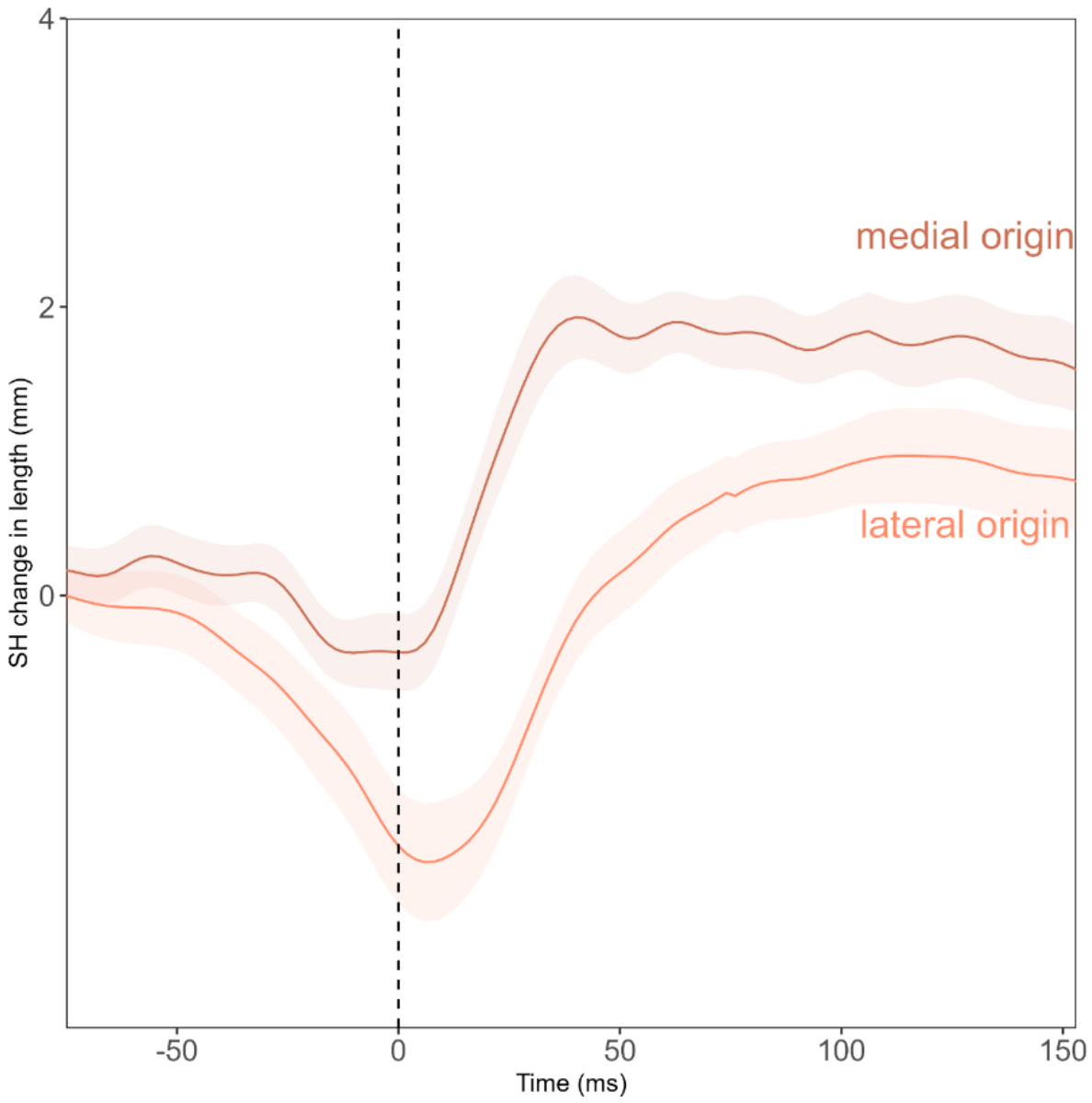

Fig. 3.5 Mean (± s.e.m.) sternohyoideus muscle length changes across all strikes. Shortening distance was calculated as the length relative to the first 25 frames of a recording, a period of relatively little intracranial movement, prior to strike onset. The "lateral origin" muscle length refers to the distance between lateral-most point of sternohyoideus origination on the cleithrum and its insertion on the ceratohyal, while "medial origin" refers to the distance between the medial-most point of sternohyoideus origination on the cleithrum and its insertion on the ceratohyal. The same insertion point was used for both measurements, as the muscle is broad at its origination and narrows to its insertion. Vertical line denotes peak gape (0 ms).

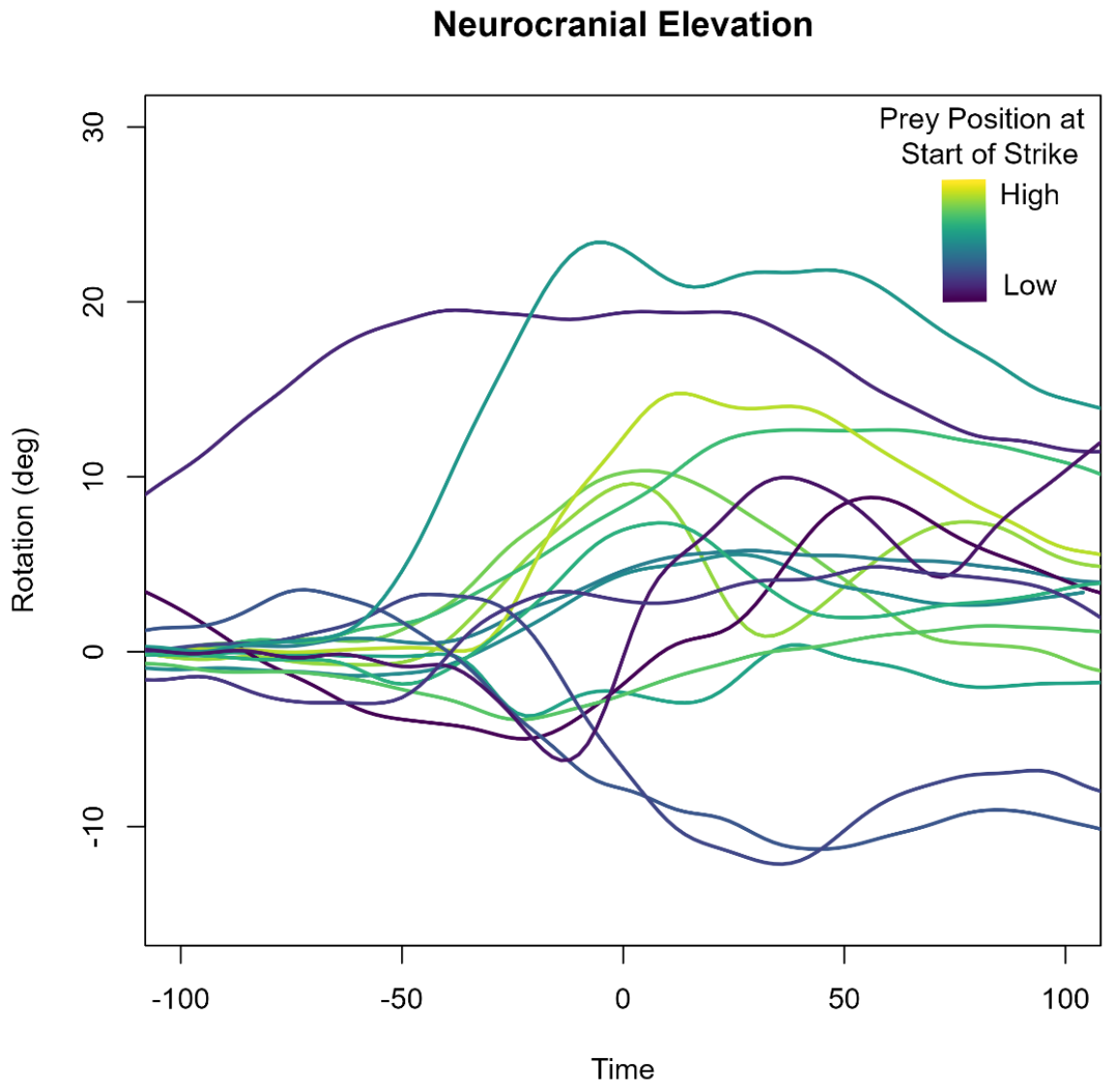

Fig. 3.6. Neurocranial elevation variability colored by starting position of prey item. Prey position was calculated as the vertical distance between the prey and the body plane of the predator at the onset of jaw rotation. Lower prey items (negative start position) are shown as darker lines, while prey mid-column are medium/greens, and prey above the predator are shown in lighter lines. Prey position was significantly associated with peak neurocranial depression (negative rotation) but not with peak elevation (positive rotation).

Prey type effects

The central result of this study is that there are highly significant differences in the velocity of cranial kinesis, hyoid motion, and pectoral girdle kinematics between strikes on evasive and non-evasive prey types by *Amia calva* (Fig. 3.7 and Fig. 3.8). A MANOVA of peak jaw, ceratohyal, and cleithral velocity found a significant prey type effect ($p = 0.001$), but no individual or individual*prey effects ($p > 0.2$). We separated velocity from onset and magnitude variables for statistical testing, as the timing and magnitude of a rotation relate strongly to its velocity. A MANOVA of peak jaw, ceratohyal, and cleithral onset and magnitude was nearly significant for prey type effects ($p = 0.057$) and for an individual effect ($p = 0.051$), but not for individual*prey effects ($p = 0.71$). Subsequent univariate tests for this model show that the onsets of each variable were significantly associated with food type ($p < 0.03$) but peak magnitudes were only significant for cleithrum ($p = 0.026$), not jaw ($p = 0.085$) or ceratohyal ($p = 0.057$).

Oral cavity volume reached a similar overall peak, but expanded faster in strikes on feeder fish, achieving a higher maximum rate of volume change in strikes on feeder fish ($p = 0.029$) (Table 3.1). Rate of oral cavity volume expansion was also statistically different across individuals ($p = 0.024$), but with no individual*prey type effect ($p = 0.295$). Peak prey velocity did not differ significantly by prey type ($p = 0.062$) or individual ($p = 0.729$).

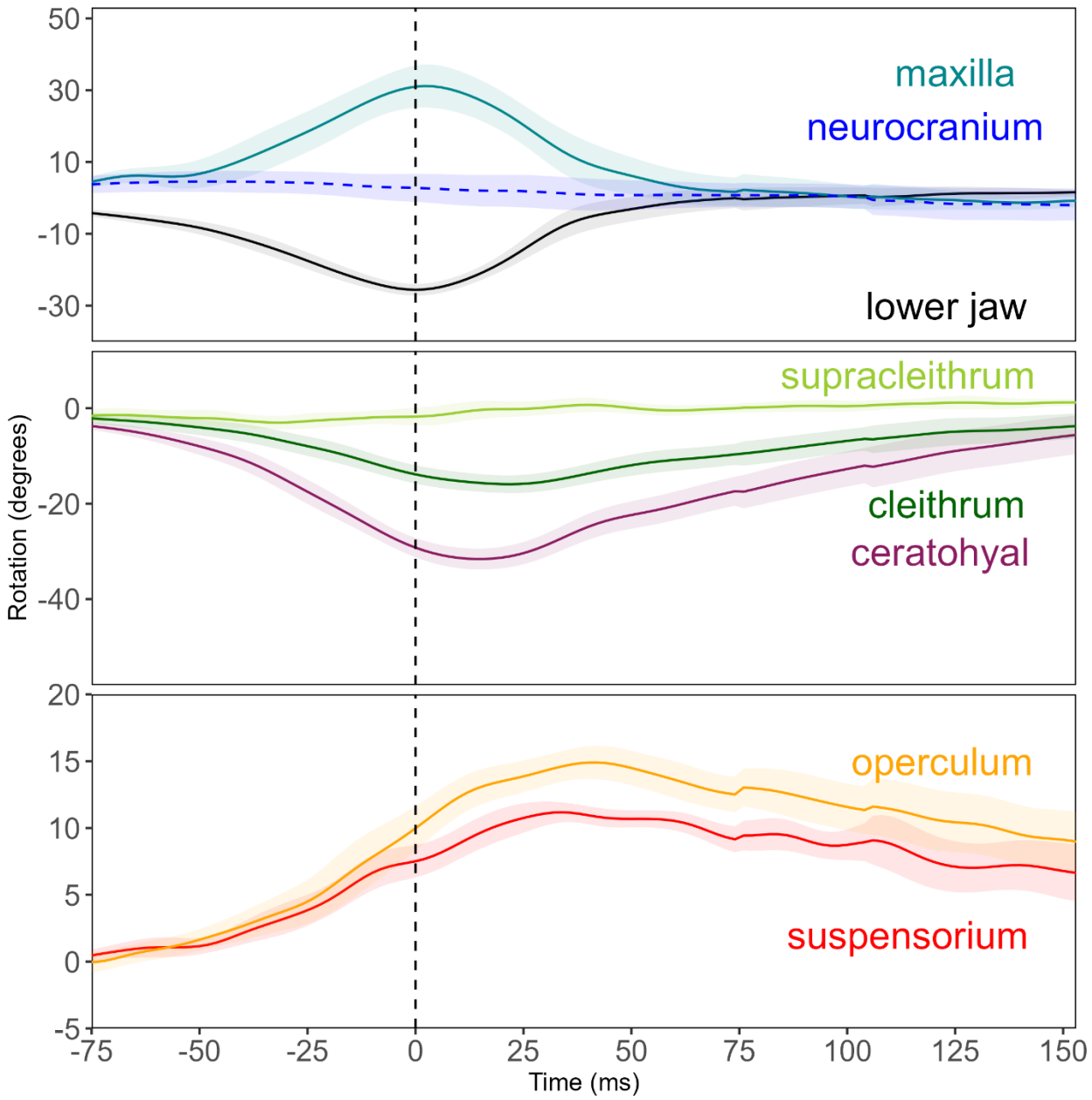

Fig. 3.7. Mean primary axis rotations from worm strikes. Shows mean ± SEM of z-axis rotations (largest axis of expected rotation) of bones from tracked strikes on worms across three individuals (5 trials for neurocranium, 8 for all other variables). Axes measured shown in Fig. 3.2: maxillary protrusion, lower jaw depression, neurocranial elevation, supracleithral retraction, cleithral retraction, ceratohyal depression, opercular abduction, and suspensorial abduction. All rotations were zeroed to average resting position by subtracting average motion during the first 25 frames recorded. Dashed line (neurocranium) was measured relative to a body plane and solid lines were measured relative to the neurocranium. Vertical line denotes peak gape (0 ms).

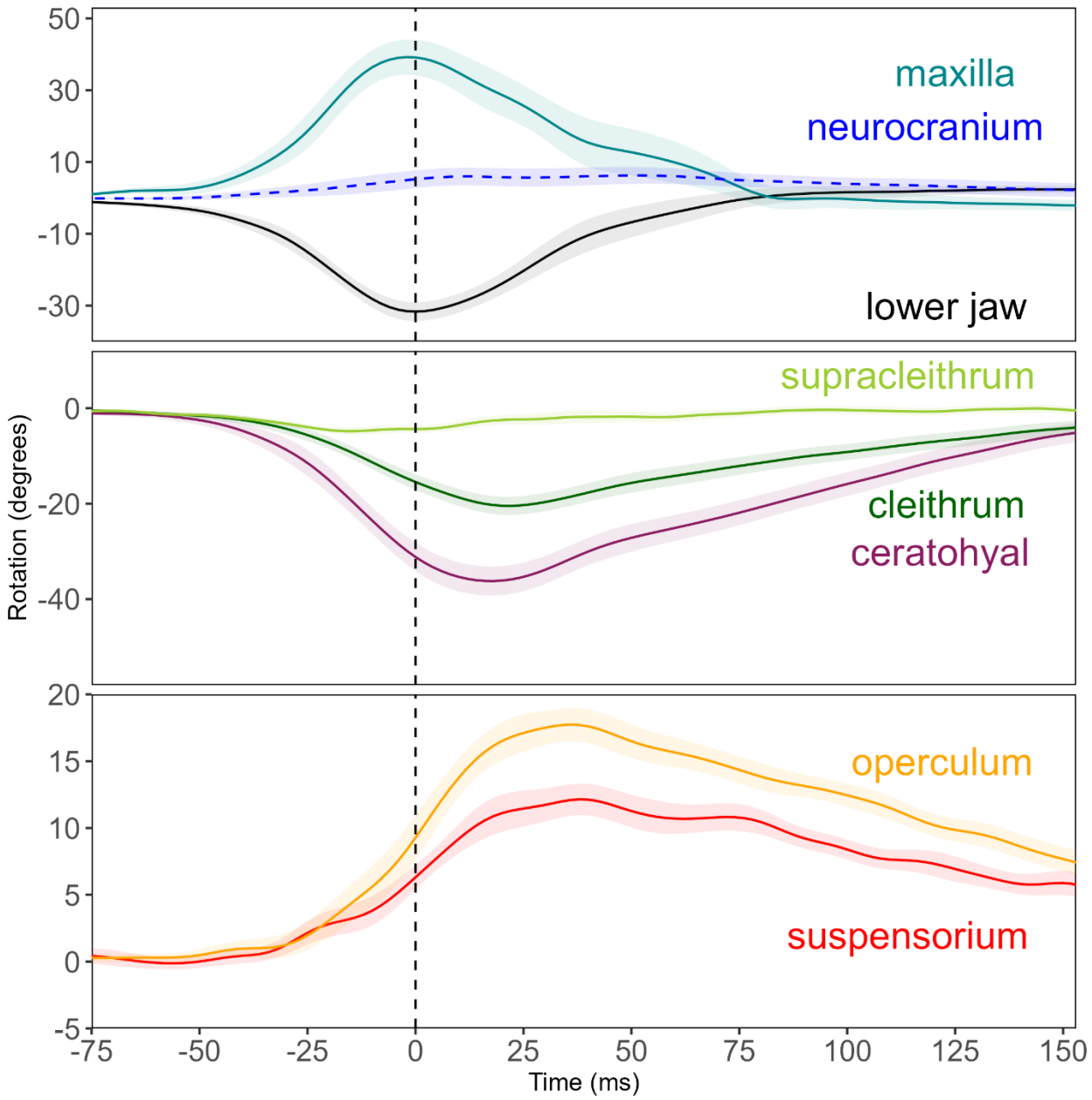

Fig. 3.8. Mean primary axis rotations from feeder fish strikes. Shows mean ± SEM of z-axis rotations (largest axis of expected rotation) of bones from tracked strikes on feeder fish across three individuals (10 trials for maxilla, 12 for all other variables). Axes measured shown in Fig. 3.2: maxillary protrusion, lower jaw depression, neurocranial elevation, supracleithral retraction, cleithral retraction, ceratohyal depression, opercular abduction, and suspensorial abduction. All rotations were zeroed to average resting position by subtracting average motion during the first 25 frames recorded. Dashed line (neurocranium) was measured relative to a body plane and solid lines were measured relative to the neurocranium. Vertical line denotes peak gape (0 ms).

DISCUSSION

The overall kinematic pattern of feeding strikes in *Amia calva* is similar to that of other fish species, with an anterior to posterior wave of motion where jaw depression peaks first, followed by maxillary protrusion, ceratohyal depression, opercular abduction, and finally suspensorial abduction. This pattern is maintained in strikes on differing food types, specifically worms and feeder fish, both of which are live prey items commonly consumed by wild *A. calva.* However, significant differences in skeletal element rotation magnitude, timing, and velocity were found for several kinematic variables across food types. These differences demonstrate that feeding strikes are highly variable in *Amia calva* and the ability of vertebrates to substantially modulate their feeding mechanics may be a primitive trait for bony fishes, or even jawed vertebrates.

Prey type effects on strike kinematics

This study demonstrates that the peak velocity of the lower jaw, ceratohyal, and cleithral rotations are all significantly higher in strikes on feeder fish than in strikes on worms. This difference is primarily driven by a later onset (i.e., shorter duration strike) of these motions in feeder fish strikes, although the cleithrum reaches a significantly higher magnitude, jaw and ceratohyal magnitudes did not vary significantly with prey type at current sample sizes. As all strikes were aligned to peak gape, an early onset is due to an overall greater strike duration for worm strikes. This means that while most bones may not have reached a significantly higher

overall magnitude for either prey type, they reached the same magnitudes over a longer period of time (i.e., a slower strike) when eating worms.

The peak magnitude of ceratohyal depression differed between prey types, but at current samples sizes the difference was not statistically significant ($p = 0.057$). Interestingly, changes in sternohyoideus muscle length throughout a strike did not differ between prey types. This implies that the observed increases in pectoral girdle retraction and ceratohyal depression in strikes on feeder fish are driven by greater shortening of the axial musculature, which is then transferred through the rotating cleithrum and a shortening sternohyoideus. This may account for the discrepancy between the current study and a previous investigation of *A. calva* feeding strikes, which described them to be invariant to the presented prey item (Lauder, 1980), but did not measure activity in the body musculature for this species.

Strikes on worms may produce less suction force than strikes on feeder fish, because the expansion of the oral cavity is happening at a slower rate. The present study found a significantly higher rate of oral cavity volume expansion in feeder fish strikes than worm strikes, though the total volumes reached were comparable across prey types (Table 1). Indeed, studies measuring oral cavity pressure during suction feeding strikes have shown pressure varies substantially by prey type, and therefore by presumed predator motivation (Ferry-Graham et al., 2001b; Lauder and Lanyon, 1980; Nemeth, 1997a). We did not find statistical differences in the induced velocity of feeder fish vs. worms in this study, but this comparison is complicated by the varying shape and weight of the prey items (i.e., the long, slender worms may travel faster or further per unit force applied than the broader, rounder feeder fish).

Numerous studies have found similar effects, such as higher attack speeds and greater cranial expansion when feeding on elusive prey (Ferry-Graham et al., 2001b; Nemeth, 1997b). Evidence even suggests that at least in piscivorous predators, sensory feedback about the prey position (Aerts, 1990) and attempted escape responses (Van Wassenbergh and De Rechter, 2011) are integrated to alter the kinematics of a strike. Indeed, experiments have shown altered kinematics in fishes and sharks in response to lateral line and visual sensory deprivation (Gardiner and Motta, 2012; Gardiner et al., 2017), though these manipulations do not definitively demonstrate whether such sensory information is only utilized by the predator *a priori* or if the predator may alter kinematics mid-strike in response to sensory feedback. Both possibilities fall under our broad definition of modulation, and we therefore term changes based on incoming sensory information that is actively integrated to alter a behavior once it is underway to be feedback modulation, specifically.

Researchers have worked to understand, define, and discuss the many ways variance can be partitioned and understood. The degree to which an animal consistently changes their behavior for different stimuli, here referred to as modulation (Matott et al., 2005), is distinct from the degree to which trials under the same set of conditions vary, termed stereotypy (Wainwright et al., 2008). We note that both of these phenomena exist on a sliding and relative scale, rather than being binary states. Here, we find evidence that *A. calva* can modulate their strikes substantially by shifting the velocity and timing of cranial rotations for evasive vs. non-evasive prey and that their strikes may be less stereotyped in general than previously proposed. Specifically, there is a relatively high degree of variance within the same set of experimental conditions (i.e., prey type) in the current dataset (Table 3.1), and these differences are further not

accounted for by individual fish. Factors like the position of the prey item relative to the sides of the tank or other unmeasured factors may be additional inputs that *A. calva* use to modulate strike kinematics.

Similar findings have been recorded in other fishes, like bluegill, who alter their kinematics and force produced despite consistent experimental controls (Holzman et al., 2007). Furthermore, the ability to modulate feeding patterns appears to be ubiquitous across vertebrates, ranging from primates (Iriarte-Díaz et al., 2011; Vinyard et al., 2008) and other mammals (Ross et al., 2007b) to lizards (Montuelle et al., 2009; Montuelle et al., 2012a) and sharks (Ferry-Graham, 1998; Matott et al., 2005). Naturally, the behaviors employed by these species range from suction feeding to capture prey to biting and chewing to process food, and the goal of these behaviors varies greatly. The coordination patterns employed to achieve these behaviors likely also vary within taxa or even individuals (see Olsen et al., 2019, for example). This demonstrates a widespread ability of vertebrates to modulate feeding behavior in a variety of circumstances and with a diversity of goals.

Additional kinematic variation across A. calva *feeding strikes*

We found substantial variation that was not accounted for by prey type effects, in addition to the modulation for prey type described above. Specifically, neurocranial elevation relative to the body plane was inconsistent across strikes on both worms and feeder fish. The neurocranium elevated in just over half of strikes where it was measured, but in several strikes it either did not elevate notably, or even depressed relative to the body plane (Fig. 3.4). This effect was not significantly associated with prey type or individual fish, but is, in part, associated with the starting position of the predator relative to the prey. Specifically, we hypothesized that if the

prey item is low in the tank, the predator may orient the body and head downwards and reduce cranial elevation to ensure prey capture. We tested this by calculating the vertical position of the prey relative to the body plane of the predator at the onset of the strike and found that peak neurocranial depression was significantly associated with prey position, though neurocranial elevation was not.

We found that while the two strikes with dramatic neurocranial depression were on prey items low in the water column, *A. calva* also used high cranial rotation on some strikes at prey below their body (Fig. 3.6; dark lines). Furthermore, this figure shows that several strikes on prey items level with or above the predator resulted in little to no neurocranial elevation (light lines; Fig. 3.6). We further verified that this variation did not affect our prey type effect results by including prey position as a covariate in our initial models and by confirming that prey position was not significantly associated with prey type ($p > 0.05$). This is because feeder fish were able to choose their position in the water column, sometimes hovering near the bottom of the tank, and worms were dropped in from above the tank, sometimes being captured by the predator mid-water column.

The substantial variation seen in neurocranial elevation and depression relative to the cranium is another line of evidence that *A. calva* are able to modulate their feeding strikes. Not only do they employ faster kinematics for evasive prey, but they also may shift from elevating the cranium to depressing depending on the position of the prey item in the water column. While we did not quantify additional information about the predator's approach in this study, such variables would be useful in understanding differences in suction feeding behavior in future

studies. Indeed, previous studies have found that predator approach is an important factor in variation across feeding strikes (Longo et al., 2016; Moran et al., 2018).

Ventral expansion in A. calva *feeding strikes*

This study expands upon a growing body of work demonstrating the variation in and importance of the body musculature and sternohyoideus muscle in generating and directing forces transferred through the pectoral girdle to the ventral cranium during suction feeding strikes. The sternohyoideus muscle connects the anterior hyoid arch to the ventral pectoral girdle, along the cleithrum, and while it's thought to be consistently active during feeding strikes, it may not contribute much power, if any to complex hyoid motions that are central to generating suction through ventral expansion of the oral cavity (Camp et al., 2015; Whitlow et al., 2022).

In some fishes, such as largemouth bass, clariid catfishes, and bichirs, the sternohyoideus muscle contracts but maintains a consistent length as the pectoral girdle retracts and the ceratohyals depress (Camp and Brainerd, 2014; Camp et al., 2015; Van Wassenbergh et al., 2005; Van Wassenbergh et al., 2007; Whitlow et al., 2022). These are cases where this muscle is described as ligament-like and the power generated is attributed solely to the hypaxial musculature. In other groups, like one clariid catfish, bluegill sunfish, and striped surfperch, the sternohyoideus may shorten in addition to transferring power from the body muscles, a case where it is said to have a bifunctional role in feeding strikes (Camp et al., 2018; Lomax et al., 2020; Van Wassenbergh et al., 2007). In the present study, we assign a bifunctional role to the sternohyoideus muscle, although its contributions were variable across strikes. While on average the sternohyoideus shortened near peak gape and then lengthened during the compressive phase of the strike (Fig 3.4), it did not shorten substantially in all strikes.

Relative cranial mobility in A. calva *and comparisons with* Polypterus bichir

P. bichir kinematics, described in the previous chapter of this thesis, follow the same anterior to posterior wave of motion seen here (Whitlow et al., 2022). Fig. 3.8 demonstrates the primary rotation magnitude and timing for *A. calva* strikes on feeder fish only and is therefore comparable to Fig. 2.3 (care was taken to align the JCSs in a homologous manner, though there may still be artifacts when comparing Tait Bryan angles taken on morphologically distinct specimens). Strikes in *Amia* show a similar degree of jaw depression and lateral abduction in the suspensorium and operculum when compared with *P. bichir*. However, neurocranial elevation is highly variable and much lower in *Amia*, even in strikes with a strong and clear neurocranial elevation (Fig. 3.4). Furthermore, *A. calva* utilize a lower degree of hyoid depression and cleithral retraction than *P. bichir*. We hypothesize that the mobile maxilla of *Amia* allows for the suction forces generated to be directed more efficiently towards a prey item, enabling similar suction forces with a slightly less mobile skull (though we did not explicitly measure suction force or power in this study, the prey items consumed by *A. calva* reached higher raw speeds than those of *P. bichir*).

Conclusion

This study expands our knowledge of the evolution of suction feeding kinematics in fishes, demonstrating that *A. calva* utilize similar kinematics to other non-teleost fishes, but with increased maxillary mobility to effectively direct suction forces towards a prey item. They further utilize a bifunctional sternohyoideus muscle and modulate their strike velocity and duration to successfully feed on different prey types. This work has implications for the neural control of strikes, suggesting that the ability to at least select between two or more pre-

programmed strikes existed prior to the evolution of teleosts. While we were unable to examine the exact nature of the neural control of strike modulation (*a priori* strike selection vs. mid-strike integration based on sensory feedback), the extent of variation seen in neurocranial elevation and sternohyoideus length changes suggests that *Amia calva* may integrate peripheral sensory information to alter their strike kinematics. Combined with evidence demonstrating modulation of feeding mechanics in tetrapods, gars, teleosts, and sharks, we conclude that the ability to modulate strikes is likely common to gnathostomes.

CHAPTER 4: QUANTIFYING THE CONTRIBUTION OF CRANIAL BONES TO ORAL CAVITY VOLUME CHANGE DURING SUCTION FEEDING: A COMPARATIVE STUDY IN LUNGFISH, BICHIR, BOWFIN, AND KNIFEFISH

ABSTRACT

Many fishes use suction feeding, driven by rapid expansion of the oral cavity, to capture prey. Computational fluid and geometric approaches can model water flow patterns and oral cavity volume change in live feeding animals, enhancing our understanding of the forces driving successful suction feeding. Here, we measured the role of individual skeletal elements in driving oral cavity shape and volume change with a combination of XROMM and dynamic endocast modeling. We used an iterative bone freezing approach to quantify the role of each bone's motion in expanding the oral cavity, not allowing the bone to move relative to the neurocranium for short rolling intervals across the strike. The ratio of volume change when a bone is frozen to the overall volume change quantifies the relative contribution to volume change (RCVC) of cranial bones animated in an XROMM dataset (Whitlow et al., 2022). Volumetric and RCVC data for *Chitala blanci*, *Amia calva*, *Polypterus bichir*, and *Protopterus annectens* are used to compare the skeletal elements driving successful suction feeding in these morphologically distinct taxa. *P. annectens* have a highly fused, relatively immobile cranium with suction driven by the jaws and ceratohyal. *P. bichir* have higher cranial mobility with a mobile suspensorium and operculum enabling lateral expansion of the skull, but their ceratohyal is the primary driver of rapid volume change. *A. calva* has lower hyoid mobility and a stronger role of the lower jaws, and *C. blanci* are laterally compressed and drive volume change with the suspensorium and operculum. We use these species to examine the importance of bone

morphology and mobility in estimating RCVC data. We hypothesized that the jaw and ceratohyal would have the highest RCVCs across taxa, with the jaw peaking first and ceratohyal after peak gape/ We further explore the inclusion of mobile elements of the pectoral girdle to define the posterior oral cavity boundary and find that the placement of endocast markers may dramatically influence the measurement of RCVC values and interpretations of how oral cavity volume change is generated.

INTRODUCTION

Actinopterygian skulls are highly complex and kinetic musculoskeletal systems, enabling rapid expansion of the oral cavity to draw prey into the mouth via suction feeding. Suction is achieved through increases in the volume of the oral cavity via precisely coordinated neurocranial elevation, suspensorial and opercular flaring, jaw and hyoid depression, and premaxillary protrusion, although the relative contribution or importance of each of these motions to successful suction feeding is poorly understood. This progressive anterior to posterior wave of volume increase creates a pressure gradient between the mouth and surrounding water, pulling a bolus of water, hopefully containing a prey item, into the oral cavity. The prey item is frequently then snagged on teeth or gill rakers to prevent escape, while the jaws close and the operculum opens to allow the water to continue flowing out through the gills.

Fishes can achieve successful suction generation in a variety of ways, and importantly, not all species that suction feed show the same degree of mobility in each skeletal element. For example, bowfin (*Amia calva*) expand their skulls relatively evenly in all directions: laterally, dorsoventrally, and anteriorly, while slingjaw wrasses (*Epibulus insidiator*) emphasize anterior expansion by throwing the oral jaws forward. In alligator gar (*Atractosteus spatula*) and

polypterid fishes the maxillae and premaxillae (or lacrimal maxillae) are immobile relative to the cranium and suspensorium (Allis, 1922), removing anterior expansion from their suction feeding repertoire, yet they are successful suction feeders and follow the classic anterior-to-posterior wave of skull expansion (Lauder, 1980; Lemberg et al., 2019; Whitlow et al., 2022). In these fishes with dorsoventrally flattened skulls, previously unappreciated degrees of lateral expansion, alongside high mobility in the hyoid arch, are responsible for oral cavity expansion following suction initiation through flat-plate suction (Lemberg et al., 2019; Whitlow et al., 2022). Other taxa have skulls compressed laterally, such as the uniquely shaped knifefishes, which are thought to power suction through lateral mobility and neurocranial elevation, driven by extensive epaxial musculature (Li et al., 2022). In perhaps the most mobility-limited suction feeders, lungfishes, the highly fused skulls do not appear to allow for lateral expansion, meaning that suction forces are driven by the jaws, hyoid, and pectoral girdle (Gartner et al., 2022).

Each axis of mobility increases sub ambient pressure by expanding the volume of the buccal cavity, increasing the rate or magnitude of forces imparted on a water bolus. However, the extent to which each bone contributes to this increase in oral cavity volume has yet to be investigated: in this study we quantified how (and how much) each mobile element in the skull contributes to the generation of suction.

A common approach to investigating mechanisms of suction generation is to quantify the association between musculoskeletal kinematics and suction strength, via proxies like pressure change or particle image velocimetry (Bishop et al., 2008; Camp and Brainerd, 2014; Higham et al., 2005; Holzman et al., 2007; Jacobs and Holzman, 2018; Muller and Osse, 1984; Svanbäck et al., 2002; Van Wassenbergh and Aerts, 2009). These studies have emphasized the importance of precise timing (Holzman et al., 2007), orientation (Higham et al., 2006) and proximity to prey

(Ferry et al., 2015) for the success of a suction feeding event. Researchers have also modeled the oral cavity volume throughout a strike using a variety of cone-like shapes (Muller and Osse, 1984; Muller et al., 1982) and elliptical cylinders based on lateral and ventral videos (Bishop et al., 2008; Van Wassenbergh and Aerts, 2009). The X-ray Reconstruction of Moving Morphology (XROMM) workflow (Brainerd et al., 2010) enables precise tracking of prey (Provini et al., 2022; Weller et al., 2020) and modeling of the bones that bound the oral cavity volume (Camp et al., 2015), providing precise and consistent quantifications of the shape of the oral cavity and rate of volume change throughout a strike. XROMM can also be used to generate a model that can be manipulated in a data-driven way to understand how the motion of these bones impacts oral cavity volume change, and recent increases in taxonomic and morphological diversity of fishes whose feeding has been animated using XROMM sets us up to ask interesting questions about how impacts to oral cavity volume change across species.

Here we use XROMM to model oral cavity volume change and iteratively freeze bone's motion relative to the neurocranium for short intervals, measuring each bone's impact on volume change during feeding strikes using recently developed methods (Whitlow et al., 2022). Briefly, using the measured impacts, we calculate each bone's relative contribution to overall oral cavity volume change (RCVC), explicitly testing the contribution of main aspects of cranial motion to oral cavity volume change throughout a strike. The neurocranium is excluded because it serves as a reference bone for freezing the rest of the cranial elements (i.e., the motion of each other bone follows the neurocranium during that bone's freeze intervals, but the neurocranium cannot be frozen relative to itself). Specifically, we compare *Protopterus annectens*, *Polypterus bichir*, *Amia calva*, and *Chitala blanci*, morphologically distinct species across a broad range of the vertebrate phylogeny.

Our primary goal is to understand which components of cranial kinesis are most important for changing oral cavity volume. We investigated this question by comparing RCVC traces across four species with unique morphologies and different levels of cranial kinesis to understand how these factors impact the important contributors to oral cavity volume expansion. We hypothesized that the jaw and ceratohyal would have the highest RCVCs across taxa, with the jaw peaking first and ceratohyal after peak gape. However, the extreme lateral compression of *C. blanci* means that in this species the suspensorium and operculum may play a larger role than in the other species.

We also examined RCVC at a specific time-point of interest, the peak rate of oral cavity volume expansion, to explore which bones play a key role in generating suction. We expected a large contribution from the ceratohyal at this time-point in all species, though again we hypothesized that *C. blanci* might also have a higher contribution from laterally mobile elements. Finally, we explored RCVC measurements both with and without the contribution of the cleithrum (where feasible) to understand how extending the measured endocast volume posteriorly impacts our results. We hypothesized that including the cleithrum would reduce the RCVC of the ceratohyal more than that of other bones, as these bones are directly connected by the sternohyoideus muscle and their motions are strongly temporally associated.

METHODS

We used motion data that were collected from other kinematics studies. All data for *Amia calva* (see Chapter 3) and *Protopterus annectens* (Gartner et al., 2022), along with most data for *Polypterus bichir* (Whitlow et al., 2022), were collected at the University of Chicago XROMM facility, under husbandry and experimental protocols approved by the University of Chicago

IACUC (protocol #72365). The full dataset for *Chitala blanci* (Li et al., 2022) and a subset of two strikes for *P. bichir* were collected at the Brown University Keck Facility under Brown University IACUC approval. *P. bichir*, *A. calva*, and *C. blanci* were all recorded striking at feeder fish, while *P. annectens* were striking at living worms. Animal sizes may be found in Table 4.1.

Table 4.1. Individual fish sizes included in the study, all listed in mm.

Chitala blanci (SL)	*Polypterus bichir* (SL)	*Amia calva* (TL)	*Protopterus annectens* (TL)
356	235	410	480
308	230	460	540
433	250	510	

Details of surgical protocols, animal care, and data collection can be found in published work (Gartner et al., 2022; Li et al., 2022; Whitlow et al., 2022). In brief, fish were implanted with radio-opaque tantalum markers in bones of interest under MS-222 anesthesia. In all fish, the lower jaw, ceratohyals, and neurocranium were implanted. In *P. bichir*, *C. blancii*, and *A. calva*, the suspensorium, operculum, and cleithrum were implanted as well. In *C. blancii* and *A. calva*, the maxilla was implanted as it is mobile relative to the cranium in these groups. All data were collected using biplanar x-ray videography, and XMALab (Knorlein et al., 2016) was used to remove image distortion, compute camera positions, and track tantalum markers in each sequence. CT scans of each fish were used to generate 3D meshes of the bones and to check subsequent animations.

XROMM animations were generated using varying methods for the four species considered here. Data from lungfish and bichir were animated fully using rigid body transformations from XMALab, Maya (Autodesk, Inc., San Rafael, California) and the XROMM

Maya Tools shelf (https://bitbucket.org/xromm/xromm_mayatools/src/master/) (Gartner et al., 2022; Whitlow et al., 2022). Rigid body motions for knifefish were calculated using the 'matools' R package (Olsen, 2019b) and subsequently applied to skeletal bone meshes in Maya (Li et al., 2022). *Amia* data were exported using the 'xromm-tools' R package (https://github.com/jdlaurence/dynamicEndocastByBone), which applies rigid body motions calculated in XMALab to ACSs and locators placed on skeletal meshes in Maya, enabling automation of the data export process (described in Chapter 3 of this thesis). Several trials were spot checked using full Maya visualization for accuracy.

Endocasts were generated using locators in one half of the oral cavity following previously established methods (Camp et al., 2015), described in detail for each species in their respective papers. The positions of these endocast locators were then exported from Maya (animated for all species but *Amia*, *Amia* animated in R). Endocast volumes computed for each hemi-volume were doubled to estimate the full buccal cavity volume.

All trials were aligned to peak gape at time 0 ms, though definitions of peak gape vary slightly by species. For bichir and bowfin, peak gape is defined as the raw linear distance between the tip of the neurocranium and the tip of the lower jaw. For lungfish, peak gape is defined as the peak z-axis rotation (in sagittal planes) between the upper and lower jaws. Finally, for knifefish, peak gape was defined as "as the maximum gape distance directly following the rapid increase in gape during the start of the strike" and was calculated by choosing the first instance of major inflection in gape distance using a 10% threshold of maximum rate of gape change (Li et al., 2022).

Volumetric analysis:

We used a dynamic digital endocast to measure the instantaneous volume of the oral cavity by attaching locators to the oral surfaces of the animated cranial bones in Maya (*sensu* Camp et al., 2015). These locator positions were then imported into Matlab (R2020a) and their positions over time were calculated using rigid body transformations in the xromm-tools package (https://github.com/jdlaurence/xromm-tools). We then used the dynamicEndocastByBone package to calculate an alpha shape for every frame using the constellation of locators and an alpha of 2.

Following methods described in Whitlow et al. (2022) we calculated the impact of each bone by freezing that bone relative to the neurocranium on a rolling basis throughout the strike and comparing the "frozen volume" to the volume measured in the actual strike. The duration of the rolling freeze interval was determined by examining the rate of volume change curves across a series of intervals to check for over-smoothing and time-shifts. The intervals varied depending upon species strike durations (approximately 10% of strike duration) and data collection settings and were as follows: *P. bichir* 5 frames or 10 ms, *A. calva* 15 frames or 30 ms, *C. blanci* 5 frames or 10 ms, and *P annectens* (20 frames or 40 ms). All volumetric data were smoothed using a three-frame moving average filter.

The instantaneous relative contribution to volume change (RCVC) of the *i*th bone ($RCVC_{Bone_i}$) is represented by the following equation:

$$RCVC_{Bone_i} = \frac{\Delta V_{Full} - \Delta V_{FrozenBone_i}}{\sum_{j=1}^{n} \left| \Delta V_{Full} - \Delta V_{FrozenBone_j} \right|}$$

Where for a given time increment: ΔV_{Full} is the change in endocast volume without any bones frozen, $\Delta V_{FrozenBone_{i/j}}$ is the change in endocast volume with the *i*th or *j*th bone frozen, and n is the number of bones frozen (i.e., does not include the neurocranium).

Due to high degrees of noise because of relatively little motion before and after the strike, we trimmed each dataset prior to extracting peak magnitudes and timings. For *Polypterus,* strikes were trimmed from -35 ms to 50 ms relative to peak volume, for *Chitala,* strikes were trimmed from -50 ms to 50 ms, *Amia* strikes were trimmed from -75 ms to 75 ms, lungfish from -250 ms to 250 ms.

For each species, we measured the significance of each bone's RCVC using a one-way ANOVA both across each strike and at a key time point within each strike. Specifically, we first compared the maximum RCVC for each bone in each trial. We then calculated the time at the highest rate of volume expansion for each trial and compared the RCVC values for each bone at that time point. We examined any significant results using post-hoc Tukey HSD tests to determine which bones' RCVCs were different for a given species and treatment. Across species, we qualitatively compare the progression of RCVC peaks and the meaningful contributors to expansion at the peak rate of volume change. However, we do not statistically compare RCVC values across species because of the unique anatomy and differing bone numbers in each taxon.

Soft tissue analysis using contrast-enhanced µ-CT

A high-resolution µ-CT scans of a contrast-enhanced *Polypterus* specimen was reconstructed to examine soft tissues bounding the oral cavity. Specimen was immersed in a 2.5% phosphomolybdic acid (PMA) solution (weight by volume) and set to mix on an orbital shaker at room temperature until adequately penetrated (17 days total). The PMA solution was

refreshed periodically and the container was covered with foil to prevent photoreaction. Following staining, specimens were scanned at the University of Chicago Paleo-CT facility using a GE Phoenix v|tome|x 240 kv/180 kv scanner (http://luo-lab.uchicago.edu/paleoCT.html) and segmented using a combination of automated thresholding and manual segmentation in 3D slicer (https://www.slicer.org/; Fedorov et al., 2012).

RESULTS

RCVC without cleithrum

In lungfish, we see that the jaws contribute steadily to oral cavity volume early in the strike, with a maximal RCVC of 0.94 ± 0.019 at -138 ± 13.21 ms (Table 4.2). The ceratohyal contributions slowly take over well before peak gape (Fig. 4.1B), reaching a peak of 0.988 ± 0.003 at -33.3 ± 14.33 ms. The ceratohyal reached a significantly higher RCVC than that of the lower jaw ($p = 0.0135$), regardless of time point. The highest rate of volume change was 30.7 ± 2.27 cm s^{-1} and occurred at -64.5 ± 13.48 ms (Fig. 4.1A, Table 4.2). At the peak rate of volume change across trials, the ceratohyal RCVC was 0.73 ± 0.035, while the lower jaw RCVC was only 0.25 ± 0.039 ($p < 0.00001$).

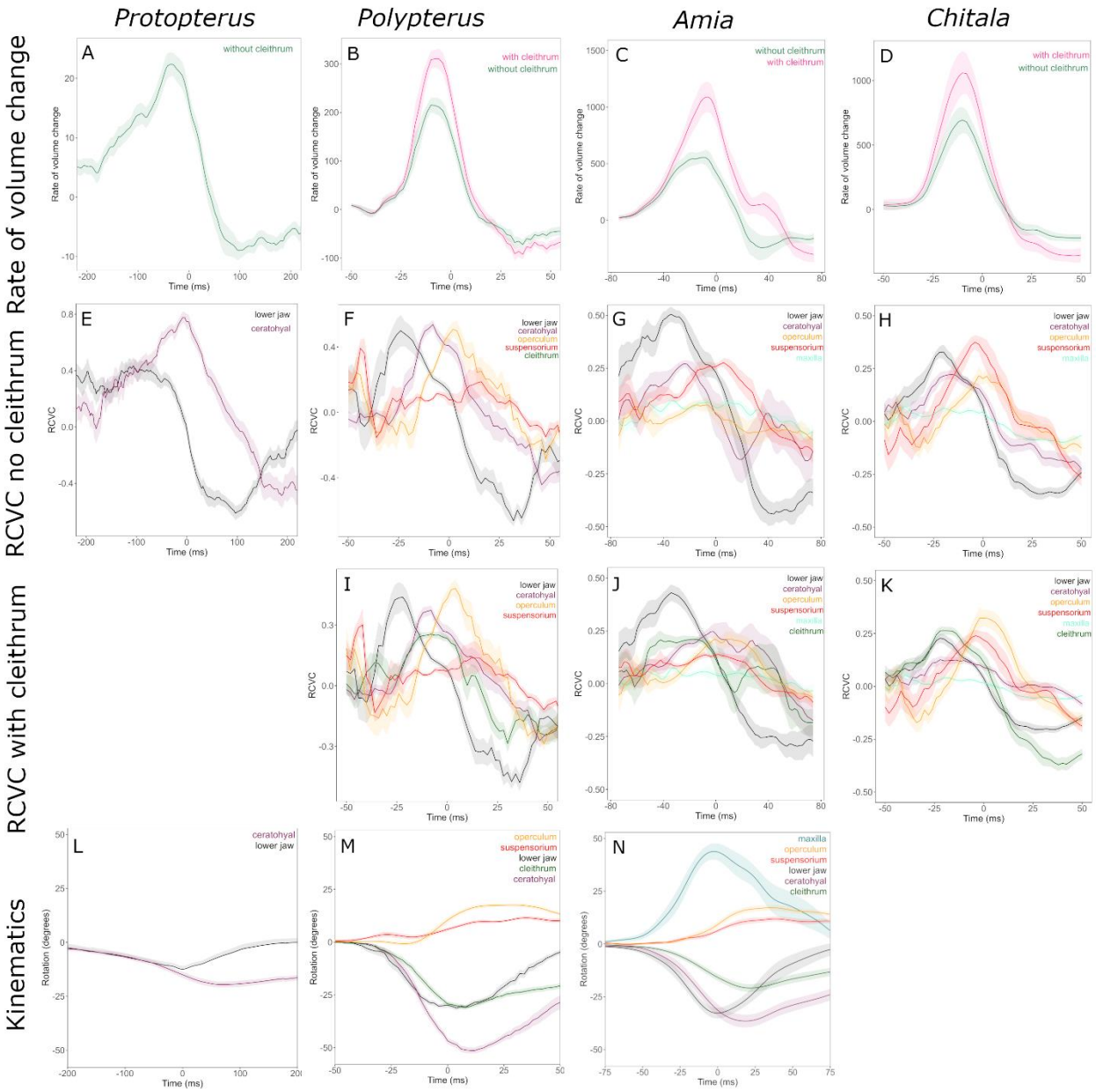

Fig. 4.1. Rate of volume change, RCVC with and without cleithrum, and kinematics of all species. (A-D) Rate of volume change, without cleithrum (green) and with cleithrum (pink) where applicable. (E-F) RCVC without the cleithrum included. (I-K) RCVC with the cleithrum included. (L-N) Kinematics measured, where applicable. All lines show mean ± SEM of strikes, with trials centered to peak gape (0 ms). Data for *Protopterus annectens* (A, E, L) are from two individuals; 36 strikes total and are reproduced with permission from Gartner et al (2022). Data for *Polypterus bichir* (B, F, I, H) are from two individuals; 7 strikes for suspensorium (red), 11 strikes for operculum (orange), 13 for all other variables and are reproduced with permission from Whitlow et al (2022). Data for *Amia calva* (C, G, J, N) are from 3 individuals; 10 strikes total. Data for *Chitala blanci* (D, H, K) are from 3 individuals; 23 strikes total and are reproduced with permission from Li et al (2022).

Table 4.2. Volume Expansion Rate and Bone RCVC peaks and timings without cleithrum.

		Expansion Rate ($cm^3 s^{-1}$)	Lower Jaw RCVC	Ceratohyal RCVC	Operculum RCVC	Suspensorium RCVC	Maxilla RCVC
Polypterus	Peak magnitude	259 ± 20.3	0.76 ± 0.039	0.63 ± 0.028	0.65 ± 0.066	0.48 ± 0.063	- ± -
	Time at peak	-9.8 ± 1.21	-20.3 ± 6.06	-4.9 ± 3.18	1.6 ± 3.72	-6.6 ± 6.94	- ± -
	Magnitude at peak expansion rate	- -	0.26 ± 0.024	0.50 ± 0.011	0.25 ± 0.021	0.06 ± 0.009	- ± -
Chitala	Peak magnitude	873 ± 106	0.52 ± 0.023	0.37 ± 0.019	0.44 ± 0.031	0.56 ± 0.020	0.21 ± 0.022
	Time at peak	-8.7 ± 2.43	-28.1 ± 2.36	-19.8 ± 3.18	-7.9 5.55	-3.1 ± 3.48	-25.3 ± 3.47
	Magnitude at peak expansion rate	- -	0.14 ± 0.013	0.19 ± 0.017	0.20 ± 0.013	0.43 ± 0.020	0.03 ± 0.008
Protopterus	Peak magnitude	30.7 ± 2.27	0.94 ± 0.018	0.99 ± 0.003	- -	- -	- -
	Time at peak	-64.5 ± 13.48	-137.7 ± 13.21	-33.3 ± 14.33	- -	- -	- -
	Magnitude at peak expansion rate	- -	0.25 ± 0.039	0.73 ± 0.035	- -	- -	- -
Amia	Peak magnitude	678 ± 56	0.61 ± 0.027	0.47 ± 0.047	0.26 ± 0.039	0.43 ± 0.016	0.22 ± 0.029
	Time at peak	-16.2 ± 3.37	-42.4 ± 8.20	-16.8 ± 14.21	-17.6 ± 12.92	-18.2 ± 11.08	-11.6 ± 13.80
	Magnitude at peak expansion rate	- -	0.38 ± 0.027	0.23 ± 0.039	0.09 ± 0.013	0.18 ± 0.021	0.11 ± 0.036

In bichir the relative contribution to volume change (RCVC) of the lower jaw reached the highest peak of 0.76 ± 0.039 first in the strike at -20.3 ± 6.06 ms (Table 4.2). The ceratohyal RCVC peaked later in the strike and contributed slightly less to instantaneous volume change (Fig 4.1F), reaching a peak of 0.63 ± 0.028 at -4.9 ± 3.18 ms. The operculum RCVC reached the latest peak of 0.65 ± 0.065 at 1.6 ± 3.72 ms, and the suspensorium reached the lowest peak RCVC of 0.48 ± 0.063 shortly before peak gape at -6.6 ± 6.94 ms. The rate of volume change peaked at -9.8 ± 1.21 ms (Fig 4.1B, Table 4.2), and at this time point the ceratohyal's RCVC was 0.497 ± 0.0111, significantly higher than all other bones ($p < 0.0001$). The lower jaw and operculum (which were not statistically different, $p = 0.965$) contributed 0.26 ± 0.024 and 0.25 ± 0.021, respectively, while contributions from the suspensorium were smallest at 0.059 ± 0.009.

In bowfin the lower jaw RCVC peaks highest and earliest in the strike (Fig. 4.1G), reaching 0.61 ± 0.027 at -42.4 ± 8.20 ms (Table 4.2), significantly higher than other bones' peaks ($p < 0.04$). The remaining cranial bones all contribute to smaller degrees, with the ceratohyal RCVC peaking at 0.47 ± 0.047 at -16.8 ± 14.21 ms, the suspensorium peaking at 0.43 ± 0.016 at -18.2 ± 11.08 ms, the operculum peaking at 0.26 ± 0.039 at -17.6 ± 12.92 ms, and the maxilla peaking at 0.22 ± 0.029 at -11.6 ± 13.8 ms. Rate of volume change peaked at 678 ± 56 cm s^{-1} at -16.2 ± 3.37 ms (Fig. 4.1C, Table 4.2). At this time, the jaw has the highest RCVC of 0.38 ± 0.027, statistically different from all other variables ($p < 0.005$). The ceratohyal has an RCVC of 0.23 ± 0.039, statistically higher than the operculum and maxilla at peak rate of volume change ($p < 0.04$). The suspensorium's RCVC at peak rate of volume change is 0.176 ± 0.021 and is not statistically different from the contributions of the operculum or maxilla.

In knifefish we see an initial high lower jaw RCVC (Fig 4.1H), peaking at 0.52 ± 0.023 at -28.1 ± 2.36 ms (Table 4.2), that is quickly overtaken by the suspensorium. The suspensorium

reaches the highest overall RCVC, peaking at 0.56 ± 0.02 at -3.1 ± 3.48 ms, and is statistically higher than all other bones' peaks except the lower jaw ($p < 0.01$). The ceratohyal RCVC also overtakes the lower jaw prior to peak gape, reaching a lower overall peak of 0.37 ± 0.019 at -19.8 ± 3.18 ms. The opercular RCVC overtakes the ceratohyal RCVC right around peak gape but does not overtake the suspensorium until well into the compressive phase. The operculum reaches an overall peak RCVC of 0.44 ± 0.031 at -7.9 ± 5.55 ms. Rate of volume change peaked to 873 ± 106 cm s^{-1} at -8.7 ± 2.43 ms (Fig. 4.1D, Table 4.2). At this time, the suspensorium contributes the most to volume change with an RCVC of 4.29 ± 0.02, statistically different from all other bones ($p < 0.0001$). The operculum and ceratohyal are distant seconds, with RCVCs of 0.2 ± 0.013 and 0.19 ± 0.017 at peak rate of volume change, respectively, statistically higher than the maxilla ($p < 0.0001$). The RCVC of the operculum is also higher than the RCVC of the jaw at this point ($p = 0.049$). The jaw RCVC is next at 0.14 ± 0.013 and is significantly higher than the small maxillary contributions ($p < 0.00001$) of 0.027 ± 0.008.

RCVC with cleithrum

In bichir, when including the cleithrum the RCVC pattern is similar, but with a necessary decrease in RCVC magnitudes across all bones and a steeper decrease in ceratohyal RCVC (Fig. 4.1F and Fig. 4.1I). Patterns of which bones drive the peak rate of volume expansion do not change (Table 4.2, Table 4.3). The lower jaw peaks at 0.64 ± 0.037 first in the strike, at -26.8 ± 1.64 ms (Table 4.3), a peak higher than that of all other bones ($p < 0.01$). The cleithrum is second, peaking at 0.37 ± 0.027 at -10.3 ± 3.77 ms. Next, the ceratohyal peaks at 0.45 ± 0.016 at -3.5 ± 3.98 ms, just before peak gape. The operculum peaks last, at 0.59 ± 0.043 at 5.6 ± 2.6 ms. The suspensorial peak is noisy, reaching its by trial peak of 0.39 ± 0.051 at -15.7 ± 5.27 ms. The peak rate of volume change is 365 ± 26.7 cm^3 s^{-1} and occurs at -8.8 ± 1.21 ms, both larger and

slightly later than when the cleithrum is not considered as a part of the oral cavity volume. At this time point, the ceratohyal RCVC is still highest at 0.36 ± 0.015 and statistically higher than all other bones ($p < 0.0001$). The cleithrum and operculum contribute equally at peak rate of volume change, with RCVCs of 0.25 ± 0.011 and 0.25 ± 0.017, respectively, and are statistically different from all other bones ($p < 0.0001$). The jaw contributes 0.15 ± 0.013, a higher contribution than the suspensorium's RCVC of 0.05 ± 0.009 at this time ($p < 0.001$).

In bowfin including the cleithrum does not substantially affect the RCVC curves (Fig. 4.1G, Fig. 4.1J), but it does shift the rate of oral cavity volume change peak later in the strike (Fig. 4.1C, Table 4.3), and therefore shifts the primary drivers of this peak rate. The lower jaw still peaks first and highest, to an RCVC of 0.48 ± 0.033 at -40.8 ± 4.34 ms (Table 4.3). The cleithrum is next, reaching a peak RCVC of 0.40 ± 0.047 at -15.2 ± 15.34 ms. The ceratohyal RCVC is the same, reaching a peak of 0.40 ± 0.04, but later in the strike, at 13.8 ± 6.85 ms. The opercular RCVC peaks near maximum gape, reaching 0.34 ± 0.022 at -1 ± 9.58 ms. The suspensorium and maxilla are highly variable in their peak timing, reaching maximal RCVCs of 0.28 ± 0.03 at -28.2 ± 12.54 and 0.17 ± 0.029 at -15.4 ± 14.56, respectively. As in *Polypterus*, the peak rate of volume change is larger and later when the cleithrum is included, reaching 1165 ± 154 $cm^3\ s^{-1}$ at -6.4 ± 2.27 ms. At this time the contributions of the ceratohyal, cleithrum, lower jaw, and operculum are all similar (0.18 - 0.23) and statistically indistinguishable from one another ($p > 0.05$). The suspensorium and maxilla are lower, at 0.13 ± 0.013 and 0.05 ± 0.012, respectively.

Table 4.3. Volume Expansion Rate and Bone RCVC peaks and timings with cleithrum.

		Expansion Rate (cm3 s-1)	Lower Jaw RCVC	Ceratohyal RCVC	Cleithrum RCVC	Operculum RCVC	Suspensorium RCVC	Maxilla RCVC
Polypterus	Peak mag.	365 ± 26.7	0.64 ± 0.037	0.45 ± 0.016	0.37 ± 0.027	0.59 ± 0.043	0.39 ± 0.051	- ± -
	Time at peak	-8.8 ± 1.21	-26.8 ± 1.64	-3.5 ± 3.98	-10.3 ± 3.77	5.6 ± 2.60	-15.7 ± 5.27	- ± -
	Mag. at peak exp. rate	- ± -	0.15 ± 0.013	0.36 ± 0.015	0.25 ± 0.011	0.25 ± 0.017	0.05 ± 0.009	- ± -
Chitala	Peak mag.	1303 ± 176	0.37 ± 0.027	0.25 ± 0.021	0.36 ± 0.018	0.54 ± 0.027	0.40 ± 0.023	0.14 ± 0.017
	Time at peak	-8.0 ± 2.35	-29.0 ± 2.48	-22.3 ± 4.48	-19.8 ± 3.05	0.9 ± 4.19	-18.3 ± 4.38	-30.9 ± 3.03
	Mag. at peak exp. rate	- ± -	0.08 ± 0.011	0.11 ± 0.014	0.20 ± 0.014	0.27 ± 0.020	0.30 ± 0.023	0.02 ± 0.005
Amia	Peak mag.	1165 ± 154	0.48 ± 0.033	0.40 ± 0.040	0.40 ± 0.047	0.34 ± 0.022	0.28 ± 0.030	0.17 ± 0.029
	Time at peak	-6.4 ± 2.27	-40.8 ± 4.34	13.8 ± 6.85	-15.2 ± 15.34	-1.0 ± 9.58	-28.2 ± 12.54	-15.4 ± 14.56
	Mag. at peak exp. rate	- ± -	0.18 ± 0.025	0.23 ± 0.022	0.21 ± 0.015	0.20 ± 0.028	0.13 ± 0.013	0.05 ± 0.012

In *Chitala*, including the cleithrum expands the posterior oral cavity volume boundaries drastically, making the operculum a primary driver of lateral, and overall, volume expansion (vs. the suspensorium only in treatments without the cleithrum; Fig. 4.1H and Fig. 4.1K). The maxillary RCVC peaks first and is lowest, reaching 0.14 ± 0.017 at -30.9 ± 3.03 ms ($p < 0.01$; Table 4.3). Its followed immediately by the lower jaw, which reaches a peak RCVC of 0.37 ± 0.027 at -29 ± 2.48 ms. Next, the ceratohyal peaks to 0.25 ± 0.021 at -22.3 ± 4.48 ms. The cleithrum reaches a higher peak RCVC of 0.36 ± 0.018 at -19.8 ± 3.05 ms. Next the suspensorium peaks to 0.4 ± 0.023 at -18.3 ± 4.38 ms. Finally, the operculum peaks the highest, reaching an RCVC of 0.54 ± 0.027 at 0.9 ± 4.19 ms ($p < 0.001$). Peak rate of volume change is higher, at 1303 $cm^3 s^{-1}$, but occurs at roughly the same time as when the cleithrum is not considered, -8 ± 2.35 ms (Fig. 4.1D). At this time, the suspensorium still drives volume change with an RCVC of 0.3 ± 0.023 but is not statistically different from the opercular RCVC of 0.27 ± 0.02 ($p = 0.842$). These two bones' RCVCs are both higher than the next highest, the cleithrum, which reaches 0.2 ± 0.14 at peak rate of volume change ($p < 0.02$). The ceratohyal, jaw, and maxillary RCVCs are all quite low at this time point; 0.11 ± 0.014, 0.08 ± 0.011, and 0.02 ± 0.005, respectively.

DISCUSSION

All species show a high lower jaw RCVC indicative of flat plate suction early in the strike (Fig. 4.1, Table 4.2, Table 4.3). In lungfish and bichir, this is followed by a ceratohyal RCVC peak that overlaps and drives the period of rapid volume expansion. The drivers of peak volume expansion for knifefish and bowfin depend on whether the cleithrum is included.

RCVC without cleithrum

In all four species examined here, the lower jaw has the highest RCVC at the beginning of the strike, as gape increase is the first component of oral cavity volume expansion. In all species but *Amia*, the ceratohyal overtakes the jaw RCVC before peak gape. In knifefish, the suspensorium quickly overshadows the jaw and ceratohyal, while in bichir the ceratohyal has a clear peak prior to being overtaken by the opercular and suspensorial RCVCs. In species with a mobile maxilla, the maxillary RCVCs remained relatively low across the strike, never rising above 0.2.

These RCVC traces give us important insight into the contributions each bone has for overall oral cavity volume change that we cannot glean from kinematic traces alone. For example, maxillary protrusion relative to the cranium in *Amia calva* is substantial, averaging up to 60° in some strikes (Chapter 3), but it does not directly contribute much to overall volume expansion (Fig. 4.1). Meanwhile, the suspensorial rotations in *C. blanci* are relatively small but this bone overshadows all others in knifefish RCVC due to its large size as these fish are very laterally compressed and dorsoventrally tall.

The primary drivers of peak rate of volume expansion vary across species. In lungfish, the peak rate of volume expansion is driven by both the lower jaw and ceratohyal, with a higher overall peak from the ceratohyal. In bichir, the peak rate of volume expansion is driven primarily by the ceratohyal. In bowfin the lower jaw appears to drive expansion during this time, while in knifefish the suspensorium contributes the highest RCVC during peak rate of volume expansion.

Role of bone morphology and mobility

Both the morphology of a bone and its relative mobility have implications for the degree to which it may drive relative volume changes in the oral cavity volume. This is perhaps an intuitive property of RCVC measurements – bones that are larger or move more should expand the oral cavity more than other bones. However, the details of RCVC give us a unique insight into the details of such mechanisms. First, it is not just the relative size of a bone, but specifically its surface area facing the buccal cavity that matters for an increased role in oral cavity volume change. For example, in *Amia* the lower jaw is quite robust, with a large cross-sectional area (likely to enable the high bite strength of this species). However, only a relatively small proportion of the bone, on its medial aspect facing the tongue and oral cavity, is modeled with the dynamic endocast. On the other hand, a relatively flat bone with low cross-sectional area, such as the suspensorium, will have a higher impact for its total size. While we did not directly measure the impact of bone surface area in this study, it is represented by the area covered by the locators in the animations, and this would be a useful avenue for future work aiming to further understand ways that RCVC may be impacted and utilized. Second, researchers may introduce bias in the way that bones are measured and must take care to place virtual points consistently across individuals and taxa. The virtual point constellations utilized to create the endocast must be applied carefully and the resultant alpha shapes scrutinized, as they can strongly influence the shape of the endocast in a way that may not always be expected or realistic. Lastly, the mobility of a bone also plays a substantial role in determining the RCVC. For instance, in *Amia* the ceratohyal is relatively larger than that of *Polypterus*, but because it does not undergo as drastic

of motions as it does in *Polypterus*, the ceratohyal plays a lesser role in expanding the oral cavity volume for *Amia* strikes.

Inclusion of the cleithrum

When the cleithrum is included as the posterior bound of the oral cavity, notable shifts in patterns may occur. In *Amia* and *Polypterus* the lower jaw still has the highest RCVC at the beginning of the strike, but in *Chitala* the cleithral RCVC is also very high at the same time point when included (Fig. 4.1). The point at which the ceratohyal peaks is muddied by the inclusion of the cleithrum, but it still overtakes the jaw RCVC before or at peak gape. In knifefish, the suspensorium and operculum quickly overshadow the jaw, ceratohyal, and cleithrum. While the suspensorium does not have a clear peak in bichir or bowfin regardless of cleithral inclusion, and the opercular peak becomes less clear in bowfin when considering the cleithrum vs. not. In both knifefish and bichir, the opercular RCVC has a clearer peak when considering the cleithrum, likely due to the posterior expansion of the alpha shape. The role of the maxilla does not appear to change when including the cleithrum (Fig. 4.1).

In all four species, including the cleithrum necessarily increases the overall oral cavity volume and the rate of volume change, as a larger posterior area is captured by the endocast (Fig. 4.1A-D). In both *Polypterus* and *Amia*, including the cleithrum also shifts the time of peak rate of volume change later in the strike. Ongoing and future investigations of things like prey motion and suction force may help to elucidate the relative validity of these rate of volume change curves with or without the pectoral girdle, as peak prey motion and peak suction force should be temporally associated with the peak rate of volume change.

In the bichir examined here, the bones which drive the peak rate of volume expansion do not change, but in bowfin, including the cleithrum does shift the primary drivers of maximal expansion rate. This is likely due to the time shift of peak volume expansion rate, because in *Amia* the lower jaw is the only bone with a clear, independent peak in RCVC, but this peak occurs relatively early in the strike. Therefore, shifting the time point of peak volume expansion later in the strike means that no bone has a clear driving role above the others at this time point. In *Chitala*, including the cleithrum expands the posterior oral cavity volume boundaries drastically, making the operculum and suspensorium both primary drivers of lateral, and overall, volume expansion, while in treatments without the cleithrum the suspensorium alone plays this role. However, the key takeaway from the knifefish data is still that lateral expansion drives oral cavity volume expansion in these laterally compressed fish.

Overall, these RCVC results change with the inclusion of the cleithrum, most notably for *Amia* and less substantially for *Chitala.* In *Polypterus*, the key drivers do not change, except for the inclusion of the cleithrum itself. In bichir and knifefish, the cleithrum is a secondary or third contributor at peak volume expansion rate, behind the ceratohyal in the bichir and behind the operculum and suspensorium in the knifefish. In bowfin, the cleithral contributions at peak volume expansion rate are second only to the ceratohyal, a drastic shift from the significant contributions of the lower jaw during peak volume expansion when the cleithrum is not considered.

These metrics give us important insight into the contributions of each bone to overall oral cavity volume change that we cannot glean from kinematic traces alone. For example, the maxillary protrusion relative to the cranium in *Amia calva* is substantial, but it does not directly

contribute much to overall volume expansion. Meanwhile, the suspensorial rotations of *C. blanci* are relatively small, but this bone overshadows all others in knifefish RCVC due to its large size as these fish are very laterally compressed and dorsoventrally tall.

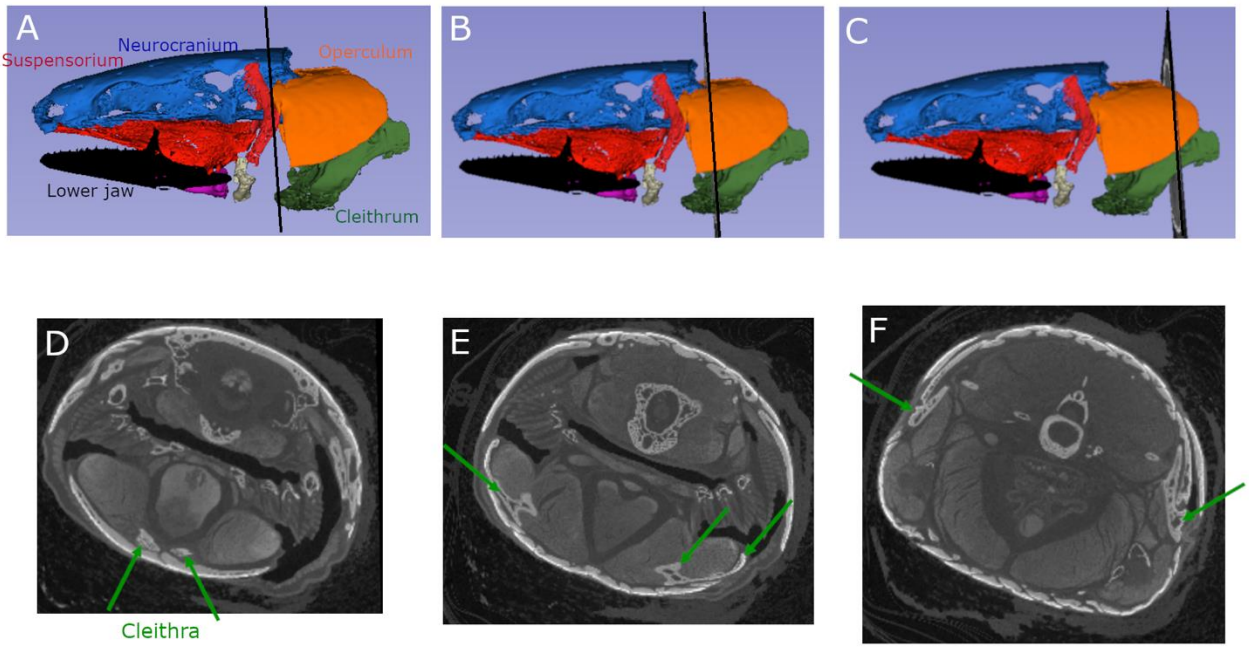

Fig. 4.2. CT reconstructions and slice images from PMA-stained Polypterus bichir demonstrating the extensive soft tissue around the cleithrum. A-C show reconstruction of ossified elements with a plane (black line) demonstrating the point on the anteroposterior axis for context for the corresponding panels below, D-F. D-F show transverse planes at different sections through the cleithra (green arrows). The plane shown in A corresponds to the slice shown in D, B to E, C to F. Here, brighter/white colors are bone or ossified elements, black is air, and gray is soft tissue (a lot of muscle shown in the ventral portions of D-F). The difference in black space (air) between E and F demonstrates that the esophagus has begun in F, as there is no longer any air present in this portion of the specimen.

The comparison of RCVCs with and without the cleithrum in this study emphasizes the importance of ensuring that the endocast representation of an oral cavity volume is realistic and based in the anatomy of the fish. These endocasts so far rely solely on motion of rigid bodies, and do not include the motion of soft tissues. Most studies take soft tissues on the bones measured into account in some way, but the degree to which soft tissues are involved in defining

oral cavity volume *in vivo* varies greatly. Furthermore, the methods for including soft tissue in endocasts have rarely been discussed and best practices are not yet established.

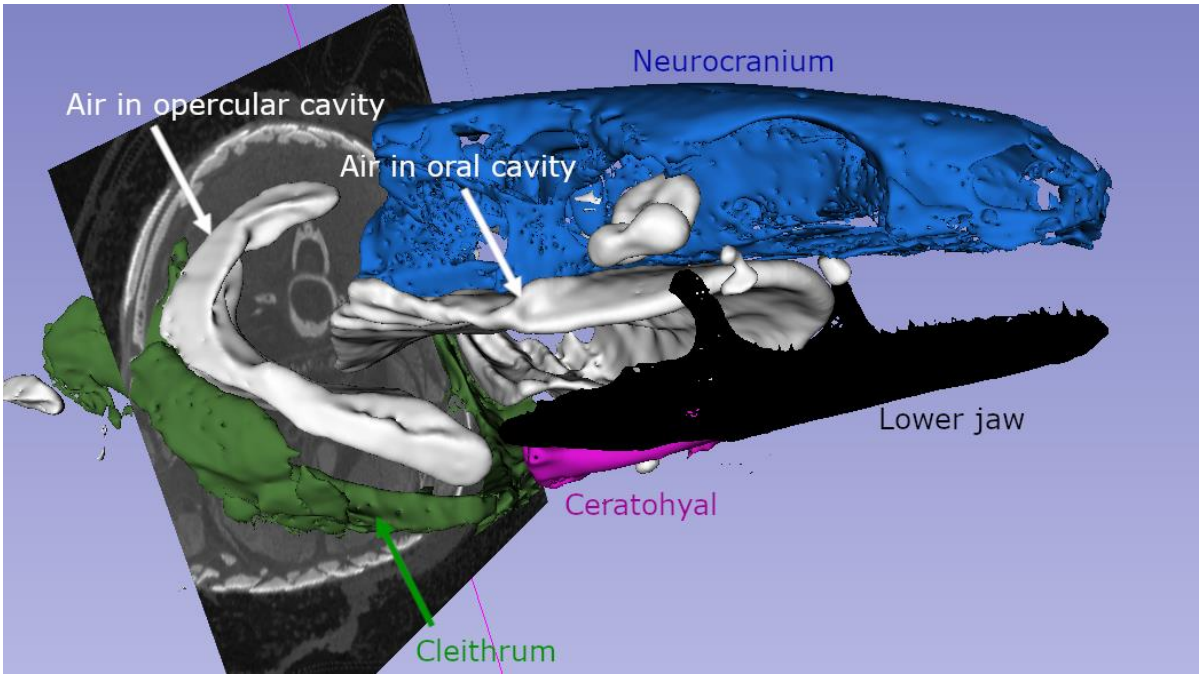

Fig. 4.3. CT reconstructions from PMA-stained *Polypterus bichir* demonstrating the air pockets found in the oral and opercular cavities. A few bones are shown for reference, the cleithrum, ceratohyal, lower jaw, and neurocranium, but the operculum and suspensorium are removed for visibility.

Here, we examine the soft tissues vs. air spaces seen in *Polypterus bichir* using a PMA-stained CT scan (Fig. 2, Fig. 3). These considerations led the authors of Whitlow et al (2022) to exclude the cleithrum from their RCVC measurements. Fig. 4.2 shows the extensive soft tissue around the cleithrum, demonstrating that endocasts including the full cleithrum may be substantially overestimating the true volume of the oral cavity. Here we also see that the esophagus opens anterior to the posterior end of the cleithrum, roughly along the same antero-posterior plane as the neurocranium. Fig. 4.3 shows the air pockets that remain in a dead specimen with mouth closed, allowing for a distinction between the air occupying the oral cavity

and the air occupying the opercular cavities (i.e., outside and around the gill rakers). This demonstrates again that the volume of the strictly defined oral cavity tapers off dramatically towards the midline (i.e., is not as laterally expanded) as we approach the cleithrum. Furthermore, we can see a clear separation between the opercular air pockets and the cleithrum on the ventral aspect of the bone. This leads us to conclude that if the cleithrum is included in RCVC measurements, the specific portions of the bone used to model the oral cavity endocast should be selected with care.

Consideration of other bones

There are additional mobile elements in the skull that we did not directly measure in these studies, but that may further shape or constrain the oral cavity. In *Polypterus* and *Amia* the gular plates may function as boundaries to the ventral floor of the oral cavity *sensu stricto* at some times during the strike, but our investigations suggest that they do not add directly to volume expansion. Instead, these bones appear to respond to motions of the anterior hyoid arch and tongue: in *Polypterus* both plates are pushed ventrally and laterally during feeding, while in *Amia* the central gular pivots around a tight connection with the anterior mandible, flicking the posterior end of the bone anteriorly when it is pushed upon by the ceratohyal and urohyal.

Additionally, when interpreting RCVC results care must be taken to not discount the role of bones with a low RCVC to successful suction generation. This could overlook critical bones that enable or mediate mobility of other bones which directly generate suction. For example, the kinethmoid in carp mediates protrusion of the oral jaws (Gidmark et al., 2012) but is a very small bone that would not directly contribute to oral cavity volume change. Other bones, such as those in the opercular system or hyoid arch, like the interhyal in *Polypterus*, are thought to provide

additional degrees of freedom to distal portions of the hyoid arch (Lauder, 1980). Without this added mobility relative to the suspensorium, the ceratohyal would be limited in its depression and lateral flaring and would likely contribute substantially less to suction generation (Whitlow et al., 2022). In sum, RCVC metrics can be used to identify bones whose motions drive oral cavity volume expansion directly but should not discount the roles of other structures that may mediate or enable such mobility.

Essential considerations when analyzing RCVC measurements

Caution must be used when describing the results and implications of RCVC data. First, we consider the sign of RCVCs and what they tell us regarding the contribution of bones to expansion or compression of the oral cavity volume – versus simply *change* in oral cavity volume. The way that RCVCs are calculated (with absolute value signs in the denominator of the equation, a necessity for dealing with periods where bones are moving in opposition to one another) removes the directionality of volume change. This means that only when all bones are contributing to expansion (RCVC is positive for all bones) or all bones are contributing to compression (RCVC is negative for all bones), can RCVC be interpreted as the relative contribution to overall oral volume expansion or contraction, respectively. For example, if a bone's RCVC is positive, then that bone is contributing to oral cavity volume expansion, but the oral cavity could be experiencing either net expansion or contraction at that time. Therefore, we recommend that RCVC values always be referred to as contributions to volume change, unless it is explicitly stated that all bones are contributing expansion or contraction, or the volume change is analyzed at that given time point and proven to be positive or negative.

Another important consideration of RCVC measurements is that they are *relative* to the overall volume change occurring at a given time point throughout a strike. Therefore, to address questions like the relative importance of a given bone for generating suction, we need to compare RCVCs at key time-points in the strike. We selected the time at maximal rate of volume expansion, as the speed of volume increase is a key factor in the overall amount of suction force generated during a strike. Furthermore, time of peak suction power overlaps nearly perfectly with time of peak rate of volume change (Li et al., 2022). At the time of peak rate of volume change, the ceratohyal is driving oral cavity volume change for lungfish and bichir. For bowfin, the peak rate of volume change is driven instead by the lower jaw, although the ceratohyal still has a higher RCVC than other bones at this time-point. In knifefish, the suspensorium contributes the most to overall volume change at the time of peak volume change rate, with the ceratohyal again playing a secondary role above other bones. Future studies should investigate the motion of the prey item in congruence with peak rate of volume change and explore the drivers of volume change when the prey item is moving or accelerating the fastest, as well as when the prey item first begins to move towards the predator (assuming that intrinsic prey motions can be controlled for).

We urge that researchers further consider the time duration, degree of motion, and skeletal linkages in their datasets before applying RCVC measurements. The iterative freezing of bones can be restricted to a very short time scale, but caution should be taken to ensure that anatomically inaccurate poses are not generated. The connected nature of fish skulls makes this a difficult consideration to tackle definitively, and we encourage the selective inclusion of bones whose motions rely heavily on the motions of other bones that are also included. Furthermore,

the time-course of the strike should be taken into account when selecting a freeze interval: shorter strikes should be frozen for a smaller duration of time, and trace data at several freeze intervals should always be examined to avoid over-smoothing.

The presence of unanimated tissues throughout the fish skull and bounding the true oral cavity volume is another caveat to RCVC data which must be considered. Likely areas of soft tissue or other unanimated tissue overlap include the tongue, gill arches, and various muscles. The tongue should occupy a consistent volume in the oral cavity, so we believe that the impact of the tongue on RCVC should be low – while including the tongue-occupied volume in the endocast means the raw oral cavity volume measured is an over-estimate, if this volume is always included it will not impact RCVC. The gill arches should similarly occupy a consistent volume, though how close individual filaments are to one another may change their resistance to water and should be explored in the future. Any muscle bodies that are always included or excluded should similarly not impact RCVC measurements, but the issue with a few muscles is maintaining this consistency as the muscles and bones change position throughout an animation. For example, jaw adductor muscles lateral to the suspensorium are sometimes partially included in the endocast volume (see Fig. 3.3). While the total volume included here is low, this inaccuracy fluctuated throughout a strike and is therefore a source of noise in the data. One possible solution for muscles like this that bound bone is to explore options for collision detection in Maya and fully constrain the endocast mesh to never overlap a bone mesh. The posterior boundary of the oral cavity is a particularly problematic group of muscle surrounding the opening to the esophagus, which falls on the same transverse plane as the cleithrum. However, often the esophageal opening musculature attaches to the epibranchials or

pharyngobranchials, all anterior to the cleithrum (Lauder, 1983; Liem, 1970; Liem, 1978). Therefore, this important soft tissue boundary does not have an easily animated rigid body to dictate its movement in the endocast reconstructions. In the absence of tantalum markers in these soft tissues precisely and accurately animating the full oral cavity volume is impossible, and we must do our best to minimize inconsistencies and be mindful of them, particularly when comparing between species. Future work manipulating dead specimens and/or using radio-opaque liquids to measure the true oral cavity volume *in-vivo* would be fruitful avenues for ground-truthing the accuracy of these endocasts.

Finally, we emphasize that while RCVC is a useful tool for understanding how a given bone contributes to volume change in the oral cavity and can be strongly associated with the ability of that bone to drive successful suction feeding, lower RCVCs should not be taken as a sign that a given bone is not important for feeding success. As discussed above, there may be bones that bound the oral cavity volume but are too thin or membranous to be included in marker-based XROMM studies. Other bones may be critical for enabling mobility but are small or relatively immobile themselves and therefore have negligible RCVC values (discussed above). Lastly, sometimes highly mobile bones bound the oral cavity but are redundant in some way for the generation of the endocast models that RCVC measurements are based on. For example, this study demonstrates that the maxillae of *Chitala* and *Amia* have low RCVCs throughout the strike, but this is due to the position of those bones: they run between the cranium and the lower jaw, an area that will be included in the endocast without mobility in the maxilla. This does not mean that they are not important for suction feeding success, but they may serve more to direct suction forces towards a prey item than to generate suction directly.

Implications and potential uses of RCVC

RCVC provides an avenue for comparing the relative roles of mobile skeletal elements in the cranium to volume expansion and compression during suction feeding strikes across species. While the importance of the hyoid arch to generating suction has long been appreciated, many studies still focus solely or primarily on changes in gape as a predictor of performance (see Ferry-Graham et al., 2001b; Higham et al., 2006; Hill et al., 2018; Holzman et al., 2008; Motta, 1984; Westneat, 2004; Wilga et al., 2000), perhaps in part because it is relatively easy to measure jaw motion during strikes and relatively difficult to accurately measure hyoid or suspensorial rotations. The jaws are undoubtedly important, and definitionally must be open in order to capture prey, RCVC metrics in the present study demonstrate that it is often the hyoid or suspensorium that is driving volume change during the critical period of prey capture (here, time of maximal volume expansion). As other researchers have emphasized, the anterior to posterior wave of motion and coordination of cranial kinesis is critical to successful suction feeding (Bishop et al., 2008; Holzman et al., 2007).

RCVC also allows insight into any point of interest throughout a strike due to the rolling nature of the freeze increments (rather than providing a single measure of the entire strike). The present study focuses on the time of peak rate of volume change, but other points in the strike can be examined as well, such as the onset of prey motion, time of peak prey velocity or acceleration, or time of peak suction force. RCVC may also be used to explore the compression of the oral cavity and has implications not only in the realm of suction feeding but also in prey processing and even air breathing.

Another potential future application for RCVC measurements is to attempt to understand the role of bones in species that have not yet been studied using XROMM. In situations where we have a reasonable estimate of the mobility of each bone (like methods of Manafzadeh, 2020) and we know a bone's surface area and orientation relative to the oral cavity, we may estimate the impacts of that bone to overall oral cavity volume change. This may even be applied to extinct taxa where fossil specimens are sufficient to provide accurate joint morphology reconstruction. For example, models of feeding mechanics in *Dunkelosteus* could be combined with bone models to model the oral cavity volume and estimate the roles of each bone to generating flat-plate suction that combats the bow wave during biting (Anderson and Westneat, 2009). Other recent work has estimated both the rotations and resultant oral cavity volume from cranial cartilages in extinct elasmobranchs (Coates et al., 2019), and such datasets are ripe for exploration with RCVC.

Key takeaways and remaining questions:

Each species examined here has a high lower jaw RCVC early in the strike, indicative of flat plate suction kicking off the expansion of the oral cavity volume. Regardless of cleithral inclusion, lungfish and bichir follow this initial lower jaw RCVC with a high ceratohyal RCVC, as we predicted. Bowfin utilize the lower jaw to expand the oral cavity even more than we anticipated, with its RCVC dwarfing those of the other bones regardless of cleithral inclusion, though the timing of peaks still matched our predictions. In knifefish, the suspensorium and/or operculum overshadow the RCVCs of other bones in both scenarios, likely due to the relative size of those bones and the extreme lateral compression of this species.

The drivers of peak oral cavity expansion velocity vary across species, with the ceratohyal driving volume change at this time in lungfish and bichir regardless of cleithral inclusion. In bowfin the lower jaw appears to drive expansion during this time when the cleithrum is not considered, and no bone has a clear driving role above the others when the cleithrum is included. In knifefish the suspensorium (without cleithrum) and operculum (with cleithrum) contributes the highest RCVC during peak rate of volume expansion.

Ultimately, we see that lateral motions drive the primary period of volumetric expansion in *Chitala* while dorsoventral motions are stronger drivers in all other species at this time point. We suggest that future work consider including the cleithrum in part and taking care to apply locators in a way that minimizes overlap with soft tissues. This is certainly a challenge, as we do not yet have an accurate picture of how these soft tissues may deform in a live-feeding animal, and their size, orientation, and attachments may vary by species. However, ensuring the best feasible accuracy of the oral cavity volume endocast is critical to the results and implications of RCVC measurements.

Future investigations of more taxa from the phylogeny of aquatic feeding vertebrates will enhance our understanding of the evolution and constraints to suction feeding. Many questions remain that may be explored productively using RCVC data: Are there species that do not generate a high jaw RCVC early in the strike? What do taxa with extremely dorsoventrally compressed heads do, vs. those with more “standard” fish skulls? Do piscivorous fishes use a different pattern of volume contributions than species that eat benthic or hard-shelled prey? Are there predictable patterns or consistent constraints to how peak volume expansion rates are generated? The expansion of aquatic suction feeding XROMM datasets to numerous teleost taxa,

extending recently into basal actinopterygians and even sarcopterygians, means the time is ripe to leverage these datasets and answer some of these questions.

Conclusions

RCVC measurements can give us unique insight into the strategies that different species utilize to generate suction. Future work should examine additional taxa, especially teleosts with less specialized cranial morphology than that seen in *C. blanci.* Additional efforts should be dedicated to validating the inclusion of various bones for RCVC modeling, and promising avenues for this validation include examining prey motion and suction forces during the strike. Despite varying morphology and feeding specializations, all three non-teleost species show a central role of the jaw and ceratohyal in driving volume expansion, with varying degrees of contribution from other mobile cranial elements, whether the pectoral girdle is included or not. However, bowfin volume expansion is driven more by the jaw, while in lungfish and *Polypterus* the ceratohyal plays a larger role. Knifefish, on the other hand, have drastically laterally compressed skulls and volume expansion driven largely by lateral expansion of the suspensorium. *P. bichir* and *A. calva* also have clear contributions from lateral expansion driven by the operculum and suspensorium following peak gape, but these do not overlap the peak rate of volume expansion curve as they do in knifefish.

CHAPTER 5: CONCLUSIONS AND FUTURE DIRECTIONS

The XROMM workflow for biomechanical studies provides new avenues for investigating important questions in functional morphology. The integration of new dynamic imaging technologies such as biplanar x-ray videoradiography with high resolution computed tomography (CT) to create XROMM animations allows us to visualize internal structures, precisely measure joint motions and muscle length changes, and visualize intra-oral water flow in aquatic feeding fishes. The aquatic feeding community has gained insights regarding the primary sources of power for suction feeding (Camp and Brainerd, 2014; Camp et al., 2015; Camp et al., 2017; Camp et al., 2018; Camp et al., 2020; Li et al., 2022; Lomax et al., 2020; Olsen et al., 2019), the mechanisms for several specific joint motions (Camp, 2021; Camp and Brainerd, 2015; Gidmark et al., 2012; Jimenez et al., 2018), and intra-oral water flows used to process and swallow prey (Olsen et al., 2019; Provini et al., 2022; Weller et al., 2020).

More specifically, the research presented in this dissertation has yielded new insights into cranial kinematics and mobility, ventral jaw opening linkages, and drivers of volume change in *Polypterus bichir* and *Amia calva*, evolutionarily important actinopterygian taxa. By leveraging relative contribution to volume change data for further comparisons with a teleost *Chitala blanci* and the lungfish *Protopterus annectens*, I provide additional insights into the ways distantly related and morphologically distinct species drive volumetric expansion of the oral cavity and successful suction feeding. These insights significantly advance our understanding of mechanics and evolution among fishes.

SUMMARY OF INSIGHTS FROM XROMM ON CRANIAL KINEMATICS

This thesis has demonstrated that *Amia* and *Polypterus* have similar degrees of lateral mobility, with both suspensoria flaring to around 12° and similar degrees of opercular flaring (Fig. 2.3, Fig. 3.4, Fig. 3.7, Fig. 3.8). The hyoid in *Polypterus* undergoes complex 3D motions, depressing an average of 55° along with 80° of long axis rotation and 28° of lateral flaring (Fig 2.4). In *Amia* hyoid motion appears to be more constrained, only depressing to 36° on average (Table 3.1). We further demonstrate that the pectoral girdle is highly mobile in both species, though somewhat less so in *Amia* with an average cleithral retraction of 20° compared to 32° in *Polypterus*.

The two species are also distinguished by the apparent role of the sternohyoideus muscle during suction feeding. In *Polypterus*, as in bass, some clariid catfishes, and bichirs (Camp and Brainerd, 2014; Camp et al., 2015; Van Wassenbergh et al., 2005; Van Wassenbergh et al., 2007) the sternohyoideus does not shorten while it is active, meaning it serves to transfer forces rather than add to the forces generated by the axial musculature (Fig. 2.7). *Amia*, on the other hand, shorten their sternohyoideus during suction feeding in most strikes (Fig. 3.5). Therefore, bowfin sternohyoideus muscles, like those of bluegill sunfish, striped surfperch, and one clariid catfish, actively contribute power to the anterior/ventral hyoid arch and jaws, rather than only transferring power generated by the axial muscles (Camp et al., 2018; Lomax et al., 2020; Van Wassenbergh et al., 2007). Continuing to investigate not only the activity and kinematic outputs, but also the length and strain of such muscles will solidify our understanding of the interplay of cranial and axial muscles during feeding.

CONCLUSIONS REGARDING VENTRAL JAW OPENING LINKAGES

The data presented in this thesis support the hypothesis that *P. bichir* depresses the lower jaw primarily through retraction of the ceratohyal, putting the mandibulohyoid ligament into tension and applying a posteriorly and dorsally directed force behind and below the axis of rotation of the jaw (Lauder, 1980; Whitlow et al., 2022; Fig. 2.7). Two additional mechanisms may also contribute to jaw opening, through suspensorial motions driven by the elevation of the neurocranium or abduction of the suspensorium, or through ceratohyal retractions transferred to the jaw through muscles that connect to the tip of the jaw (Whitlow et al., 2022). These mechanisms should be explored further by modeling the potential lines of action of the relevant muscles and combining these data with temporal associations of translation and rotation data collected here using XROMM.

I further explored the role of the sternohyoideus and axial muscles in driving the pectoral girdle-hyoid component of the pectoral girdle-hyoid-jaw opening linkage in both *Amia* and *Polypterus*. In both taxa retraction of the ceratohyal is clearly driven at least in part by cleithral retraction. In *Polypterus* the sternohyoideus muscle connecting the cleithrum to the ceratohyal does not shorten during suction strikes (Whitlow et al. 2022; Fig. 2.7), while in *Amia* the sternohyoideus shortens briefly during suction strikes (Fig 3.5). Therefore, *Polypterus* hyoid motions appear to be driven by the axial muscles and directed through isometric activity of the sternohyoideus, while *Amia* hyoid motion receives contributions from activity in both sets of muscles. Recent work suggests the distinction between these roles in teleosts is associated with the relative size of the sternohyoideus and hypaxial musculature (Lomax et al., 2020), so

measuring the cross-sectional area of these muscles in these non-teleost species would be a fruitful next step.

NEW INSIGHTS FROM RCVC AND THE BASIC BUILDING BLOCKS OF SUCTION FEEDING

All species show a high lower jaw RCVC indicative of flat plate suction early in the strike, followed by a ceratohyal RCVC peak that overlaps the period of rapid volume expansion (Fig 4.1). We considered the time at peak rate of volume change across species, as this time has been shown to correspond with the strongest pressure differential in the oral cavity. We further examined how including the cleithrum as a mobile posterior boundary to the oral cavity changes the results of these analyses, as there is some debate as to how best define this area with extensive soft tissues (Chapter 4).

In lungfish, the peak rate of volume expansion is driven by both the lower jaw and ceratohyal, with a greater contribution from the ceratohyal. In bichirs the peak rate of volume expansion is driven primarily by the ceratohyal. In bowfin the lower jaw appears to drive volume change during peak expansion rate when the cleithrum is not considered, but when the cleithrum is included, bowfin have statistically equal contributions from all bones. Peak rates of cranial expansion in knifefish are primarily driven by lateral flaring; with the cleithrum this period is driven by both operculum and suspensorium, while without the cleithrum the suspensorium leads peak volume expansion rates (Fig 4.1). There is not a clear maxillary peak in *C. blanci* or *A. calva*, suggesting that anterior swing of the maxilla in these groups may serve more to direct suction forces than to generate them.

Despite varying morphology, cranial mobility, and feeding specializations, all three non-teleost species show a central role of the ceratohyal in driving volume expansion, with varying degrees of contribution from other mobile cranial elements. The teleost representative in this study, *Chitala blanci*, is extremely laterally compressed and therefore suspensorial and opercular RCVCs play a leading role in driving volume change. Recent work suggests that the jaws and a mobile hyoid arch are all that is required to generate substantial suction in aquatic feeding fishes (Gartner et al., 2022). Furthermore, in species with lateral cranial mobility the ceratohyal may still be a key driver of volume change (Fig. 3.5). However, with the evolution of unique morphologies, such as extreme lateral compression, other bones can also be utilized which reduce the necessity of a mobile hyoid for expanding the floor of the mouth to drive suction generation (Fig 4.1). We expect that species with dramatic dorsal compression will have an even higher RCVC from the ceratohyal or other mechanism driving ventral expansion.

Furthermore, these results emphasize that while jaw depression or gape is often measured as a primary determinant of suction feeding performance, the morphology and cranial mobility of the species of interest should be considered, as the role of the lower jaw is often overshadowed by the ceratohyal or laterally expanding elements at moments of peak suction generation. Future work should continue to expand the diversity of species analyzed for the relative contribution to volume change of each mobile element in the cranium. The number of suction feeding species for which XROMM-based 3D kinematic data are available is nearing or already in the double digits, documenting morphological and kinematic diversity, allowing broad evolutionary questions related to the primary drivers of volumetric expansion in the oral cavity to be addressed (Fig. 5.1). While not all available datasets can be utilized to generate endocast models,

the time is ripe to apply this technique where possible and continue to collect more data for a broad, comparative analysis of the drivers of oral cavity volume change in aquatic suction feeders. Clear targets for future analysis are additional teleosts (as this branch accounts for most of actinoptyergian diversity), Lepisosteiformes, and aquatic-feeding tetrapods.

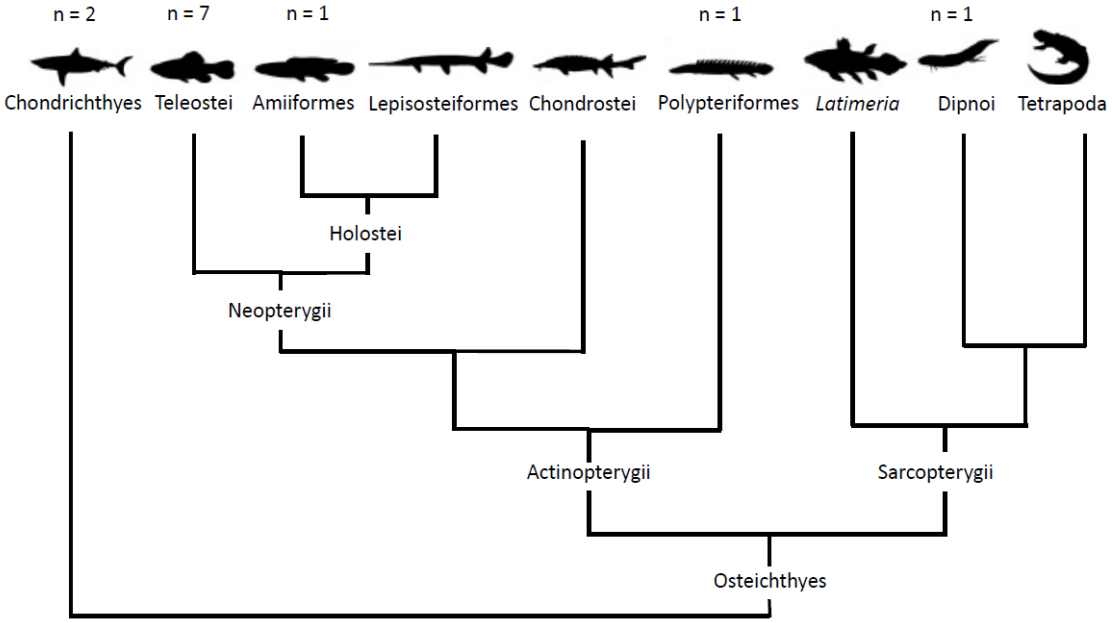

Fig. 5.1. Phylogeny of jawed vertebrates with species studied using XROMM noted. Adapted from Giles et al., 2017; Wilhelm et al., 2015.

IMPLICATIONS FOR EVOLUTION OF SUCTION FEEDING

The nature of the Tait-Bryan angles applied to intuitively measure rotations in XROMM datasets makes comparing magnitudes of rotations measured in these studies to those measured using light cameras (or even a different JCS) fraught with potential errors and misunderstandings (Manafzadeh and Gatesy, 2020). I therefore limit broader taxonomic comparisons to relative

timing variables measured in this dissertation and encourage exploration of additional mechanisms for measuring cranial mobility in the future directions.

The speed of a suction feeding strike (when other factors are equal) will increase the force applied to a prey item and in theory increase the chance of the strike being successful. Time from strike onset to peak gape is longest in *Amia calva*, approximately 55 ms in strikes on feeder fish, while the holostean relative *Atractosteus spatula* completes gape expansion in only 17 ms. *Polypterus bichir*, the outgroup to all other ray-finned fishes, strikes with intermediate speed, with peak gape occurring after an average of 28 ms from initiation of gape increase. Similarly, the durations of hyoid rotation, neurocranial elevation, suspensorial abduction, and cleithral retraction from onset to peak all increase in the order of gar, bichirs, and bowfin. While larger fish may have higher strike times when all other factors are equal, the *Polypterus* studied here were smaller than *A. spatula* and still used slower strikes. Furthermore, these findings are comparable to those of Lauder (1980), who measured strike kinematics in *Polypterus senegalus*, *Lepisosteus occulatus*, and *Amia calva* (*P. senegalus* and *L. occulatus* are close relatives to *P. bichir* and *A. spatula*, respectively).

This thesis also has implications for the neural control of feeding strikes in fishes. The data show that bowfin modulate their strikes in response to variation in prey type (Fig. 3.7, Fig. 3.8) and prey position (Fig. 3.6). Teleosts have also been shown to modulate strikes when feeding on elusive prey (Ferry-Graham et al., 2001; Nemeth, 1997a, Holzman 2007). Sensory feedback about the prey position (Aerts, 1990) and attempted escape responses (Van Wassenbergh and De Rechter, 2011) are likely integrated by the nervous system to alter the strike kinematics, though there are still debates about whether such sensory information is only

utilized by the predator *a priori* or if the predator may modulate kinematics mid-strike in response to sensory feedback. The data presented here, in combination with modulation found in shark feeding (Ferry-Graham, 1998; Gardiner et al., 2017; Matott et al., 2005) and tetrapods (Montuelle et al., 2012b; Vinyard et al., 2008) suggests that the ability to modulate feeding behaviors or kinematics is probably primitive for jawed vertebrates.

As an outgroup to teleosts and an outgroup to all other living ray-finned fishes, respectively, *Amia's* and *Polypterus'* cranial kinematics can be used to address important questions regarding skeletal mobility and suction feeding mechanics across the tree of life. Chapters 2 and 3 of this thesis, combined with findings from teleosts and gar (Camp and Brainerd, 2014; Lemberg et al., 2019) demonstrate that a mobile pectoral girdle is likely ubiquitous among ray finned fishes; recent data on lungfish feeding (Kaczmarek et al., 2022), suggests that this feature may also have been primitive for all bony fishes. A mobile pectoral girdle enables contracting hypaxial muscles and an active (isometric, concentric, or eccentric) sternohyoideus to work in concert, directly driving complex ceratohyal motions which enable jaw opening and successful suction feeding. Similar mechanisms have been described in clariid catfishes (Van Wassenbergh et al., 2007), largemouth bass (Camp and Brainerd, 2014), bluegill (Camp et al., 2018), catfish (Camp et al., 2020), and now *P. bichir* and *A. calva* - emphasizing that hypaxial muscle contraction is likely to be important for suction feeding in many fishes (Tchernavin, 1948). Additional power contributions from the sternohyoideus are variable (Lomax et al., 2020; Van Wassenbergh et al., 2007), and this thesis demonstrates they are not always consistent within a single species or individual (Fig. 3.4). Additional work into this variability in *Amia* sternohyoideus and hypaxial muscle activity would be fruitful, as we did not

find a clear driving factor for an actively shortening vs. isometric sternohyoideus muscle across strikes.

Datasets generated in this thesis could be further leveraged to model cranial mobility of fossil taxa, in particular the *Amia* lineage has a long history of morphological similarity and a strong fossil record (Grande and Bemis, 1998). *Polypterus* may also be used to model specific features of early tetrapods or closely related extinct taxa (see Ch. 2; Giles et al., 2017; Molnar et al., 2017). The newly developed method of using endocast measurements and iterative bone freezing to understand the relative contribution to volume change (RCVC) of a given bone could also be applied to fossil taxa using mobility estimates bound by those measured in live fishes. Such studies could greatly enrich our understanding of species ecology in a paleontological context.

FUTURE DIRECTIONS

Many questions remain regarding suction feeding generally, as well as in the taxa studied here. Here I highlight a few that closely follow from the data and findings in this thesis. Future work should attempt to 1) quantify the relative mobility of cranial elements more explicitly and explore ways to make 3D datasets comparable to traditional light camera feeding studies, 2) model the jaw opening mechanisms in *Polypterus* and *Amia*, and 3) investigate mechanics of prey processing and swallowing in these groups.

Comparability of XROMM data and quantifying joint mobility

XROMM data provide unique insights and precision to measuring joint mobility and skeletal elements that are largely or partly inaccessible with traditional light camera methods and have transformed the way we look at feeding biomechanics in fishes. However, XROMM is still a relatively new technique that is not only costly but and has a steep learning curve. It is not needed for every type of question and has substantial processing times, particularly for datasets less amenable to tracking with neural networks (Laurence-Chasen et al., 2020). Furthermore, it is currently difficult to compare XROMM data to all the wealth of what we have learned from light camera video because Tait-Bryan angles are plotted in Euler space, which intrinsically distort the measurements in ways that are rarely intuitive (Manafzadeh and Gatesy, 2020). In brief, the X, Y, and Z positions are not independent from one another and depend heavily on the orientation of a JCS as well as the rotations of the other axis. Furthermore, the X axis moves with the distal bone while the Z axis moves with the proximal bone, while Y is calculated between these two axes. Therefore, using a full JCS system to compare to straight sagittal, coronal, transverse plane angles is invalid, as the planes generated by Tait-Bryan angles in XROMM datasets do not remain orthogonal to one another. One approach to enable these broader comparisons is to only consider primary axis rotations around axes through biologically meaningful planes.

Recent work discovered a transformation that can be applied to 3D joint mobility envelopes which undistort the measurements and allow us to compare the size of the envelope (i.e., relative joint mobility; Manafzadeh, 2020; Manafzadeh and Gatesy, 2020). While these methods have so far only been applied to limbs, relative mobility of bones like the ceratohyal are of particular interest in fish feeding studies and should be amenable to such methods of

undistortion. Future work could also explore methods of moving the XROMM space away from Tait Bryan angles, and in fact the initial rigid body transformations are in transformation matrix form (which are not distorted and therefore should be more readily comparable). However, these 16-variable transformation matrices are not intuitive or easy to translate to a biomechanically meaningful context, and we encourage further exploration of measurements that can minimize unexpected distortions while maintaining a context that is biologically meaningful.

Modeling jaw opening mechanisms

Why model the mechanisms of jaw opening in *Polypterus* and *Amia*? Such modeling would help us to evaluate the relative importance of different mechanisms of jaw opening in *Polypterus* and *Amia*. The data presented here emphasize the role of the pectoral girdle-hyoid-jaw mechanism of jaw depression but do not explicitly rule out another mechanism in *Polypterus* because the jaw is already starting to open at roughly the same time or slightly before ceratohyal depression. It is possible this mechanism is sufficient, but it is equally feasible that another mechanism helps initiate jaw depression. For example, perhaps neurocranial elevation helps open the jaw (as described in bass by Camp and Brainerd, 2015) or maybe there is a role played by the relative mobility of the hyomandibula in *Polypterus*. The role of the pectoral girdle-hyoid-jaw linkage should also be explored further in *Amia* and should additionally be compared with the mechanism of opercular-driven jaw opening. These opercular driven mechanics have been recently re-evaluated in bass, where the importance of cranial and suspensorial elevation has been emphasized (Camp and Brainerd, 2015). Historically the opercular jaw opening mechanism of *Amia* has been considered functionally comparable to that of teleosts (Lauder, 1980) but the precise, *in-vivo* data generated from XROMM provide a unique opportunity to test this

hypothesis. Furthermore, the datasets gathered in this thesis provide an avenue for comparing the hyoid-driven and opercular-driven jaw opening mechanisms and may allow us to parse the relative contribution of each linkage in *Amia calva*.

Furthermore, *Amia* has an additional morphological novelty related to jaw opening which has not been studied explicitly and is only briefly mentioned in the feeding literature (Westneat, 2004) (but see Allis, 1897; Grande and Bemis, 1998; Patterson, 1982 for morphological considerations). The suspensorial-mandibular connection in this group is comprised of not one, but two joints, each with a clear articular surface. Most fishes possess the quadrato-articular joint, where the quadrate element of the suspensorium articulates with the jaw. However, *Amia* also has a connection between the jaw and the symplectic, a distinct element of the suspensorium that sits lateral and posterior to the quadrate (Fig. 1.2). Interestingly, the distal and proximal bones are solidly fused to each other; the symplectic and quadrate are immovable relative to one another and comprise two components of the suspensorium, while the surfaces they articulate with on the lower jaw are similarly fused in living specimens. Both joints can be described as approximating a ball and socket, though the articular surfaces don't fit together as snuggly as they do for other species. Interestingly, the quadrate contains the "ball" or "peg" for it's joint with the lower jaw, while the jaw contains the "peg" surface for the jaw-symplectic joint – i.e., these joints are almost mirrored in terms of their joint surface anatomy (though the quadrate joint is a closer approximation to a true ball and socket, while the symplectic is less rounded and closer to two posts).

The function of this double jaw joint remains a mystery. Perhaps the additional surface area serves to better distribute joint-reaction forces during hard biting, but this explanation alone

is insufficient. If resisting joint reaction forces was the sole function, it's not clear why these joints evolved as two distinct articular surfaces rather than simply expanding the existing surface area in the quadrate-articular joint. This hypothesis could be tested using finite element modeling to elucidate the load paths during biting. Another (not mutually exclusive) possibility is that there is a shift in the fulcrum of the jaw for closing vs. opening, where perhaps the axis of rotation shifts from quadrate to symplectic (or vice versa) during transition to the compressive phase of a strike. Helical axis modeling and examination of the translations at each joint may reveal how the axis of rotation changes throughout a strike.

Prey processing and swallowing

Fish suction feed to acquire a prey item but processing the food is not complete once the strike ends. These phases of repositioning the food item can be termed food transport or handling (Provini et al., 2022; Weller et al., 2020). Much of what we know about detailed mechanisms of prey transport and swallowing comes from a single XROMM dataset on channel catfish (*Ictalurus punctatus*; Olsen et al., 2019; Olsen et al., 2020; Weller et al., 2020), with one other study describing intraoral water flow during processing in carp and tilapia (Provini et al., 2022). Fishes use inertia-driven filtration during the initial strike to parse water out through the gills while trapping the prey item in the branchial basket, subsequently re-suspending the prey item and transporting it to the esophagus using coordinated cranial bone movements (Provini et al., 2022). While these behaviors are less coordinated than suction strikes and are thought to generate multiple flows (as opposed to unidirectional during strikes) to effectively reposition prey (Olsen et al., 2019), prey transport has been shown to utilize the same number of functional degrees of freedom used for suction feeding (Olsen et al., 2020). Catfish also employ a unique

pattern of cranial expansion that moves the prey item through the esophagus (Weller et al., 2020). This surprising result suggests that esophageal peristalsis in this group is not always sufficient to move the prey and is therefore sometimes accompanied by pectoral girdle retractions to aid in movement of the prey item (Weller et al., 2020). Several fishes also employ rhythmic chewing behaviors to process the food item prior to swallowing (Gidmark et al., 2014; Gintof et al., 2010; Laurence-Chasen et al., 2019).

Given our severely limited understanding of each of these behaviors (intra-oral processing or chewing, intra-oral transport, and swallowing) and their diversity across taxa, the time is ripe for further work to investigate their mechanics and variability. Prior to the advent of videoradiography and the XROMM workflow, understanding anything about these behaviors was limited as it was not possible to track a prey item inside the oral cavity. Throughout this thesis, biplanar x-ray video data on prey processing and swallowing have been opportunistically collected following the captured strikes. Future work will utilize these data to explore how *Polypterus* and *Amia* process, transport, and swallow food items acquired via suction feeding. This will enhance our understanding of the processes by which fish acquire the energy needed to grow and reproduce, allow new opportunities to explore hydrodynamics and biomechanics of a complex musculoskeletal system, and provide insight into the evolution of neural control and rhythmic feeding behaviors.

BIBLIOGRAPHY

Aerts, P. (1990). Variability of the fast suction feeding process in *Astatotilapia elegans* (Teleostei: Cichlidae): a hypothesis of peripheral feedback control. *J. Zool. London* **220**, 653–678.

Alexander, R. M. (1967). The functions and mechanisms of the protrusible upper jaws of some acanthopterygian fish. *J. Zool.* **151**, 43–64.

Allis, E. P. (1897). The cranial muscles and cranial and first spinal nerves in *Amia calva*. *J. Morphol.* **12**, 487–809.

Allis, E. P. (1922). The cranial anatomy of *Polypterus*, with special reference to *Polypterus bichir*. *J. Anat.* **56**, 189-294.43.

Anderson, P. S. L. and Westneat, M. W. (2009). A biomechanical model of feeding kinematics for *Dunkleosteus terrelli* (Arthrodira, Placodermi). *Paleobiology* **35**, 251–269.

Berme, N., Cappozzo, A. and Meglan, J. (1990). Rigid body mechanics as applied to human movement studies. In *Biomechanics of human movement: applications in rehabilitation, sports and ergonomics*, pp. 89–102.

Bermingham, E. and Avise, J. C. (1986). Molecular zoogeography of freshwater fishes in the Southeastern United States. *Genetics* **113**, 939–965.

Bernstein, N. (1967). *The co-ordination and regulation of movements*. Oxford, New York, Pergamon Press.

Bishop, K. L., Wainwright, P. C. and Holzman, R. (2008). Anterior-to-posterior wave of buccal expansion in suction feeding fishes is critical for optimizing fluid flow velocity profile. *J. R. Soc. Interface* **5**, 1309–1316.

Brainerd, E. L., Baier, D. B., Gatesy, S. M., Hedrick, T. L., Metzger, K. A., Gilbert, S. L. and Crisco, J. J. (2010). X-ray reconstruction of moving morphology (XROMM): precision, accuracy and applications in comparative biomechanics research. *J. Exp. Zool.* **313A**, 262–279.

Camp, A. L. (2019). What fish can teach ss about the feeding functions of postcranial muscles and joints. *Integr. Comp. Biol.* **59**, 383–393.

Camp, A. L. (2021). A neck-like vertebral motion in fish. *Proc. R. Soc. B Biol. Sci.* **288**,.

Camp, A. L. and Brainerd, E. L. (2014). Role of axial muscles in powering mouth expansion during suction feeding in largemouth bass (*Micropterus salmoides*). *J. Exp. Biol.* **217**, 1333–1345.

Camp, A. L. and Brainerd, E. L. (2015). Reevaluating musculoskeletal linkages in suction-feeding fishes with X-Ray Reconstruction of Moving Morphology (XROMM). *Integr. Comp. Biol.* **55**, 36–47.

Camp, A. L., Roberts, T. J. and Brainerd, E. L. (2015). Swimming muscles power suction feeding in largemouth bass. *Proc. Natl. Acad. Sci.* **112**, 8690–8695.

Camp, A. L., Scott, B., Brainerd, E. L. and Wilga, C. D. (2017). Dual function of the pectoral girdle for feeding and locomotion in white-spotted bamboo sharks. *Proc. R. Soc. B Biol. Sci.* **284**, 2–8.

Camp, A. L., Roberts, T. J. and Brainerd, E. L. (2018). Bluegill sunfish use high power outputs from axial muscles to generate powerful suction-feeding strikes. *J. Exp. Biol.* **221**,.

Camp, A. L., Olsen, A. M., Hernandez, L. P. and Brainerd, E. L. (2020). Fishes can use axial muscles as anchors or motors for powerful suction feeding. *J. Exp. Biol.* **223**,.

Coates, M. (2017). Plenty of fish in the tree. *Nature* **549**, 167–169.

Coates, M. I., Tietjen, K., Olsen, A. M. and Finarelli, J. A. (2019). High-performance suction feeding in an early elasmobranch. *Sci. Adv.* **5**, 1–9.

Fedorov, A., Beichel, R., Kalpathy-Cramer, J., Finet, J., Fillion-Robin, J.-C., Pujol, S., Bauer, C., Jennings, D., Fennessy, F., Sonka, M., et al. (2012). 3D Slicer as an image computing platform for the quantitative imaging network. *Magn. Reson. Imaging* **30**, 1323–41.

Ferry-Graham, L. A. (1998). Effects of prey size and mobility on prey-capture kinematics in leopard sharks *Triakis semifasciata*. *J. Exp. Biol.* **201**, 2433–2444.

Ferry-Graham, L. A., Lauder, G. V. and Hulsey, C. D. (2001a). Aquatic prey capture in ray-finned fishes: A century of progress and new directions. *J. Morphol.* **248**, 99–119.

Ferry-Graham, L. A., Wainwright, P. C., Westneat, M. W. and Bellwood, D. R. (2001b). Modulation of prey capture kinematics in the cheeklined wrasse *Oxycheilinus digrammus* (Teleostei: Labridae). *J. Exp. Zool.* **290**, 88–100.

Ferry, L. A., Paig-Tran, E. M. and Gibb, A. C. (2015). Suction, ram, and biting: Deviations and limitations to the capture of aquatic prey. *Integr. Comp. Biol.* **55**, 97–109.

Gardiner, J. M. and Motta, P. J. (2012). Largemouth bass (*Micropterus salmoides*) switch feeding modalities in response to sensory deprivation. *Zoology* **115**, 78–83.

Gardiner, J. M., Atema, J., Hueter, R. E. and Motta, P. J. (2017). Modulation of shark prey capture kinematics in response to sensory deprivation. *Zoology* **120**, 42–52.

Gartner, S. M., Whitlow, K. R., Laurence-Chasen, J. D., Kaczmarek, E. B., Granatosky, M. C., Ross, C. F. and Westneat, M. W. (2022). Suction feeding of West African lungfish (*Protopterus annectens*): An XROMM analysis of jaw mechanics, cranial kinesis, and hyoid mobility. *bioRxiv* 2022.05.30.493759.

Gidmark, N. J., Staab, K. L., Brainerd, E. L. and Hernandez, L. P. (2012). Flexibility in starting posture drives flexibility in kinematic behavior of the kinethmoid-mediated premaxillary protrusion mechanism in a cyprinid fish, *Cyprinus carpio*. *J. Exp. Biol.* **215**,

2262–2272.

Gidmark, N. J., Tarrant, J. C. and Brainerd, E. L. (2014). Convergence in morphology and masticatory function between the pharyngeal jaws of grass carp, *Ctenopharyngodon idella*, and oral jaws of amniote herbivores. *J. Exp. Biol.* **217**, 1925–1932.

Gidmark, N. J., Taylor, C., Lopresti, E. and Brainerd, E. L. (2015). Functional morphology of durophagy in black carp, *Mylopharyngodon piceus*. *J. Morphol.* **276**, 1422–1432.

Giles, S., Xu, G. H., Near, T. J. and Friedman, M. (2017). Early members of "living fossil" lineage imply later origin of modern ray-finned fishes. *Nature* **549**, 265–268.

Gintof, C., Konow, N., Ross, C. F. and Sanford, C. P. J. (2010). Rhythmic chewing with oral jaws in teleost fishes: A comparison with amniotes. *J. Exp. Biol.* **213**, 1868–1875.

Grande, L. and Bemis, W. E. (1998). A comprehensive phylogenetic study of amiid fishes (Amiidae) based on comparative skeletal anatomy. An empirical search for interconnected patterns of natural history. *J. Vertebr. Paleontol.* **18**, 1–696.

Grood, E. S. and Suntay, W. J. (1983). A joint coordinate system for the clinical description of three-dimensional motions: Application to the knee. *J. Biomech. Eng.* **105**, 136–144.

Grubich, J. R. (2001). Prey capture in actinopterygian fishes: A review of suction feeding motor patterns with new evidence from an elopomorph fish, *Megalops atlanticus*. *Am. Zool.* **41**, 1258–1265.

Higham, T. E., Day, S. W. and Wainwright, P. C. (2005). Sucking while swimming: Evaluating the effects of ram speed on suction generation in bluegill sunfish *Lepomis macrochirus* using digital particle image velocimetry. *J. Exp. Biol.* **208**, 2653–2660.

Higham, T. E., Day, S. W. and Wainwright, P. C. (2006). Multidimensional analysis of suction feeding performance in fishes: Fluid speed, acceleration, strike accuracy and the ingested volume of water. *J. Exp. Biol.* **209**, 2713–2725.

Hill, J. J., Puttick, M. N., Stubbs, T. L., Rayfield, E. J. and Donoghue, P. C. J. (2018). Evolution of jaw disparity in fishes. *Palaeontology* **61**, 847–854.

Holzman, R., Day, S. W. and Wainwright, P. C. (2007). Timing is everything: coordination of strike kinematics affects the force exerted by suction feeding fish on attached prey. *J. Exp. Biol.* **210**, 3328–3336.

Holzman, R., Day, S. W., Mehta, R. S. and Wainwright, P. C. (2008). Integrating the determinants of suction feeding performance in centrarchid fishes. *J. Exp. Biol.* **211**, 3296–3305.

Hughes, L. C., Ortí, G., Huang, Y., Sun, Y., Baldwin, C. C., Thompson, A. W., Arcila, D., Betancur, R., Li, C., Becker, L., et al. (2018). Comprehensive phylogeny of ray-finned fishes (Actinopterygii) based on transcriptomic and genomic data. *Proc. Natl. Acad. Sci. U. S. A.* **115**, 6249–6254.

Iriarte-Diaz, J., Terhune, C. E., Taylor, A. B. and Ross, C. F. (2017). Functional correlates of the position of the axis of rotation of the mandible during chewing in non-human primates. *Zoology* **124**, 106–118.

Iriarte-Díaz, J., Reed, D. A. and Ross, C. F. (2011). Sources of variance in temporal and spatial aspects of jaw kinematics in two species of primates feeding on foods of different properties. *Integr. Comp. Biol.* **51**, 307–319.

Jacobs, C. N. and Holzman, R. (2018). Conserved spatio-temporal patterns of suction-feeding flows across aquatic vertebrates: A comparative flow visualization study. *J. Exp. Biol.* **221**,.

Jimenez, Y. E., Camp, A. L., Grindall, J. D. and Brainerd, E. L. (2018). Axial morphology and 3D neurocranial kinematics in suction-feeding fishes. *Biol. Open* **7**, 1–10.

Kaczmarek, E. B., Gartner, S. M., Westneat, M. W. and Brainerd, E. L. (2022). Air breathing and suction feeding kinematics in the West African lungfish, *Protopterus annectens*. *Integr. Comp. Biol.* **icac109**,.

Kane, E. A. and Higham, T. E. (2014). Modelled three-dimensional suction accuracy predicts prey capture success in three species of centrarchid fishes. *J. R. Soc. Interface* **11**, 20140223.

Kane, E. A. and Higham, T. E. (2015). Complex systems are more than the sum of their parts: Using integration to understand performance, biomechanics, and diversity. *Integr. Comp. Biol.* **55**, 146–165.

Knorlein, B. J., Baier, D. B., Gatesy, S. M., Laurence-Chasen, J. D. and Brainerd, E. L. (2016). Validation of XMALab software for Marker-based XROMM. *J. Exp. Biol.* **219**, 3701–3711.

Lacepède, B. (1803). *Histoire naturelle des poissons*. Biodiversity Heritage Library.

Lauder, G. V. (1979). Feeding mechanics in primitive teleosts and in the halecomorph fish *Amia calva*. *J. Zool. London* **187**, 543–578.

Lauder, G. V. (1980). Evolution of the feeding mechanism in primitive actionopterygian fishes: A functional anatomical analysis of *Polypterus*, *Lepisosteus*, and *Amia*. *J. Morphol.* **163**, 283–317.

Lauder, G. V. (1982). Patterns of evolution in the feeding mechanism of actinopterygian fishes. *Am. Soc. Zool.* **285**, 275–285.

Lauder, G. V. (1983). Functional design and evolution of the pharyngeal jaw apparatus in euteleostean fishes. *Zool. J. Linn. Soc.* **77**, 1–38.

Lauder, G. V. (1985). Aquatic feeding in lower vertebrates. In *Functional vertebrate morphology*, pp. 210–229.

Lauder, G. V. and Lanyon, L. E. (1980). Functional anatomy of feeding in the bluegill sunfish, *Lepomis macrochirus*: *in vivo* measurement of bone strain. *J. Exp. Biol.* **84**, 33–55.

Laurence-Chasen, J. D., Ramsay, J. B. and Brainerd, E. L. (2019). Shearing overbite and asymmetrical jaw motions facilitate food breakdown in a freshwater stingray, *Potamotrygon motoro*. *J. Exp. Biol.* **222**,.

Laurence-Chasen, J. D., Manafzadeh, A. R., Hatsopoulos, N. G., Ross, C. F. and Arce-McShane, F. I. (2020). Integrating XMALab and DeepLabCut for high-throughput XROMM. *J. Exp. Biol.* **223**,.

Lemberg, J. B., Shubin, N. H. and Westneat, M. W. (2019). Feeding kinematics and morphology of the alligator gar (*Atractosteus spatula*, Lacépède, 1803). *J. Morphol.* **280**, 1548–1570.

Lemberg, J. B., Daeschler, E. B. and Shubin, N. H. (2021). The feeding system of *Tiktaalik roseae*: an intermediate between suction feeding and biting. *Proc. Natl. Acad. Sci. U. S. A.* **118**, 1–10.

Li, E. Y., Kaczmarek, E. B., Olsen, A. M., Brainerd, E. L. and Camp, A. L. (2022). Royal knifefish generate powerful suction feeding through large neurocranial elevation and high epaxial muscle power. *bioRxiv (preprint)*.

Liem, K. F. (1970). Comparative functional anatomy of the Nandidae (Pisces: Teleostei). *Fieldiana Zool.* **56**, 1–166.

Liem, K. F. (1978). Modulatory multiplicity in the functional repertoire of the feeding mechanism in cichlid fishes. I. Piscivores. *J. Morphol.* **158**, 323–360.

Liem, K. F. (1980). Adaptive significance of intra-and interspecific differences in the feeding repertoires of cichlid fishes. *Am. Zool.* **20**, 295–314.

Linnaeus, C. (1766). *Systema naturae per regna tria naturae, secundum classes, ordinus, genera, species, cum characteribus, differentiis, synonymis, locis. Laurentii Salvii, Holmiae*.

Lomax, J. J., Martinson, T. F., Jimenez, Y. E. and Brainerd, E. L. (2020). Bifunctional role of the sternohyoideus muscle during suction feeding in striped surfperch, *Embiotoca lateralis*. *Integr. Org. Biol.* **2**,.

Longo, S. J., McGee, M. D., Oufiero, C. E., Waltzek, T. B. and Wainwright, P. C. (2016). Body ram, not suction, is the primary axis of suction-feeding diversity in spiny-rayed fishes. *J. Exp. Biol.* **219**, 119–128.

Manafzadeh, A. R. (2020). A practical guide to measuring *ex vivo* joint mobility using XROMM. *Integr. Org. Biol.* **2**,.

Manafzadeh, A. R. and Gatesy, S. M. (2020). A coordinate-system-independent method for comparing joint rotational mobilities. *J. Exp. Biol.* **223**,.

Markey, M. J. (2006). *In vivo* cranial suture function and suture morphology in the extant fish *Polypterus*: implications for inferring skull function in living and fossil fish. *J. Exp. Biol.* **209**, 2085–2102.

Markey, M. J. and Marshall, C. R. (2007). Terrestrial-style feeding in a very early aquatic tetrapod is supported by evidence from experimental analysis of suture morphology. *Proc. Natl. Acad. Sci. U. S. A.* **104**, 7134–7138.

Matott, M. P., Motta, P. J. and Hueter, R. E. (2005). Modulation in feeding kinematics and motor pattern of the nurse shark *Ginglymostoma cirratum*. *Environ. Biol. Fishes* **74**, 163–174.

McAllister, C. T., Robison, H. W. and Drive, W. M. (2019). A novel food item (Diptera : Stratiomyidae) of Spotted Gar, *Lepisosteus oculatus* and Bowfin, *Amia calva*, from Southeastern Oklahoma. **49**, 47–49.

Michel, K. B., Heiss, E., Aerts, P. and van Wassenbergh, S. (2015). A fish that uses its hydrodynamic tongue to feed on land. *Proc. R. Soc. B Biol. Sci.* **282**,.

Molnar, J. L., Johnston, P. S., Esteve-Altava, B. and Diogo, R. (2017). Musculoskeletal anatomy of the pelvic fin of *Polypterus*: implications for phylogenetic distribution and homology of pre- and postaxial pelvic appendicular muscles. *J. Anat.* **230**, 532–541.

Montuelle, S. J., Herrel, A., Schaerlaeken, V., Metzger, K. A., Mutuyeyezu, A. and Bels, V. L. (2009). Inertial feeding in the teiid lizard *Tupinambis merianae*: The effect of prey size on the movements of hyolingual apparatus and the cranio-cervical system. *J. Exp. Biol.* **212**, 2501–2510.

Montuelle, S. J., Herrel, A., Libourel, P.-A., Daillie, S. and Bels, V. L. (2012a). Flexibility in locomotor-feeding integration during prey capture in varanid lizards: effects of prey size and velocity. *J. Exp. Biol.* **215**, 3823–3835.

Montuelle, S. J., Herrel, A., Libourel, P., Daillie, S. and Bels, V. L. (2012b). Prey capture in lizards: differences in jaw – neck – forelimb coordination. *Biol. J. Linn. Soc.* **105**, 607–622.

Moran, C. J., Rzucidlo, C. L., Carlowicz, R. M. and Gerry, S. P. (2018). Stereotyped feeding behaviors of polyphenic bluegill sunfish. *J. Zool.* **305**, 116–123.

Motta, P. J. (1984). Mechanics and functions of jaw protrusion in teleost fishes: A review. *Am. Soc. Ichthyol. Herpetol.* **1**, 1–18.

Muller, M. (1989). A quantitative theory of expected volume changes of the mouth during feeding in teleost fishes. *J. Zool. Lond.* **217**, 639–662.

Muller, M. and Osse, J. W. M. (1984). Hydrodynamics of suction feeding in fish. *Trans. Zool. Soc. London* **37**, 51–135.

Muller, M., Osse, J. W. M. and Verhagen, J. H. G. (1982). A quantitative hydrodynamical model of suction feeding in fish. *J. Theor. Biol.* **95**, 49–79.

Near, T. J., Eytan, R. I., Dornburg, A., Kuhn, K. L., Moore, J. a, Davis, M. P., Wainwright, P. C., Friedman, M. and Smith, W. L. (2012). Resolution of ray-finned fish phylogeny and timing of diversification. *Proc. Natl. Acad. Sci. U. S. A.* **109**, 13698–13703.

Nemeth, D. H. (1997a). Modulation of buccal pressure during prey capture in *Hexagrammos decagrammus* (Teleostei: Hexagrammidae). *J. Exp. Biol.* **200**, 2145–2154.

Nemeth, D. H. (1997b). Modulation of attack behavior and its effect on feeding performance in a trophic generalist fish, *Hexagrammos decagrammus*. *J. Exp. Biol.* **200**, 2155–2164.

Nyberg, D. W. (1971). Prey capture in the largemouth bass. *Am. Midl. Nat.* **86**, 128–144.

Olsen, A. M. (2019a). A mobility-based classification of closed kinematic chains in biomechanics and implications for motor control. *J. Exp. Biol.* **222**,.

Olsen, A. (2019b). matools.

Olsen, A. M., Camp, A. L. and Brainerd, E. L. (2017). The opercular mouth-opening mechanism of largemouth bass functions as a 3D four-bar linkage with three degrees of freedom. *J. Exp. Biol.* **220**, 4612–4623.

Olsen, A. M., Hernández, L. P., Camp, A. L. and Brainerd, E. L. (2019). Channel catfish use higher coordination to capture prey than to swallow. *Proc. R. Soc. B Biol. Sci.* **286**,.

Olsen, A. M., Hernandez, L. P. and Brainerd, E. L. (2020). Multiple degrees of freedom in the fish skull and their relation to hydraulic transport of prey in channel catfish. *Integr. Org. Biol.* **2**,.

Patterson, C. (1982). Morphology and interrelationships of primitive actinopterygian fishes. *Integr. Comp. Biol.* **22**, 241–259.

Provini, P., Brunet, A., Filippo, A. and Van Wassenbergh, S. (2022). *In vivo* intraoral waterflow quantification reveals hidden mechanisms of suction feeding in fish. *Elife* **11**, 1–20.

Ram, Y. and Ross, C. F. (2019). Jaw elevator muscle coordination during rhythmic mastication in primates: Are triplets units of motor control? *Brain. Behav. Evol.* 1–14.

Reed, D. A. and Ross, C. F. (2010). The influence of food material properties on jaw kinematics in the primate, *Cebus*. *Arch. Oral Biol.* **55**, 946–962.

Rice, A. N. and Westneat, M. W. (2005). Coordination of feeding, locomotor and visual systems in parrotfishes (Teleostei: Labridae). *J. Exp. Biol.* **208**, 3503–3518.

Rice, A. N., Cooper, W. J. and Westneat, M. W. (2008). Diversification of coordination patterns during feeding behaviour in cheiline wrasses. *Biol. J. Linn. Soc.* **93**, 289–308.

Ross, C. F., Dharia, R., Herring, S. W., Hylander, W. L., Liu, Z.-J., Rafferty, K. L., Ravosa, M. J. and Williams, S. H. (2007a). Modulation of mandibular loading and bite force in mammals during mastication. *J. Exp. Biol.* **210**, 1046–1063.

Ross, C., Dharia, R., Herring, S., Hylander, W., Lui, Z.-J., Rafferty, K., Ravosa, M. and Williams, S. (2007b). Modulation of mandibular loading and bite force in mammals during mastication. *J. Exp. Biol.* **210**, 1046–1063.

Ross, C. F., Iriarte-Diaz, J., Reed, D. A., Stewart, T. A. and Taylor, A. B. (2016). *In vivo* bone strain in the mandibular corpus of *Sapajus* during a range of oral food processing behaviors. *J. Hum. Evol.* **98**, 36–65.

Sanford, C. P. (2001). Kinematic analysis of a novel feeding mechanism in the brook trout *Salvelinus fontinalis* (Teleostei: Salmonidae): behavioral modulation of a functional novelty. *J. Exp. Biol.* **204**, 3905–16.

Sinopoli, D. (2019). Morphological variation of bowfin (Amiidae: *Amia calva* Linnaeus 1766) populations from the Mississippi River Basin: Taxonomic and conservation implications.

Svanbäck, R., Wainwright, P. C. and Ferry-Graham, L. A. (2002). Linking cranial kinematics, buccal pressure, and suction feeding performance in largemouth bass. *Physiol. Biochem. Zool.* **75**, 532–543.

Tchernavin, V. V. (1948). On the mechanical working of the head of bony fishes. *Proc. Zool. Soc. London* **118**, 129–143.

Team, R. C. (2019). R: A language and environment for statistical computing.

Thompson, A. W., Hawkins, M. B., Parey, E., Wcisel, D. J., Ota, T., Kawasaki, K., Funk, E., Losilla, M., Fitch, O. E., Pan, Q., Feron, R., Louis, A., Montfort, J., Milhes, M., Racicot, B. L., Childs, K. L., Fontenot, Q., Ferrara, A., David, S. R., McCune, A. R., Dornburg, A., Yoder, J. A., Guiguen, Y., Roest Crollius, H., Berthelot, C., Harris, M. P., Braasch, I. (2021). The bowfin genome illuminates the developmental evolution of ray-finned fishes. *Nat. Genet.* **53**, 1373–1384.

Van Wassenbergh, S. and Aerts, P. (2009). Aquatic suction feeding dynamics: Insights from computational modelling. *J. R. Soc. Interface* **6**, 149–158.

Van Wassenbergh, S. and De Rechter, D. (2011). Piscivorous cyprinid fish modulates suction feeding kinematics to capture elusive prey. *Zoology* **114**, 46–52.

Van Wassenbergh, S., Herrel, A., Adriaens, D. and Aerts, P. (2005). A test of mouth-opening and hyoid-depression mechanisms during prey capture in a catfish using high-speed cineradiography. *J. Exp. Biol.* **208**, 4627–4639.

Van Wassenbergh, S., Aerts, P. and Herrel, A. (2006). Scaling of suction feeding performance in the catfish *Clarias gariepinus*. *Physiol. Biochem. Zool.* **79**, 43–56.

Van Wassenbergh, S., Herrel, A., Adriaens, D. and Aerts, P. (2007). Interspecific variation in sternohyoideus muscle morphology in clariid catfishes: Functional implications for suction feeding. *J. Morphol.* **268**, 232–242.

Vereijken, B., van Emmerik, R., Whiting, H. T. A. and Newell, K. M. (1992). Free(z)ing degrees of freedom in skill acquisition. *J. Mot. Behav.* **24**, 133–142.

Vinyard, G. L. (1982). Variable kinematics of Sacramento perch (*Archoplites interruptus*) capturing evasive and nonevasive prey. *Can. J. Fish. Aquat. Sci.* **39**, 208–211.

Vinyard, C. J., Wall, C. E., Williams, S. H. and Hylander, W. L. (2008). Patterns of variation across primates in jaw-muscle electromyography during mastication. *Integr. Comp. Biol.* **48**, 294–311.

Wainwright, P. C. and Bellwood, D. R. (2002). Ecomorphology of feeding in coral reef fishes. *Coral Reef Fishes. Dyn. Divers. a Complex Ecosyst.* 33–55.

Wainwright, P. C. and Day, S. W. (2007). The forces exerted by aquatic suction feeders on their prey. *J. R. Soc. Interface* **4**, 553–560.

Wainwright, P. C. and Lauder, G. V. (1986). Feeding biology of sunfishes: patterns of variation in the feeding mechanism. *Zool. J. Linn. Soc.* **88**, 217–228.

Wainwright, P. C., Bellwood, D. R., Westneat, M. W., Grubich, J. R. and Hoey, A. S. (2004). A functional morphospace for the skull of labrid fishes: Patterns of diversity in a complex biomechanical system. *Biol. J. Linn. Soc.* **82**, 1–25.

Wainwright, P. C., Mehta, R. S. and Higham, T. E. (2008). Stereotypy, flexibility and coordination: key concepts in behavioral functional morphology. *J. Exp. Biol.* **211**, 3523–3528.

Wainwright, P. C., McGee, M. D., Longo, S. J. and Patricia Hernandez, L. (2015). Origins, innovations, and diversification of suction feeding in vertebrates. *Integr. Comp. Biol.* **55**, 134–145.

Weller, H. I., Olsen, A. M., Camp, A. L., Manafzadeh, A. R., Hernandez, L. P. and Brainerd, E. L. (2020). An XROMM study of food transport and swallowing in channel catfish. *Integr. Org. Biol.* **2**,.

Westneat, M. W. (1990). Feeding mechanics of teleost fishes (Labridae; Perciformes): A test of four-bar linkage models. *J. Morphol.* **205**, 269–295.

Westneat, M. W. (2004). Evolution of levers and linkages in the feeding mechanisms of fishes. *Integr. Comp. Biol.* **44**, 378–389.

Westneat, M. W. and Wainwright, P. C. (1989). Feeding mechanism of *Epibulus insidiator* (Labridae; Telesotei): evolution of a novel functional system. *J. Morphol.* **205**, 269–275.

Westneat, M. and Walker, J. (1997). Motor patterns of labriform locomotion: kinematic and electromyographic analysis of pectoral fin swimming in the labrid fish *Gomphosus varius*. *J. Exp. Biol.* **200**, 1881–1893.

Whitlow, K. R., Ross, C. F., Gidmark, N. J., Laurence-Chasen, J. D. and Westneat, M. W. (2022). Suction feeding biomechanics of *Polypterus bichir*: Investigating linkage mechanisms and the contributions of cranial kinesis to oral cavity volume change. *J. Exp. Biol.* **225**,.

Wilga, C. D., Wainwright, P. C. and Motta, P. J. (2000). Evolution of jaw mechanics in vertebrates: Insights from Chondrichthyes. *Biol. J. Linn. Soc.* **71**, 165–185.

Wilhelm, B. C., Du, T. Y., Standen, E. M. and Larsson, H. C. E. (2015). *Polypterus* and the evolution of fish pectoral musculature. *J. Anat.* **226**, 511–522.